Asymptotic Giant Branch Variables in NGC 6822

By

Francois Nsengiyumva

Department of Astronomy

University of Cape Town

South Africa

Supervisors: Prof. Patricia Whitelock [1,2], Dr. John Menzies[1] &

Prof. Michael Feast[2,1]

A dissertation submitted in partial fulfilment of the requirements for the degree of M.Sc. in the Department of Astronomy, as part of the National Astrophysics and Space Science Programme

November 2010

[1]South African Astronomical Observatory

[2]University of Cape Town

Abstract

NGC 6822, a Local Group dwarf irregular galaxy, was observed in the near-infrared JHK$_S$ bands using the Japanese-SAAO Infrared Survey Facility (IRSF) telescope over a period of about four years. An extensive search for large amplitude asymptotic giant branch variables over the observed 7.5$'$x 21.1$'$ area of NGC 6822 found 162 probable variables. In particular, 30 Miras and 9 semiregulars have been identified and characterised. Their peak-to-peak J, H and K$_S$ amplitudes, pulsation periods and Fourier mean J, H and K$_S$ as well as their bolometric magnitudes have been determined. The periods (P) fall within the range $190 < P < 900$ d whereas the K amplitudes ($\triangle$K) fall within the range $0.2 < \triangle K < 1.8$ mag. Many of these stars are fainter than predicted by the K period-luminosity (PL) relation, because of high circumstellar extinction. Stars with the largest pulsation amplitudes show the largest circumstellar extinction. The slope of the apparent bolometric PL relation for NGC 6822 Miras is similar to its LMC counterpart. This leads to a distance modulus of 23.43$\pm$ 0.04 for NGC 6822, on the assumption that the distance modulus to the LMC is 18.39. This is in reasonable agreement with other determinations.

Acknowledgements

I sincerely thank my supervisors, Prof. Patricia Whitelock, Dr. John Menzies and Prof. Michael Feast, for their invaluable support and guidance over the duration of this project. You have been very supportive and helpful throughout and I really appreciate the time and effort you put into your suggestions and feedback. I have learnt so much from you.

In no particular order, I would like to thank the following people for their contribution to this work, in one way or the other: Mr Oyirwoth Patrick Abedigamba, Mr Geoffrey Okeng'o, Miss Zara Randriamanakoto, Mr Solohery Randriamampandry, Mr Rudi Kuhn, Mr Andry Rajoelimanana, Mr Paul Kotze, Ms Shireen Davis, Dr. Enrico Olivier, Dr. Luis Balona, Mr Ed Elson, Dr. Matsunaga Noriyuki and Dr. Lakhan Lal Yadav.

Spending a year at the SAAO working on this thesis was a great pleasure to me. I thank the SAAO community for their hospitality.

This work was made possible and funded by the South African National Astrophysics and Space Science Program (NASSP). I am very grateful to this program.

Contents

1 Introduction **9**

1.1 NGC 6822 9

1.2 Asymptotic Giant Branch (AGB) stars 13

1.2.1 Introduction 13

1.2.2 TRGB of NGC 6822 15

1.2.3 Characteristics and properties of AGB stars 16

1.3 AGB stars in NGC 6822 20

1.4 Long-period AGB variables and aim of the project 21

2 Near-infrared observations of NGC 6822 **25**

2.1 Observations of NGC 6822, data reduction and photometric measurements 25

2.2 Data processing and selection of variables 27

2.2.1 Data processing 27

2.2.2 Selection of large amplitude variables 33

3 Data analysis and results **37**

3.1 Identification and characterisation of large amplitude AGB variables in NGC 6822 37

3.2 Colour-Magnitude Diagram and carbon stars 46

3.2.1 Colour-Magnitude Diagram 46

3.2.2 Carbon stars 48

3.3 Colour-colour diagram 49

3.4 K period-luminosity relation for Miras 53
3.5 Bolometric period-luminosity relation for Miras 58
3.6 Distance to NGC 6822 65

4 Discussion of the results and recommendations 67

5 Conclusion 69

A Probable large amplitude AGB variables in NGC 6822 76

B Potential large amplitude variables observed less than 10 times in NGC 6822 81

C Other red objects detected in NGC 6822 82

D Phased K light curves for Miras in NGC 6822 84

E Phased K light curves for SRs in NGC 6822 100

List of Figures

2.1 Histogram of the number of sources detected in NGC 6822 as a function of J, H and K_S magnitudes. 29

2.2 Histogram of number of objects with $16.5 \leq K < 17.4$ as a function of standard deviations of K magnitudes (σ_K) in that bin. A Gaussian curve is fitted and from the Gaussian fit, the mean (μ_{σ_K}) and standard deviation (σ_{σ_K}) of the standard deviations of K magnitudes are obtained. 33

2.3 The K standard deviations (σ_K) as a function of K magnitudes of all sources detected in NGC 6822. The line is given by equation 2.3 and all the objects above it are selected as candidate large amplitude variables. 34

3.1 Comparison of our data and the AGB stars identified in NGC 6822 by Kang et al. (2006), using a colour-magnitude diagram. Filled ellipses and rectangles represent, respectively, the 141 carbon and 522 M stars identified by Kang et al. (2006) whereas crosses represent objects in our data. The estimated slanted line is given by $K_S = -3.12(J - K_S) + 19.49$ whereas the horizontal line represents the TRGB in K band and is given by K_S=17.2mag. 38

3.2 K Light curve of Mira 20784. 40

3.3 K Light curve of Mira 10807. 41

3.4 Histogram of the number of Miras as a function of their pulsation periods. 45

3.5 Colour-magnitude diagram for the sources detected in NGC 6822, emphasing the location of large amplitude AGB variables. Only sources with at least 10 observations at K_S are illustrated here. Objects brighter than the TRGB (K_S=17.2) and fainter than the slanted line given by $K_S = -3.12(J - K_S) + 19.49$ (see also Figure 3.1) are considered as the most probable AGB stars. Miras and SRs are shown by filled ellipses and rectangles, respectively, whereas other probable large amplitude AGB variables are indicated by filled triangles. Crosses indicate other objects detected in NGC 6822. . 47

3.6 Colour-colour diagram of the sources detected in NGC 6822, emphasing the location of large amplitude AGB variables. Symbols are the same as in Figure 3.5. The solid line shows the locus of Galactic carbon Miras and is given by $(H-K)_0 = -0.428 + 1.003(J - H)_0$. This is equation 2 from Whitelock et al. (2006), converted on to the 2MASS system. The dashed line represents infrared colours of black bodies given in Glass (1999). 51

3.7 The location of large amplitude carbon/oxygen variables on a two-colour diagram. Filled ellipses represent the probable carbon variables, whereas filled rectangles represent the probable oxygen ones. 52

3.8 PL(K) relation for Miras and SRs in NGC 6822, on the assumption that the distance modulus to NGC 6822 is 23.43 (see section 3.5). Filled ellipses represent Miras while filled rectangles represent SRs. The line is the PL(K) relation for Miras in the LMC and is given by $M_K = -3.51[log(P) - 2.38] - 7.15$ (Whitelock et al., 2008). 54

3.9 The differences (dM_{K_S}) between the observed K magnitudes and those predicted from the LMC PL(K) as a function of J-K_S colours. Symbols are the same as in Figure 3.8. The arrowed line indicates the locus of interstellar reddening of strength A_V=10 mag. This value of A_V was found using the colour excess ratios given in Table 5.2 in Glass (1999). 56

3.10 The differences (dM_{K_S}) between the observed magnitudes and those predicted from the LMC PL(K) as a function of K amplitudes of pulsation. Symbols are the same as in Figure 3.8. 57

3.11 m_{bol} PL relation for Miras and SRs in NGC 6822. Symbols are the same as in Figure 3.8. The line is given by $m_{bol} = -3.31[\log(P)\text{-}2.5] + 19.154$ (equation 3.4). 60

3.12 M_{bol} PL relation for Miras and SRs in NGC 6822 and LMC. Filled ellipses and rectangles represent, respectively, Miras and SRs in NGC 6822 while filled triangles represent 22 C Miras in the LMC (Whitelock et al., 2009). The solid line is a result of a least squares fit to the NGC 6822 Miras and is given by $M_{bol} = -2.81[log(P)-2.5]-4.32$, whereas the dashed line results from a least squares fit to the LMC C Miras and is given by $M_{bol} = -3.31[log(P)-2.5]-4.271$ (Whitelock et al., 2009). 64

D.1 Phased K light curve for 11032. 84

D.2 Phased K light curve for 10807. 85
D.3 Phased K light curve for 12208. 85
D.4 Phased K light curve for 1059. 86
D.5 Phased K light curve for 11296. 86
D.6 Phased K light curve for 11299. 87
D.7 Phased K light curve for 12147. 87
D.8 Phased K light curve for 20417. 88
D.9 Phased K light curve for 20439. 88
D.10 Phased K light curve for 20784. 89
D.11 Phased K light curve for 11140. 89
D.12 Phased K light curve for 11174. 90
D.13 Phased K light curve for 11226. 90
D.14 Phased K light curve for 12400. 91
D.15 Phased K light curve for 13364. 91
D.16 Phased K light curve for 20569. 92
D.17 Phased K light curve for 13106. 92
D.18 Phased K light curve for 12466. 93
D.19 Phased K light curve for 30920. 93
D.20 Phased K light curve for 12751. 94
D.21 Phased K light curve for 20542. 94
D.22 Phased K light curve for 10817. 95
D.23 Phased K light curve for 12445. 95
D.24 Phased K light curve for 13293. 96
D.25 Phased K light curve for 12177. 96
D.26 Phased K light curve for 21419. 97
D.27 Phased K light curve for 20356. 97
D.28 Phased K light curve for 21671. 98
D.29 Phased K light curve for 21234. 98
D.30 Phased K light curve for 31168. 99

E.1 Phased K light curve for 11389. 100
E.2 Phased K light curve for 10935. 101
E.3 Phased K light curve for 11372. 102
E.4 Phased K light curve for 11794. 103
E.5 Phased K light curve for 10412. 104
E.6 Phased K light curve for 10439. 105
E.7 Phased K light curve for 10635. 106
E.8 Phased K light curve for 10876. 107
E.9 Phased K light curve for 20539. 108

List of Tables

2.1 Data obtained from observations of NGC 6822 using IRSF . . 28
2.2 K data for the star 12208 31
2.3 JHK data for the star 12208 32

3.1 List of Mira (M) and semiregular (SR) variables identified in NGC 6822 and their positions 42
3.2 Characteristic parameters of Miras and SRs in NGC 6822 . . 44
3.3 Parameters associated to the equation 3.5 61
3.4 Values of the slope and scatter of the LMC Mira PL(bol) relations from the literature 62
3.5 Estimates of the distance modulus to NGC 6822 from the literature 65

Chapter 1

Introduction

1.1 NGC 6822

Dwarf irregular galaxies are known to be gas-rich with a low metallicity, suggesting that they are still in an early stage of star formation. They are characterised by a simple structure, compared to other types of galaxy, which makes it easier to study stellar populations and star formation history in them. In particular, dwarf irregular galaxies of the Local Group are of special interest since their proximity allows us to study them in greater detail than more distant galaxies. A study of the stellar population in dwarf galaxies provides clues to stellar evolution and star formation history in galaxies. Due to their small size and low luminosity, photometric studies of the resolved stars in dwarf galaxies are possible only for those in the Local Group (LG). Asymptotic giant branch (AGB) stars are among the bright resolved stars in the LG dwarf galaxies.

NGC 6822 is an isolated, Local Group, barred, dwarf irregular galaxy of Magellanic type (Hubble, 1925). Its equatorial coordinates are $\alpha = 19^h44^m56^s$ (2000), $\delta = -14°48'06''$ (2000) and its Galactic coordinates are $l = 25°.34$, $b = -18°.39$ (van den Bergh, 2000).

Hubble (1925) was the first astronomer to study NGC 6822 in detail and

his observations led to the discovery of 11 Cepheid variables and 9 nonstellar objects some of which are young star clusters whereas others appear to be old star clusters. In addition to Hubble's discovery, Hodge (1977) found a number of open clusters as well as other nonstellar objects in NGC 6822. The work of Wyder et al. (2000) which involved the analysis of V and I images of five fields of NGC 6822 obtained by the Hubble Space Telescope, found the ages of Hubble's clusters VI and VIII to be 70 $\pm$ 10 Myr and 1.5 $\pm$ 0.2 Gyr, respectively. These workers also suggest that Hubble's cluster VII might be similar to the old, metal-poor globular clusters in the Milky Way. Several OB associations in this galaxy have been found and studied by a number of investigators (e.g. Hodge (1977)). A comparison with those in other galaxies (Hodge, 1977) shows that their spatial and size distribution as well as the relationship between size and stellar density are similar to the ones in the LMC OB associations. In addition to young stars, a large number of evolved stars have been identified in NGC 6822 (see section 1.3).

Several investigations of the star formation history of NGC 6822 (e.g. Wyder (2000)) have shown that this galaxy started forming stars at a very early epoch (12-15 Gyr ago) from low metallicity gas, and that stars span a wide range of ages. The discovery of a large number of evolved stars such as AGB stars in NGC 6822 (e.g. Cioni & Habing (2005)) indicates that the star formation rate (SFR) in NGC 6822 was high over a lengthy time scale. The rate of star formation in NGC 6822 started to increase about 3 Gyr ago (Tolstoy et al., 2001) and kept on increasing over the last 100-200 Myr (Gallart et al., 1996a). The last mentioned workers also noticed, following earlier work, that the strength of the increase in recent SFR has been different from one region of the galaxy to another. They found that the recent SFR is higher in the bar region than in regions outside the bar and that it is higher in the northern and southern edges than in the central part of the bar. They also noticed a good correlation between the regions of

the galaxy with a more pronounced recent SFR and the observed HI regions. A large extended halo of HI gas (e.g. Brandenburg & Skillman (1998)) and numerous HII regions (e.g. Hodge et al. (1988)) as well as OB associations (e.g. Hodge (1977)) found in NGC 6822, suggest that this galaxy is currently actively forming stars.

Despite its proximity, the fact that NGC 6822 is located at a relatively low Galactic latitude ($b = -18°$), in a region with a high density of foreground stars and absorbing dust, has made its study more difficult. The interstellar reddening towards NGC 6822 is relatively large. Hodge (1977) found a colour excess E(B-V)=0.28 $\pm$ 0.03 from photoelectric and photographic studies of the surface brightness and colour, and of individual stars and nonstellar objects in NGC 6822. UBV photometry of OB stars in NGC 6822 by Massey et al. (1995) found that the colour excess increases from E(B-V) $\approx$ 0.26 at the eastern and western ends to E(B-V) $\approx$ 0.45 near the center. Cioni & Habing (2005) noticed that the high reddening in the central region of NGC 6822 might be due to young objects still being associated with the dusty gas clouds from which they formed, but it hardly affects the near-infrared photometry of the AGB or red giant branch (RGB) stars. Gallart et al. (1996b) found E(B-V)=0.24 $\pm$ 0.03 from UBVRI photometry of the resolved stars in NGC 6822. In light of the results presented in section 3.4, a colour excess of the order of E(B-V)=0.25 mag which amounts to about A_K=0.07 is almost negligible in this work.

Various estimates of the distance to NGC 6822 using different approaches have been made. Clementini et al. (2003) use V photometry of six RR Lyrae variables to derive $(m\text{-}M)_0$=23.36 $\pm$ 0.17. From the bolometric magnitudes of the position of the tip of the red giant branch (TRGB), Sohn et al. (2008) found the distance modulus to NGC 6822 to be 23.41$\pm$ 0.17. Using 56 Cepheids, Gieren et al. (2006) obtained 23.31 $\pm$ 0.02 as a distance modulus to NGC 6822. In section 3.5, a new distance to NGC 6822 is determined

using the data in this work and more details of the distance to NGC 6822 are presented in section 3.6.

Venn et al. (2001) obtained high-resolution spectra of 2 supergiants in NGC 6822 and found the mean iron abundance from the two stars to be $< [Fe/H] >= -0.49 \pm 0.22$dex. From the average period of the ab-type RR Lyrae stars, Clementini et al. (2003) obtained $[Fe/H] = -1.92\pm$ 0.35dex for the mean metallicity of RR Lyrae stars in NGC 6822. On the basis of I, J and K_S observations of NGC 6822, Cioni & Habing (2005) derived, from the ratio between C- and O-rich AGB stars, a spread in metallicity in NGC 6822 which is twice as large as the spread in metallicity deduced within each Magellanic Cloud using the same technique. They found a spread in metallicity of 1.56dex for NGC 6822 (see also section 1.3). They also estimated that the average metallicity of an average AGB star of $1.5 M_{\odot}$, detected in their study, would be $< [Fe/H] >= -0.89$dex. Tolstoy et al. (2001) measured the metallicities of 23 RGB stars in NGC 6822 which led them to an estimate of the metallicity distribution for this galaxy. From the measurements of the Ca II triplet, they found that the metallicity of the RGB stars observed in NGC 6822 has a very large spread ranging from -2.0 to -0.5dex. They obtained on average $[Fe/H] = -0.9$dex. Davidge (2003) determined, from the slope of the RGB on the (J-K, K) colour-magnitude diagrams, the metallicity of the RGB in the disk of NGC 6822 as $[Fe/H] = -1.0\pm$ 0.3dex. Spectroscopic studies of Cluster VII and Cluster VI of NGC 6822 by Cohen & Blakeslee (1998) found Cluster VII to be an old globular cluster with a metallicity of $[Fe/H] = -1.95\pm$ 0.15dex while Cluster VI was found to be much younger with a metallicity of $[Fe/H] \approx -1.0$dex. The metallicity of cluster VII is comparable to that of the metal-poor Galactic globular clusters whereas that of cluster VI is similar to that of the gas currently seen in NGC 6822. In summary, these investigations suggest that NGC 6822 has a wide spread of metallicity in the range $-2.0 \lesssim [Fe/H] \lesssim -0.5$dex.

1.2 Asymptotic Giant Branch (AGB) stars

1.2.1 Introduction

In this section, I review some important aspects of stellar evolution relevant to this work.

The birth of a star takes place in dense interstellar clouds known as Giant Molecular Clouds (GMCs). These are large agglomerations of interstellar gas and dust. The GMCs are not static, they are dynamic and subject to instabilities.

Eventually, the GMC becomes gravitationally unstable and starts to collapse. As it collapses, the GMC breaks up into subclouds which may themselves break into smaller structures. This process is known as fragmentation.

At central densities below 10^{-13} g cm^{-3} (Schulz, 2005), the collapse in each of the fragments is somewhat isothermal. The density increases more rapidly in the center of the collapsing cloud than in the outer layers. When the central density exceeds 10^{-13} g cm^{-3}, the collapse is no longer isothermal. Internal temperature increases resulting in increase in pressure. Eventually, the pressure becomes high enough to slow down the rate of gravitational collapse in each of the fragments at least near the core. This results in a first stable core of few astronomical units and the object at this stage is known as protostar.

Protostars evolve in different ways depending on their masses. Only those with high masses can reach high enough core temperatures for nuclear fusion of hydrogen to start. In these protostars, the proton-proton (pp) chain reaction occurs, allowing hydrogen to fuse first to deuterium and then to helium. For protostars with masses slightly over $1M_{\odot}$, the CNO cycle contributes a considerable portion of energy generation.

As they evolve, protostars continue to contract until the internal pressure

becomes high enough to balance gravity and prevent any further gravitational collapse. At this stage, the star is in hydrostatic equilibrium, a stable phase of evolution known as the main sequence phase.

The lifetime of stars on the main sequence is a function of their masses (M). Massive stars (M$\gtrsim 8M_{\odot}$) spend a relatively short time on the main sequence and evolve to become red supergiants, eventually exploding as Type II supernovae. Stars with masses in the range $0.08 \lesssim M \lesssim 0.5M_{\odot}$ remain on the main sequence for a very long time and are never able to fuse helium even after the core ceases hydrogen fusion. More details about the early evolution of stars can be found for example in Schulz (2005).

For the purpose of the present work, I focus on low and intermediate mass stars. Low mass stars are those whose initial masses M_i lie within the range $0.5M_{\odot} \lesssim M_i \lesssim 2.3M_{\odot}$ and intermediate ones are those with initial masses within the range $2.3M_{\odot} \lesssim M_i \lesssim 8M_{\odot}$. These are the ones that evolve through the AGB phase, when they leave the main sequence.

As hydrogen fuses to helium in the core of a low or intermediate mass star, a helium-rich core develops and this is surrounded by layers where hydrogen fusion continues. After the end of the central hydrogen fusion, the star evolves quickly to become a red giant.

Following the exhaustion of the central hydrogen, the surface abundance of some chemical elements changes due to convective mixing, in a process known as first dredge-up (Iben, 1964). This results in, roughly, a doubling of the surface ^{14}N abundance, a reduction in surface ^{12}C abundance by about 30%, the formation of a surface $^{12}C/^{13}C$ ratio of about 20-30, a reduction in surface Li and Be by several orders of magnitude and small changes in the ^{16}O abundance (Iben & Renzini, 1983).

As a result of the fusion of hydrogen in the layers, the helium core grows and contracts under gravity resulting in increase in temperature and pressure in the core. Eventually, the temperature becomes high enough to ignite the

helium core. If the core is largely supported by electron degeneracy pressure, which is the case for low mass stars, the ignition of the helium core happens in an explosive manner known as the helium flash and this occurs at the tip of the red giant branch (TRGB).

The fusion of helium in the core results in the growing of a carbon/oxygen (C/O) core which gradually becomes denser. After the helium core is exhausted, the helium burning zone moves outward with an accompanying contraction of the C/O core and expansion of the envelope as well as an increase in stellar luminosity. At that time the star settles in the so-called early-AGB (E-AGB) phase. The E-AGB lifetime is defined as the time from the core helium exhaustion to the time of the first major helium shell flash (Vassiliadis & Wood, 1993).

1.2.2 TRGB of NGC 6822

In this section, I review some of the previous work which involved the determination of the luminosity of the TRGB of NGC 6822 and deduce the value which will be used in this work.

The I, J and K_S observations of NGC 6822 by Cioni & Habing (2005) found the TRGB to be at I=19.76 $\pm$ 0.01, J=18.32 $\pm$ 0.01, K_S=17.10 $\pm$ 0.01. The work of Sohn et al. (2008) found the TRGB of NGC 6822 to be at J=18.3, H=17.5, K=17.3. In the subsequent analysis, I assume the TRGB of NGC 6822 to be at K_S=17.20, which is the mean of the values found by Sohn et al. (2008) and Cioni & Habing (2005). In this work, low and intermediate mass objects brighter than K_S=17.20 are considered as AGB stars.

1.2.3 Characteristics and properties of AGB stars

An AGB star consists of a degenerate, very hot, dense C/O core surrounded by helium and hydrogen burning shells as well as a large and convective envelope. For a typical $1M_{\odot}$ star, the size of the stellar envelope is of the order of 1AU and the surface temperature is about 3000K. The low temperature in the outer layers results in the formation of molecules whose presence determines the spectral appearance of the stars.

During the E-AGB phase, while the hydrogen-burning shell is extinct, most of the energy comes from the burning of helium in the layers immediately around the C/O core. For more massive intermediate stars, $\sim$(4-8$M_{\odot}$), convective mixing takes place in the stellar envelope in a process known as second dredge-up (Kippenhahn et al., 1965). This mixes the products of the CNO cycle resulting in an increase in the surface abundances of ^{4}He and ^{14}N and a reduction of ^{12}C and ^{16}O (Iben & Renzini, 1983).

At some stage during the evolution of low or intermediate mass stars on the AGB, hydrogen is reignited in a thin shell, the star begins to thermally pulse and this marks the end of the E-AGB phase.

Thermal pulses, also called helium shell flashes, are one of the important characteristics of AGB stars. The dominant energy source for a thermal pulse is the triple alpha reaction which occurs in a region between the hydrogen-helium discontinuity and the C/O core (Iben & Renzini, 1983). The energy liberated during a thermal pulse goes into raising the local pressure, resulting in an expansion. Thermal pulses are believed to be the cause of period changes in some Mira variables (Wood & Zarro, 1981). AGB stars experiencing thermal pulses are known as thermally pulsing AGB (TP-AGB) stars.

Near the peak of a thermal pulse, the local conversion of nuclear energy into thermal energy results in the outward expansion of matter against gravity. Matter at the hydrogen-helium interface and beyond is propelled outwards to lower densities and temperatures. For stars of sufficiently large core mass (M_c=0.7$M_\odot$) and sufficiently large total mass ($M > 2M_\odot$), as the pulsation amplitude approaches the limiting strength, the base of the convective envelope extends into the region containing highly processed material (Iben & Renzini, 1983). This results in mixing ^{12}C and neutron-rich isotopes at the surface in a process called third dredge-up (Iben, 1975). As a result of the third dredge-up, there is an increase in ^{12}C (Vassiliadis & Wood, 1993) in the atmosphere. This suggests that if the third dredge-up is efficient enough, it can lead to the formation of a carbon star (Iben & Renzini, 1983). TP-AGB stars are referred to as carbon or oxygen stars depending on whether C/O >1 or C/O < 1, respectively.

It has been known for quite a while that in more massive intermediate AGB stars ($M_i \gtrsim 5M_\odot$), during the thermally pulsing phase, the convective envelope can reach high enough temperatures to initiate H-burning there. This process known as envelope-burning or hot bottom burning (Scalo et al., 1975) results in CN processing and a significant energy generation. Blöcker & Schönberner (1991) demonstrated that as a result of hot bottom burning (HBB), the concept of core-mass-luminosity relation (Paczyński, 1971) is no longer valid. Due to the HBB burning, there are changes in chemical composition within the envelope. ^{12}C is burnt to ^{14}N (Iben, 1975) turning a C star into a nitrogen-rich M star. HBB affects the transition from oxygen-rich to carbon-rich and may prevent the formation of massive carbon stars. However, in some models, a C star forms and HBB turns the star back from C-rich to M-type. The work of Sackmann & Boothroyd (1992) found that HBB leads to the formation of lithium at the surface of intermediate mass stars with initial masses 4-6$M_\odot$.

At some point during their late evolution on the AGB, the envelope of stars becomes pulsationally unstable with a characteristic time scale of the order of a hundred days. Late AGB stars are, therefore, pulsating stars. The pulsation deposits mechanical energy into the outer layers which are weakly bound by gravity, resulting in the stellar atmosphere being more extended. Consequently, the radiation pressure on dust particles in the weakly bound outer layers of the star will eventually force them to escape at a considerable rate in the form of a stellar wind, resulting in a significant mass loss from the star and a circumstellar envelope of escaping gas and dust particles.

During the evolution of low and intermediate mass stars, the AGB is a very important phase since at this stage stars lose a significant amount of their initial mass via the strong winds powered by the radiation pressure, and probably other mechanisms which are still poorly understood, on the outer layer dust particles which are very weakly bound by gravity. This high mass loss is accompanied by the formation of a circumstellar dust shell which obscures the central star such that in extreme cases the star is no longer visible in optical wavelengths, hence the necessity for AGB stars being observed in infrared wavelengths.

The mass loss from AGB stars has been the subject of a number of investigations by various authors and it turns out that the results differ from one investigation to another. Vassiliadis & Wood (1993) have proposed

$$\frac{dM}{dt} = \frac{L}{cv_{exp}} \tag{1.1}$$

as a reliable estimate of the mass-loss rate for AGB stars. In relation 1.1, L is the stellar luminosity, c is the speed of light, whereas v_{exp} denotes the stellar wind expansion velocity far from the central star.

As far as the estimate of the mass-loss rates for evolved low and intermediate mass stars is concerned, one may also be interested in having a look at the Reimers (1975) relation, for the slow mass-loss rates for red giants and E-AGB stars, and its modified form proposed by Baud & Habing (1983).

Despite their diversity, it turns out that all the estimated expressions for the mass-loss rates for evolved low and intermediate mass stars are functions of luminosity. This suggests the important role of radiation pressure in the mechanism driving the mass loss from the evolved low and intermediate mass stars.

Mass loss from AGB stars is an important source of enrichment of the interstellar medium and its strength determines the lifetimes of stars on the AGB and their populations.

Low and intermediate mass stars evolve on the AGB losing mass according to the relation 1.1. During that time, the mass of the core (M_c) increases whereas the mass of the envelope (M_e) decreases due to strong stellar winds. The stellar luminosity increases with time and when a critical luminosity is reached, M_e falls below a critical value, and at that time the envelope is ejected resulting in the so-called planetary nebula, marking the end of the AGB phase (see e.g. Iben & Renzini (1983) for more details). The remnant evolves towards the so-called white dwarf sequence, marking the end of evolution of a low or intermediate mass star. Provided $M_c \leq 1.4M_\odot$ (which is observed to be true for low and intermediate mass stars), the star during its white dwarf configuration is supported by electron degeneracy pressure. The critical mass $M_c = 1.4M_\odot$ is known as the Chandrasekhar limit.

1.3 AGB stars in NGC 6822

In this section, I review some of the previous results by some of the investigators of the AGB stellar population in NGC 6822.

Letarte et al. (2002) observed a $28^{'}$ x $42^{'}$ area of NGC 6822. From the CN-TiO vs R-I diagram of NGC 6822, they identified 904 C stars and estimated the number of M stars to be 941 ± 184. They found a C/M=1.0 ± 0.2.

Investigation of AGB stars in NGC 6822 was also carried out by Kang et al. (2006). These workers observed the central bar of NGC 6822, covering a total area of $3.^{'}6$ x $6.^{'}3$ and obtained JHK and gi images. From the near-infrared colour-colour diagram, they identified 141 C stars and 522 M stars. They found a C/M=0.27 ± 0.03.

Cioni & Habing (2005) detected a larger number of AGB stars in NGC 6822. They observed NGC 6822 in the IJK$_S$ bands, covering the $20^{'}$x $20^{'}$ central area. From the (I-J, I) and (J-K$_S$, K$_S$) colour-magnitude diagrams, they detected 2661 AGB stars, including 500 C-rich and 2161 O-rich stars. They found C/M=0.23, from which they derived a spread in metallicity of 1.56dex. However, the C/M ratio depends on how M stars are defined, which may account for some of the differences between various estimates.

Cioni & Habing (2005) found further that the average AGB star in NGC 6822 would have $M_{bol} = -4.3$. On the assumption that at least a few of the AGB stars in their sample with $M_{bol} = -4.3$ are Miras and pulsate with P ≈250 d and by using the theoretical models by Vassiliadis & Wood (1993), they roughly estimated the initial mass of an average AGB star in their sample to be about $1.5M_{\odot}$ with an age of about 2 Gyr.

These previous determinations suggest that NGC 6822 has a large population of AGB stars.

1.4 Long-period AGB variables and aim of the project

Many AGB stars brighter than the TRGB pulsate with long periods of the order of hundreds of days and amplitudes of up to a few magnitudes in the optical and somewhat less in the near-infrared bands. Some of them are multi-periodic objects. Based on the period, amplitude and regularity of the variation of their flux, we distinguish among AGB variables (Kukarkin, 1985):

1. Miras: These are located at the tip of the AGB, easily identified by their late spectral types (Me, Ce, Se, or very rarely Ke). Most of them have light-curves characterised by regular variations with well defined single periods (P) within the range $80 \lesssim P \lesssim 1000$ d and large amplitudes ($\triangle V \geq 2.5$ in V-band or $\triangle K \geq 0.4$ in K-band (Whitelock et al., 2008)).

2. Semiregulars of type "a" (SRa): These are characterised by a relatively regular variation with a smaller amplitude ($\triangle V < 2.5$ in V-band or $\triangle K < 0.4$ in K-band).

3. Semiregulars of type "b" (SRb): These are characterised by a poor regularity in their variation with a small amplitude ($\triangle V < 2.5$ in V-band or $\triangle K < 0.4$ in K-band).

Semiregulars have pulsation periods in the range $20 \lesssim P \lesssim 2000$ d.

4. Irregulars: These are AGB variables characterised by irregular variations of low amplitudes.

Most long-period variables (LPVs) are TP-AGB stars experiencing thermal pulses which result in highly extended stellar atmospheres and losing mass at an average rate of 10^{-6} $M_{\odot}$ yr^{-1} or more (e.g. Cioni et al. (2003)). The pulsation, believed to be one of the driving mechanisms of stellar winds, is an important element as far as the study of the mass-loss rate for AGB stars is concerned.

Mira variables are very bright objects at infrared wavelengths so that they can be seen to large distances and through heavy interstellar absorption. It is believed that most SRs are in the pre-Mira stage, but it is also possible that Miras go through a SR stage during the low luminosity part of the He-shell flash cycles.

Miras are known to follow a well-defined period-luminosity (PL) relation. Using 11 Miras which they discovered in the Large Magellanic Cloud (LMC), Glass & Lloyd Evans (1981) obtained infrared photometry for them and discussed the existence of a relationship between periods and bolometric magnitudes with a scatter of σ=0.22 mag. Using the same data, such relationships in J, H, and K bands were derived by Glass & Feast (1982). By combining data from Glass & Feast (1982) and Wood et al. (1985), Feast (1984) refined the latter relations and found that carbon- and oxygen-rich Miras follow the same PL relations at K. The work of Menzies & Whitelock (1985) which involved the study of Miras in Galactic globular clusters supported the existence of a PL relation for Miras. Feast et al. (1989) derived the PL relation for 29 O-rich and 20 C-rich Miras in the LMC and found that the PL relations for O- and C-Miras are very similar at K. Wood et al. (1999) detected more than one PL relation in the LMC long-period AGB variables, which fall on approximately parallel series. In these series, Miras lie on a single PL relation. Each PL relation is probably associated with a different mode of pulsation. It has been found that (e.g. Wood et al. (1999)) Miras pulsate in the radial fundamental mode whereas SRs can pulsate in

the first, second, third overtone or the fundamental.

The K PL relation for Miras has been proved to be more practical than the ones at J and H when Miras are to be used as distance indicators, since it is narrower for both O-and C-Miras and in addition to that, K is less sensitive to interstellar reddening than J and H (Feast et al., 1989). Also the K amplitude is lower, so the K PL is more useful on occassions when there is no full coverage of the light curve. Therefore, in most discussions of this work, the K band will be used rather than J and H.

Several investigations for Miras, e.g. Rejkuba (2004), suggest that the slope of the PL relation for these stars is universal. The existence of a PL relation in Miras makes them very useful as distance indicators, independent of other common methods such as the TRGB, RR Lyraes and Cepheids. Miras are known to be losing mass at high rates and therefore contribute significantly to the material entering the interstellar medium. Their circumstellar dust shell formation makes these stars no longer visible in optical wavelengths and it is therefore necessary to observe them at infrared wavelengths. The mass loss from the late stages of stellar evolution has been the subject of a number of investigations, but is still poorly understood. Most of the investigations for Miras have, so far, concentrated on the Galactic and Magellanic Clouds cases. It is very important to identify and characterise these large amplitude variables in more distant extragalactic systems, due to their importance as distance indicators. This project aims at identifying and characterising the large amplitude AGB variables in NGC 6822, with emphasis on Mira variables. Most importantly, the predicted universality for the Mira PL relation will be investigated by comparing the PL relation for Miras in NGC 6822 to the one for Miras in the LMC.

The work is organised as follows. In Chapter 2, the near-infrared observations of NGC 6822 are discussed. Photometry and data are discussed in this Chapter. The selection of a sample of large amplitude variables which

will be used in the subsequent analysis is also discussed in Chapter 2. In Chapter 3, the data are analysed and the results presented. Analysis of the light curves, periods and amplitudes of variability is an important tool in the identification and characterisation of the large amplitude periodic AGB variables. The colour-magnitude and two-colour diagrams of the sources detected in NGC 6822, with emphasis on large amplitude AGB variables are presented and discussed. A PL relation for Miras in NGC 6822, in K band and bolometric magnitudes is presented and compared to the one for Miras in the LMC. The distance to NGC 6822 is deduced from the bolometric PL relation. In Chapter 4, the results are discussed and the recommendations for future work presented, while Chapter 5 concludes.

Chapter 2

Near-infrared observations of NGC 6822

2.1 Observations of NGC 6822, data reduction and photometric measurements

Observations of NGC 6822, data reduction and photometry were entirely done by the supervisors of my MSc dissertation. However, in August 2009 (one month after the beginning of the research part of my MSc), I was given the opportunity of observing NGC 6822. This was for me not only to get experience in observing, but also to get some idea of how the data which I was going to analyse had been obtained. In addition to observing NGC 6822, I was initiated by the supervisors of my MSc project into how the data reduction and photometry had been done and below I describe the whole process which led to the data that I analysed as part of my MSc dissertation.

The galaxy was observed using the InfraRed Survey Facility (IRSF) telescope and the SIRIUS (Simultaneous 3-colour InfraRed Imager for Unbiased Survey) camera.

The IRSF is a 1.4m telescope mounted in an altitude-azimuth configuration. It is located at Sutherland ($20°49'$ E, $32°23'$ S, and 1798 metres in altitude), a place about 370 km north-east of Cape Town, in South Africa. The telescope was constructed by Nagoya University (in Japan), and is maintained in collaboration with the South African Astronomical Observatory (SAAO).

The SIRIUS camera, whose details can be found in Nagashima et al. (1999) and Nagayama et al. (2003), is a near-infrared camera which produces simultaneous J, H and K_S images covering an area of about $7.2'$x $7.2'$, after dithering, with a scale of 0.45 arcsec pixel^{-1}. A 1x3 grid was used in order to cover most of NGC 6822. Region 1 covered the central part and most of the galaxy, region 2 covered the northern part whereas region 3 covered the southern part of NGC 6822. The total area observed was $7.5'$x $21.1'$, with slight overlaps between adjacent fields.

Since the purpose was to detect the long-period variables, observations were intended to be made at 19 epochs, spread over 4 years, but poor weather and other contraints meant that only 16 observations were obtained in the south field (region 3). Depending on the seeing and brightness of the sky in the K_S band, typical exposures were of either 20 or 30s, for each image. In each field, 10 dithered images were combined and median averaged, after flat-fielding, dark and sky subtraction, using the reduction package written by Dr. Taka Nagayama from Kyoto, Japan, to produce an image for measurement.

Photometry was performed using DoPHOT (Schechter et al., 1993) in 'fixed-position' mode, using the best-seeing H-band images for each field as templates. Aladin (Bonnarel et al., 2000) was used to correct the coordinate system on each template, and RA and Dec. were determined for each measured star. Cross-correlation of IRSF images with the ones of the Two-Micron All Sky Survey (2MASS) catalogue (Cutri et al., 2003) was made

and photometric zero-points were determined by comparing IRSF photometry with that from 2MASS. In each field, stars in common with the 2MASS catalogue with photometric quality A in each colour were identified and the magnitudes were adjusted to match those from 2MASS. The number of common stars is at least 84, 75 and 71 in regions 1, 2 and 3, respectively. The standard deviations of the differences between IRSF and 2MASS measurements are 0.053mag in J, 0.061mag in H, 0.074 in K_S in region 1 and 0.044mag in J, 0.048 in H, 0.084 in K_S in region 2 as well as 0.035 in J, 0.032 in H and 0.051 in K_S in region 3.

2.2 Data processing and selection of variables

2.2.1 Data processing

The structure of the data which have been analysed in this work is illustrated in Tables 2.1, 2.2 and 2.3.

Table 2.1 illustrates, respectively, the coordinates (right ascension and declination) in degrees, identification name, arithmetic mean J, H and K_S magnitudes and the associated standard deviations (σ_J, σ_H and σ_K), the quality of observations (Q) and the number of observations in K band (NK), for each object detected in NGC 6822. Table 2.1 is a part of the full Table available at the SAAO and which contains 7076 objects with more columns than the ones illustrated here. The columns which are not illustrated here consist of the number of observations in J and H bands as well as J-H, H-K_S and J-K_S colours. The quality of observation (Q) indicates how good the observation was in J, H and K band. Q=11 means a good quality observation, Q=17 means a fair quality observation while Q= anything other than 11 or 17 means a poor quality observation. In column 10 of Table 2.1, a number such as 111117 means that the quality of observation was good at J and H, but fair at K. Objects with identification names starting with 1, 2

and 3 were observed in regions 1, 2 and 3, respectively. Those with names starting with 4 were observed in the overlap regions.

Table 2.1: Data obtained from observations of NGC 6822 using IRSF

RA (2000)	Dec (2000)	Name	J	σ_J	H	σ_H	K	σ_K	Q	NK
296.21515	-14.82656	11954	18.00	0.07	17.35	0.10	17.10	0.14	111117	19
296.21530	-14.97481	30079	15.64	0.04	14.91	0.04	14.74	0.06	111111	19
296.21533	-14.65763	21908	18.61	0.13	17.90	0.13	17.67	0.25	111117	19
296.21533	-14.78275	11249	17.70	0.06	16.82	0.06	16.52	0.08	111111	19
296.21533	-14.74448	20811	18.62	0.16	17.78	0.23	17.46	0.18	111117	19
296.21536	-14.78379	11234	17.83	0.14	16.77	0.12	16.09	0.11	111111	19
296.21539	-14.86183	11637	18.15	0.12	17.24	0.12	17.04	0.28	111117	19
296.21545	-14.91717	31565	18.41	0.08	17.77	0.12	17.73	0.20	111717	19
296.21545	-14.77108	12642	18.09	0.12	17.14	0.06	16.77	0.09	111111	18
296.21545	-14.77491	13948	18.72	0.18	17.94	0.19	17.82	0.30	171717	18
296.21555	-14.85932	11650	18.08	0.09	17.18	0.05	16.92	0.10	111111	18
296.21558	-14.94851	31445	18.62	0.13	17.96	0.08	17.62	0.13	171117	18
296.25256	-14.74493	21461	18.75	0.10	17.87	0.11	17.62	0.17	171117	18
296.25256	-14.82794	13318	18.79	0.15	18.06	0.10	17.94	0.24	171717	18
296.25256	-14.89009	31039	18.12	0.08	17.49	0.06	17.15	0.15	111117	17
296.25256	-14.77367	12622	18.73	0.12	17.75	0.13	17.49	0.20	171117	17
296.25256	-14.84586	13132	18.90	0.15	18.12	0.20	17.89	0.35	171717	17
296.25256	-14.86109	10629	17.60	0.11	16.52	0.06	15.96	0.08	111111	17
296.29581	-14.87388	30594	17.04	0.03	16.40	0.04	16.15	0.04	111111	17
296.29581	-14.88382	30563	17.32	0.04	16.40	0.04	16.17	0.06	111111	17
296.29584	-14.95035	30794	18.03	0.04	17.37	0.06	17.12	0.11	111117	17
296.29584	-14.78528	10082	15.11	0.02	14.62	0.01	14.51	0.02	111111	17
296.29590	-14.83469	10784	17.45	0.03	16.53	0.04	16.21	0.09	111111	17
296.29590	-14.79961	11080	17.35	0.04	16.60	0.04	16.41	0.08	111111	17
296.29593	-14.72771	20964	18.42	0.13	17.58	0.06	17.44	0.17	111117	17
296.29596	-14.73905	20867	18.72	0.14	17.83	0.11	17.56	0.24	171717	16

Figure 2.1 shows the histogram of the number of sources detected in NGC 6822 as a function of J, H and K_S magnitudes. It can be noted from the histogram that most of the sources were detected at $\sim$ 18 mag. The peak of the sources detected at J is at $\sim$ 18.76 mag with $\sim$ 2041 objects detected, at H and K_S the peak is at $\sim$ 17.74 mag with $\sim$ 2334 and $\sim$ 2111 objects detected, respectively. At H and K_S, the limiting magnitude is at $\sim$ 18.5 mag, while it is at $\sim$ 19.5 mag at J.

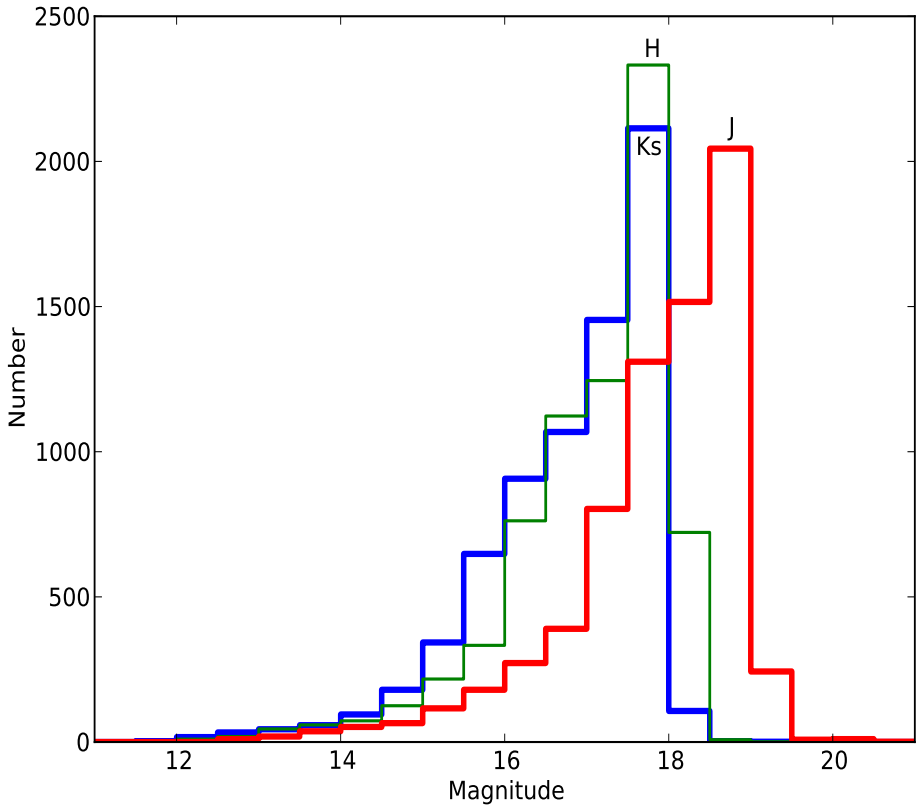

Figure 2.1: Histogram of the number of sources detected in NGC 6822 as a function of J, H and K_S magnitudes.

As a result of the slight overlaps between adjacent fields, some objects were observed twice. During the first data processing phase, my task was to identify the duplicates in the overlap regions. I identified 647 duplicates from a sample of 7076 objects observed in NGC 6822. The duplicates' measurements were dealt with by finding the weighted mean of the arithmetic mean J, H and K_S magnitudes and the associated standard deviations, using the formulae:

$$\bar{x} = \frac{\sum_{i=1}^{n} \frac{x_i}{\sigma_i^2}}{\sum_{i=1}^{n} \frac{1}{\sigma_i^2}} \tag{2.1}$$

$$\sigma_{\bar{x}}^2 = \frac{1}{\sum_{i=1}^{n} \frac{1}{\sigma_i^2}} \tag{2.2}$$

where x_i, σ_i represent the arithmetic mean J, H, and K_S magnitudes and the associated standard deviations, respectively. The coordinates (right ascension and declination) of the duplicates were arithmetically averaged.

Table 2.2 illustrates the structure of the data for a typical example of an object observed in NGC 6822, in K band. Similar data in J and H bands are available at the SAAO. In each band, column 1 shows the number of observations, column 2 illustrates the photometric measurement corresponding to each observation, column 3 shows the error on the photometric measurement for each observation, column 4 illustrates the time in Julian day, column 6 shows the sky background, column 8 illustrates the exposure time and the content of other columns are clearly explained in the Tables. The data for all the individual objects detected in NGC 6822 are available at the SAAO and consist of more columns than the ones shown in Table 2.2. Here I only use the data for one individual object to explain the structure of the data which have been analysed and show the columns which are more useful for this work.

The second phase of processing consisted of putting together the data

obtained in J, H and K bands after selecting the information relevant to this work. The content of a typical resulting data file is illustrated in Table 2.3 though some useful columns are not shown for clarity reasons, but those are already shown in Table 2.2. The second phase of data processing applied only to 236 objects of interest that I selected as explained in the next section.

Table 2.2: K data for the star 12208

No	K	eK	JD	Seeing	Sky	Quality	Exposure
1	15.257	0.024	2353.49644	1.138	6354	11	20
2	15.816	0.037	2436.50394	1.617	6389	11	30
3	15.768	0.050	2440.50422	1.523	5865	11	30
4	15.734	0.057	2441.50423	1.448	4766	17	20
5	15.752	0.035	2442.44586	1.359	3595	11	20
6	15.868	0.028	2507.29760	1.039	4318	11	20
7	15.956	0.054	2808.46756	2.785	3096	17	20
8	15.985	0.029	2809.38435	1.267	6829	11	30
9	15.866	0.026	2529.28608	1.014	3065	11	20
10	15.433	0.019	2882.34804	1.465	7519	11	30
11	15.729	0.027	3093.62506	1.260	6821	11	30
12	15.146	0.018	3173.44424	1.062	6189	11	30
13	15.419	0.017	3243.35845	1.173	4261	11	30
14	15.558	0.019	3259.26118	1.045	6206	11	30
15	15.545	0.019	3260.26279	1.010	7148	11	30
16	15.853	0.028	3293.28920	1.021	9619	11	30
17	15.642	0.018	3531.55302	1.177	3578	11	30
18	15.678	0.024	3533.40996	1.296	5010	11	30
19	16.057	0.024	3612.30425	0.979	7250	11	30

Table 2.3: JHK data for the star 12208

JD	J	H	K	eJ	eH	eK
2353.49644	17.266	16.067	15.257	0.037	0.023	0.024
2436.50394	18.218	16.830	15.816	0.098	0.054	0.037
2440.50422	18.157	16.772	15.768	0.111	0.071	0.050
2441.50423	18.121	17.028	15.734	0.101	0.075	0.057
2442.44586	18.074	16.760	15.752	0.082	0.043	0.035
2507.29760	18.411	16.867	15.868	0.082	0.039	0.028
2808.46756	18.467	17.051	15.956	0.175	0.085	0.054
2809.38435	18.474	17.009	15.985	0.090	0.048	0.029
2529.28608	18.045	16.873	15.866	0.056	0.043	0.026
2882.34804	17.390	16.261	15.433	0.028	0.020	0.019
3093.62506	18.082	16.779	15.729	0.068	0.039	0.027
3173.44424	17.019	15.963	15.146	0.024	0.017	0.018
3243.35845	17.665	16.446	15.419	0.039	0.025	0.017
3259.26118	17.905	16.611	15.558	0.046	0.029	0.019
3260.26279	17.902	16.588	15.545	0.050	0.025	0.019
3293.28920	18.380	17.067	15.853	0.076	0.039	0.028
3531.55302	18.152	16.824	15.642	0.068	0.034	0.018
3533.40996	18.111	16.733	15.678	0.063	0.032	0.024
3612.30425	18.613	17.267	16.057	0.090	0.043	0.024

2.2.2 Selection of large amplitude variables

In this section, I discuss how I selected a sample of candidate large amplitude variables from the 7076 objects detected in NGC 6822.

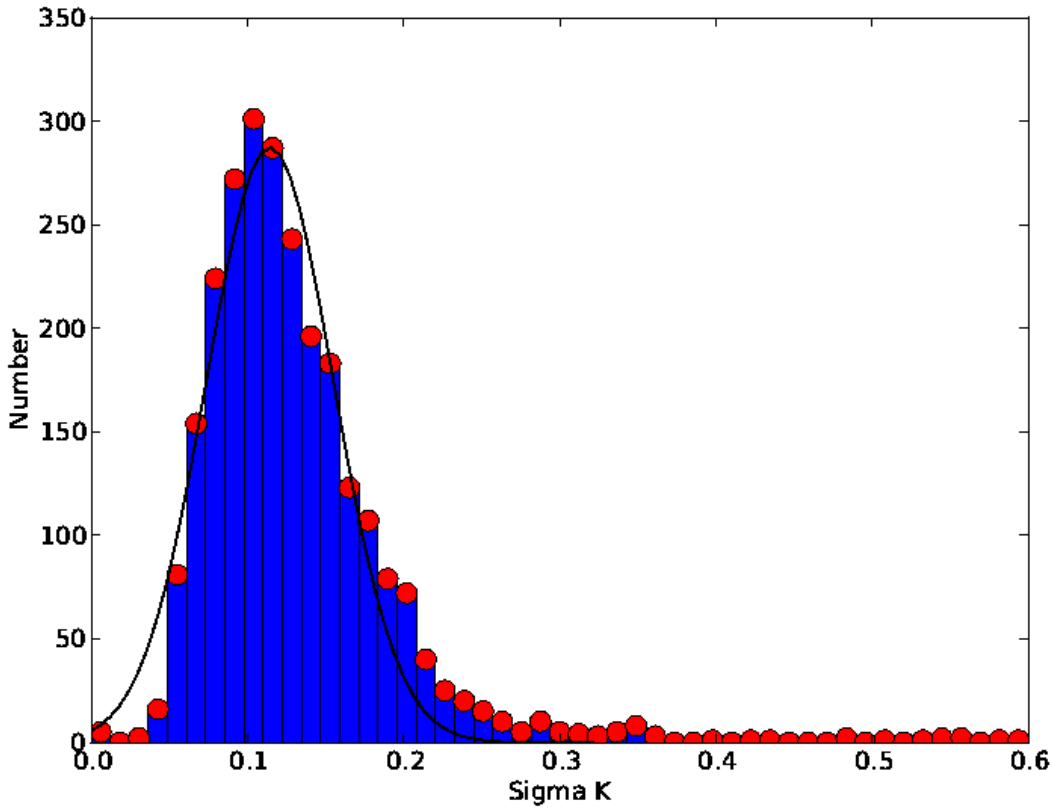

Figure 2.2: Histogram of number of objects with $16.5 \leq \mathrm{K} < 17.4$ as a function of standard deviations of K magnitudes (σ_K) in that bin. A Gaussian curve is fitted and from the Gaussian fit, the mean (μ_{σ_K}) and standard deviation (σ_{σ_K}) of the standard deviations of K magnitudes are obtained.

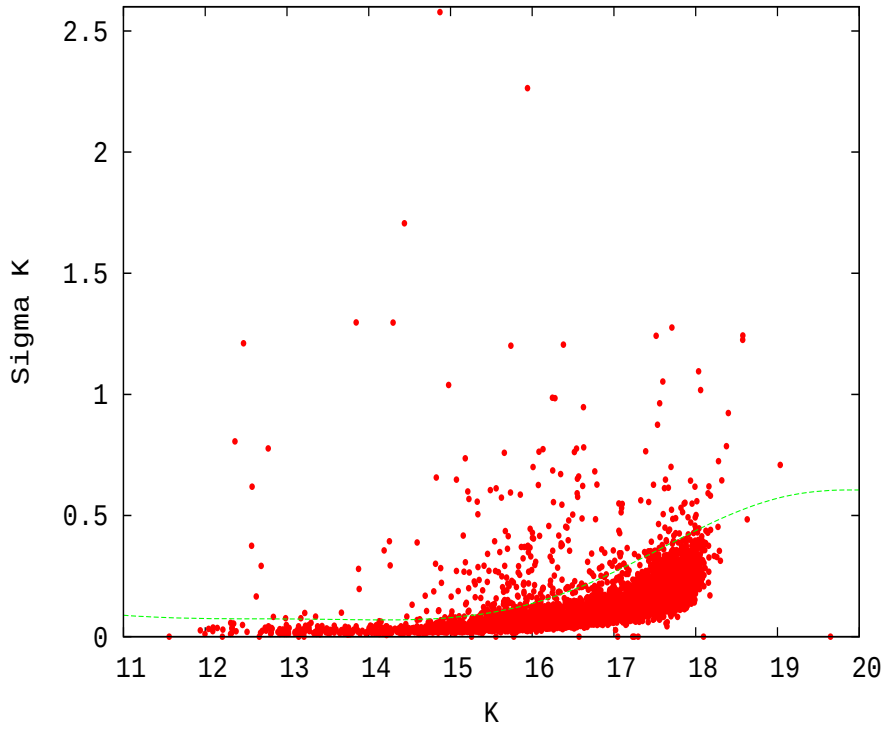

Figure 2.3: The K standard deviations (σ_K) as a function of K magnitudes of all sources detected in NGC 6822. The line is given by equation 2.3 and all the objects above it are selected as candidate large amplitude variables.

It is easy to understand that the standard deviations of the set of photometric measurements are expected to be larger for large amplitude variables than for small amplitude or non-variables. This motivated me to search for those objects whose standard deviations at K are large. To do this, data in columns 8 and 9 of Table 2.1 (full version of it) were used.

Considering K magnitudes of all 7076 objects, I defined different bins starting from 11 mag and ending at 18 mag and then selected the standard deviations corresponding to the K magnitudes in each bin. It is reasonable to think of a value greater than the mean standard deviation as a standard deviation of the photometric measurement of a large amplitude variable object. In each bin of standard deviations, I defined a value "$\mu_{\sigma_K} + 3\sigma_{\sigma_K}$" where μ_{σ_K} is the mean K standard deviation and σ_{σ_K} is the standard deviation of the K standard deviations. The reason for using three standard deviations here will soon be clear. I found μ_{σ_K} and σ_{σ_K} as follows:

In each K bin, I plotted a histogram of the number of objects as a function of standard deviation. Realizing that the standard deviations in each bin were approximately Gaussian distributed, a Gaussian curve was fitted and from that fit the mean (μ_{σ_K}) and standard deviation (σ_{σ_K}) of the K standard deviations were obtained, resulting in a number of μ_{σ_K} and σ_{σ_K} values. One example of such a histogram is illustrated in Figure 2.2. The purpose of this was to establish (x, y) points which can be used to find the coefficients of a polynomial, as illustrated in Figure 2.3. The values of y were given by $\mu_{\sigma_K}+3\sigma_{\sigma_K}$ while those of x were given by the first K magnitude of each bin of K magnitudes. The properties of a Gaussian distribution predict that most of the data under consideration fall within three standard deviations of the mean. By using $\mu_{\sigma_K}+3\sigma_{\sigma_K}$ as the value of y, I am aiming at the objects whose the K standard deviations are large compared to the mean standard deviation. I note that it would have been better to use as x value the mean K magnitude of each bin instead of the first K magnitude

of the bin, although it does not affect the selection of the large amplitude variables. The selection of large amplitude variables is mainly decided by $\mu_{\sigma_K}+3\sigma_{\sigma_K}$ rather than K mag, whichever K mag is considered within the bin. Then I used the least squares fit to the (K, $\mu_{\sigma_K}+3\sigma_{\sigma_K}$) points obtained as described above to find the coefficients of the polynomial illustrated in Figure 2.3. A smooth and reasonable fit was obtained at 7th order and the resulting polynomial is given by

$$f(x) = -837.55+422.03x-90.12x^2+10.57x^3-0.73x^4+0.03x^5-0.0007x^6+6.55E-06x^7. \quad (2.3)$$

Selecting those objects falling above the line represented by the above polynomial and considering only those which were observed at least 10 times, I obtained a sample of 236 candidate large amplitude variables. 10 observations is the minimum required to derive a reliable period from data of this type. The sample of the variables selected as discussed above will be used to identify the probable large amplitude AGB variables (see section 3.1 and Appendix A).

Objects with fewer than 10 observations, but which are likely to be large amplitude AGB variables, given their colours (J-$K_S \geq 2$), are listed in Appendix B. Sources with J-$K_S \geq 2$ which have been observed more than 10 times, but which have not been selected as candidate large amplitude variables are listed in Appendix C. It would be interesting to investigate the cause of the very red colours of these objects. Note that in Appendix A, B and C the coordinates (right ascension and declination) are in degrees.

Chapter 3

Data analysis and results

3.1 Identification and characterisation of large amplitude AGB variables in NGC 6822

The large amplitude variables selected as discussed in section 2.2.2 are expected to involve the AGB and non-AGB sources and the former constitute my main interest in the present analysis. Among AGB stars, there are those which are brighter or fainter than the TRGB. In this work, I adopted K_S=17.2 (see section 1.2.2) as the TRGB of NGC 6822. I focus on those brighter than the TRGB not only due to the fact that I have no systematic way of identifying those fainter than the TRGB but also because the large amplitude AGB stars which I am interested in are mostly, if not all, brighter than the TRGB. Futhermore, the large amplitude AGB stars are expected to involve Miras and non-Miras. In this section, I describe how I identified the most probable large amplitude AGB objects in NGC 6822 among which Miras and SRs will be my main interest in the subsequent discussion, due to their importance as discussed in section 1.4.

The objects brighter than K_S=17.2 include not only the AGB variables, but also the supergiants and foreground objects which are expected to make a non-negligible contribution due to NGC 6822 being located at a low Galactic latitude. I consider as AGB variables the objects brighter than K_S=17.2, but fainter than $K_S = -3.12(J - K_S) + 19.49$. The slanted line given by

$K_S = -3.12(J - K_S) + 19.49$, estimated by comparing our data with the AGB stars previously identified in NGC 6822 by Kang et al. (2006), see Figure 3.1 for illustration, excludes most of the supergiants and foreground sources.

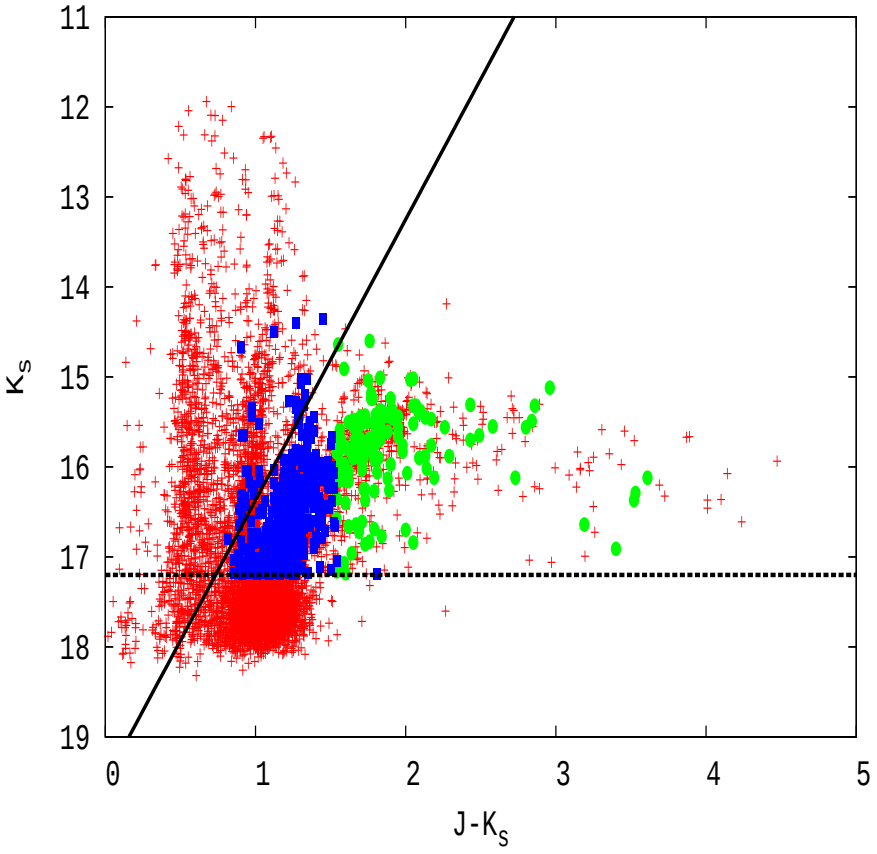

Figure 3.1: Comparison of our data and the AGB stars identified in NGC 6822 by Kang et al. (2006), using a colour-magnitude diagram. Filled ellipses and rectangles represent, respectively, the 141 carbon and 522 M stars identified by Kang et al. (2006) whereas crosses represent objects in our data. The estimated slanted line is given by $K_S = -3.12(J - K_S) + 19.49$ whereas the horizontal line represents the TRGB in K band and is given by K_S=17.2mag.

Applying the above conditions to the sample of 236 candidate large amplitude variables selected in section 2.2.2, I obtained a smaller sample of 162

objects, which will mostly be made up of large amplitude AGB variables, and these are listed in Appendix A. This sample of large amplitude AGB variables is going to be examined so as to identify Miras and SRs. Selecting the large amplitude AGB variables in this way might result in some of them being left out, but it is less likely that there are any Miras left out due to their high mass-loss rates and therefore their very red colours.

Miras are mostly characterised by a relatively regular pulsation such that they can be identified by a visual inspection of their light curves although more inputs are needed for one to be sure of the Mira nature of a given star. In this work, the identification of Miras and SRs was done by analysing the light curves and periodograms of the stars of interest. To do this, I wrote a python program which outputs the magnitudes versus time plots in J, H and K_S bands for all 162 variables. By visual inspection of each of the light curves, I could estimate which variable is likely to be a Mira or SR depending on the regularity of the light curves. Two examples of those light curves are illustrated in Figures 3.2 and 3.3. Clearly, from these Figures one can see that the stars in question are large amplitude and long-period variables whose pulsation periods and amplitudes can be estimated.

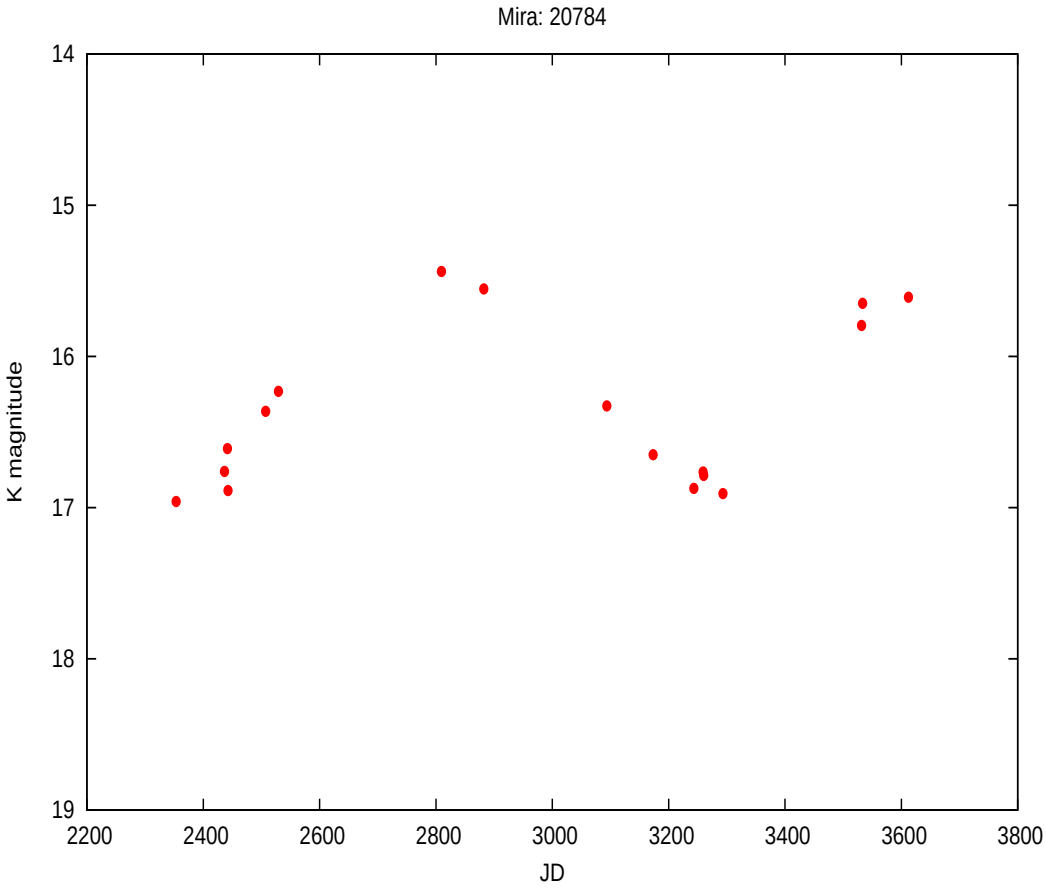

Figure 3.2: K Light curve of Mira 20784.

However, C-Miras undergo changes in mass-loss rate that sometimes can lead to erratic light curves (Whitelock et al., 2006). Such C-Miras might have been left out, in this analysis.

For those variables whose light curves show more or less regular variation, I used a Fourier type periodogram analysis to determine their periods and amplitudes of pulsation in the J, H and K_S bands and this was done by running a Fourier fitting program named "star" kindly made available by Dr. Luis Balona, one of the SAAO staff. Using the conditions on the periods and amplitudes of pulsation discussed in section 1.4 for Miras and SRs, I obtained 30 Miras and 9 SRs and these are listed in Table 3.1 which presents

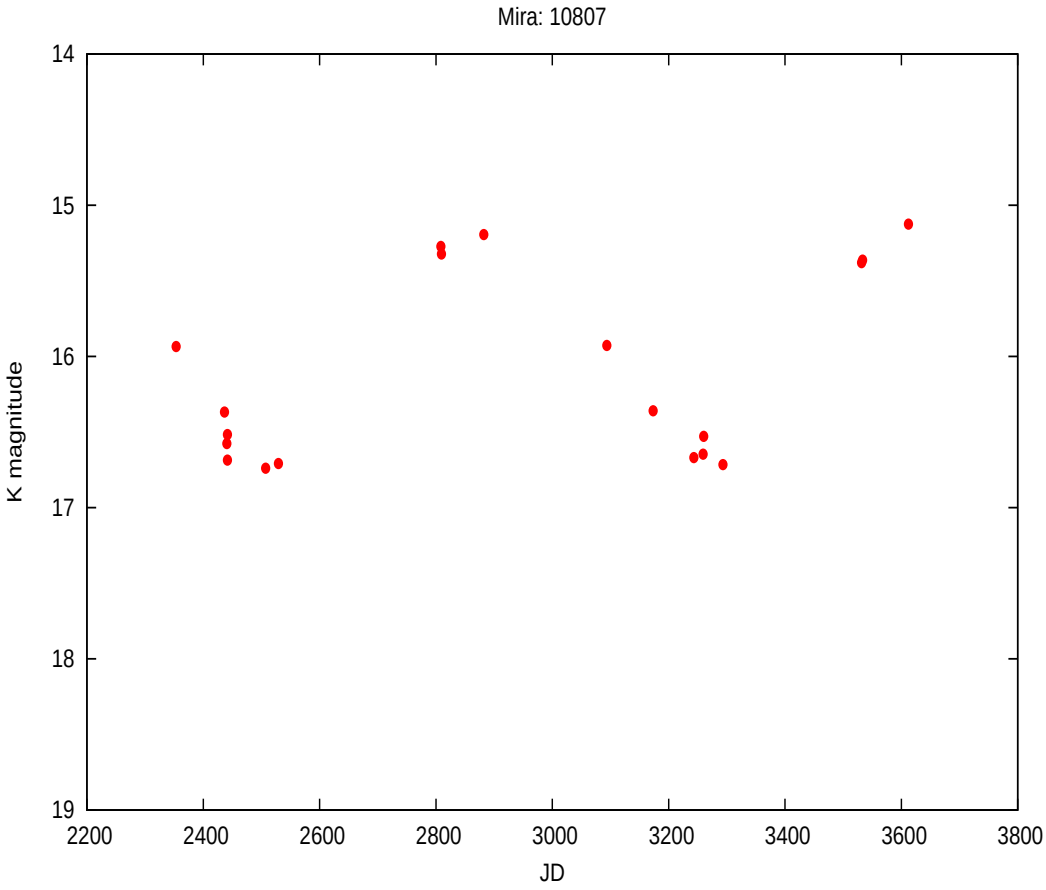

Figure 3.3: K Light curve of Mira 10807.

their identification names, equatorial coordinates in degrees, classification into Miras and SRs as well as the quality (Q) of their phased K light curves (1=very good, 2=good, 3=fair, 4=uncertain).

Table 3.1: List of Mira (M) and semiregular (SR) variables identified in NGC 6822 and their positions

Name	α(2000)	δ(2000)	Type	Q_{KLC}
12208	19:44:41.5	-14:48:24	M	1
11032	19:44:41.9	-14:48:16	M	1
11059	19:44:41.9	-14:48:05	M	1
11296	19:44:42.0	-14:46:35	M	1
11299	19:44:42.4	-14:46:35	M	1
12147	19:44:43.3	-14:48:39	M	1
20417	19:44:46.7	-14:44:25	M	1
20439	19:44:47.2	-14:44:05	M	1
20784	19:44:47.4	-14:44:49	M	1
11140	19:44:48.8	-14:47:36	M	1
11174	19:44:50.4	-14:47:22	M	2
12400	19:44:51.0	-14:47:38	M	2
10807	19:44:51.9	-14:49:55	M	1
13364	19:44:51.9	-14:49:22	M	2
20569	19:44:52.1	-14:41:52	M	1
13106	19:44:52.2	-14:50:58	M	3
12466	19:44:54.3	-14:47:19	M	2
30920	19:44:54.9	-14:54:42	M	4
12751	19:44:56.0	-14:45:35	M	1
20542	19:44:56.7	-14:42:37	M	3
10817	19:44:57.3	-14:49:50	M	2
11226	19:44:57.7	-14:47:05	M	1
12445	19:44:58.1	-14:47:26	M	1
13293	19:44:58.9	-14:49:50	M	1
12177	19:44:59.1	-14:48:32	M	1
21419	19:45:00.5	-14:44:57	M	1
20356	19:45:01.6	-14:45:04	M	3
21671	19:45:01.7	-14:43:13	M	2
21234	19:45:03.7	-14:40:26	M	1
31168	19:45:04.0	-14:52:13	M	1
11389	19:45:06.1	-14:45:48	SR	3
10935	19:45:07.4	-14:49:00	SR	2
11372	19:45:07.5	-14:46:03	SR	1
11794	19:45:08.2	-14:50:34	SR	3
10412	19:45:09.3	-14:48:10	SR	2
10439	19:45:09.8	-14:47:38	SR	2
10635	19:45:11.0	-14:51:35	SR	3
10876	19:45:11.2	-14:49:21	SR	2
20539	19:45:11.5	-14:42:41	SR	3

Table 3.2 presents the characteristic parameters for Miras and SRs that I identified in NGC 6822. Peak-to-peak amplitudes $\triangle$J, $\triangle$H, $\triangle$K in the J, H, and K_S bands, as well as the pulsation periods are presented. The mean J, H, and K_S magnitudes for Miras and SRs are also given and were found from first order Fourier fitted sine curves to the J, H and K_S light curves. In cases where the J magnitude is uncertain, due to the poor quality of the J data, the estimated J value is quoted as "J:". Such cases are those where a significant number of points have measurement errors greater than 0.2 mag. Infrared colours, for Miras and SRs, which will be discussed in detail in section 3.3 were deduced from J, H and K_S magnitudes given in Table 3.2. The bolometric apparent magnitudes are also presented in Table 3.2, but the way they were obtained will be discussed in detail in section 3.5. Examination of the results in Table 3.2 shows that the pulsation amplitudes generally decrease with increasing wavelength, except for a few cases where $\triangle$J $<$ $\triangle$ H, resulting in the ratio $\triangle$K/$\triangle$J being always less than 1.

The errors on the periods were estimated by looking at the appearance of the phased light curves when the period is varied from its mean value. Different values of the periods around the mean one were assumed until the phased light curve loses the general appearance. Then the error on the period was taken to be the difference between the extreme value (i.e its value when the phased light curve loses its general appearance) and the mean one.

The phased K light curves for Miras are given in Appendix D whereas those for SRs are given in Appendix E. As can be seen, the phased K light curve for the star 30920 suggests an odd variability. The reasons for this are not clear to me and further investigation of this star is needed.

Figure 3.4 illustrates the histogram of the number of Miras as a function of their pulsation periods. Clearly, most of the Miras have periods in the range 200 to 500 d. There are four Miras with periods greater than 500 d extending to 900 d, close to the longest period known for Galactic carbon

Table 3.2: Characteristic parameters of Miras and SRs in NGC 6822

Name	P	J	H	K	m_{bol}	$\triangle J$	$\triangle H$	$\triangle K$
12208	278 ± 10	17.87	16.61	15.62	19.02	1.36	1.08	0.76
11032	239 ± 16	18.20	16.91	15.94	19.35	1.20	0.92	0.65
11059	319 ± 20	18.37	16.90	15.79	19.11	1.20	1.01	0.75
11296	340 ± 15	18.37	16.99	15.78	19.06	1.03	0.90	0.65
11299	494 ± 15	19.06	17.30	15.73	18.57	2.16	2.07	1.67
12147	475 ± 20	19.93:	17.89	16.24	18.88	1.61	1.59	1.26
20417	432 ± 15	18.41	16.87	15.51	18.63	1.25	0.91	0.74
20439	430 ± 20	19.14	17.31	15.77	18.62	1.05	0.94	0.85
20784	897 ± 80	20.40:	18.08	16.11	18.17	1.76	1.77	1.45
11140	405 ± 15	18.74	17.24	15.93	19.11	0.91	0.95	0.83
11174	440 ± 15	19.11	17.42	15.90	18.82	1.31	1.24	0.89
12400	301 ± 15	18.00	16.75	15.88	19.30	1.11	0.84	0.60
10807	747 ± 30	20.37:	18.00	15.89	17.71	1.92	2.13	1.59
13364	286 ± 15	18.10	16.85	15.86	19.26	1.30	1.09	0.75
20569	454 ± 15	19.23	17.62	16.03	18.90	1.45	1.40	1.15
13106	354 ± 15	19.10	17.38	15.96	18.98	1.51	1.34	0.98
12466	311 ± 15	18.43	17.10	16.03	19.40	1.52	1.17	0.96
30920	384 ± 10	18.95	17.22	15.86	18.93	1.75	1.46	0.98
12751	231 ± 10	17.89	16.91	16.29	19.62	1.07	0.72	0.50
20542	255 ± 10	17.83	16.76	16.02	19.42	0.73	0.66	0.50
10817	214 ± 10	17.70	16.76	16.04	19.41	0.75	0.61	0.45
11226	257 ± 15	17.49	16.54	16.08	19.27	0.53	0.58	0.52
12445	454 ± 15	20.27:	18.35	16.43	18.75	2.42	1.78	1.25
13293	495 ± 20	20.30:	18.37	16.42	18.69	1.25	1.13	0.95
12177	590 ± 40	20.50:	18.10	16.10	18.08	1.52	1.25	1.09
21419	278 ±15	19.62:	18.27	16.57	19.29	1.50	1.42	1.05
20356	526 ± 20	19.69:	17.43	15.69	18.11	2.12	1.31	1.05
21671	436 ± 15	19.78:	17.78	16.16	18.85	1.59	1.22	0.95
21234	466 ± 15	20.16:	18.21	16.25	18.50	1.54	1.41	1.25
31168	434 ± 10	19.49:	17.49	15.82	18.45	2.05	1.40	1.01
11389	310 ± 13	17.61	16.46	15.66	19.08	0.67	0.43	0.31
10935	243 ± 10	17.48	16.53	16.12	19.25	0.50	0.42	0.37
11372	279 ± 10	17.65	16.55	15.75	19.17	0.81	0.59	0.34
11794	195 ± 15	17.78	16.84	16.42	19.56	0.62	0.39	0.35
10412	398 ± 20	17.22	15.97	15.12	18.54	0.55	0.44	0.32
10439	385 ± 20	17.58	16.27	15.47	18.89	0.77	0.56	0.30
10635	325 ± 15	17.87	16.64	15.78	19.20	0.67	0.42	0.30
10876	316 ± 20	17.67	16.36	15.45	18.87	0.76	0.58	0.37
20539	440 ± 15	17.97	16.62	15.55	18.91	0.64	0.47	0.33

stars (Feast et al., 2006). Two (10807 and 12177) of these longer period variables are from the centre, while the other two (20784 and 20356) are from the northern region of NGC 6822.

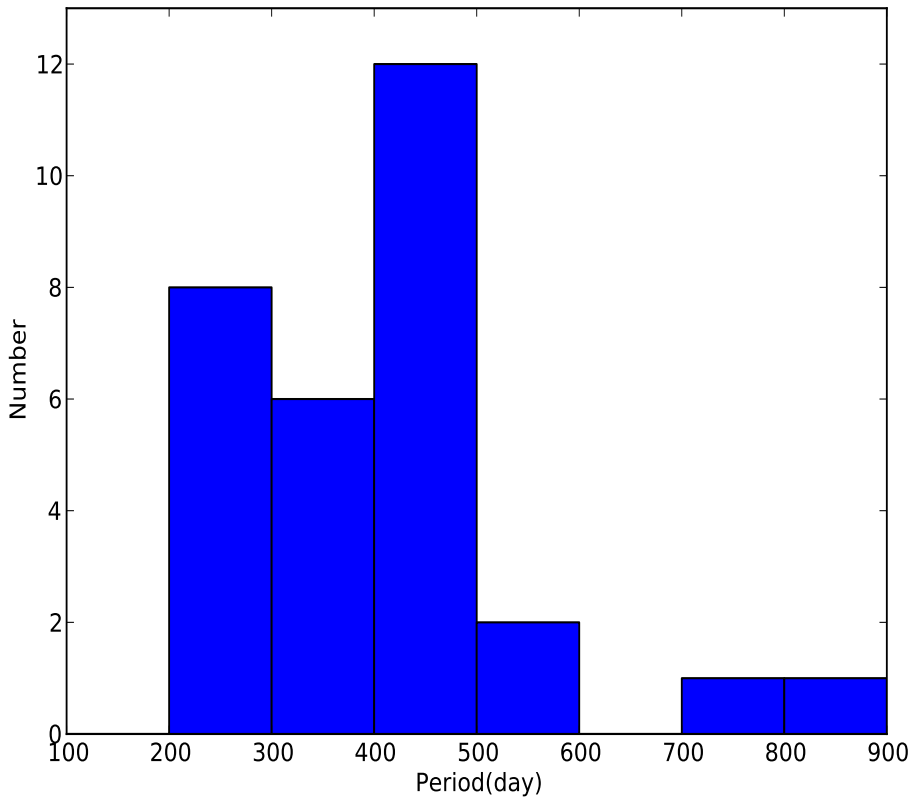

Figure 3.4: Histogram of the number of Miras as a function of their pulsation periods.

Feast et al. (2006) have shown, in their study of Galactic C Miras, that the kinematics of C Miras (like O Miras) are a function of their pulsation periods. They specifically found that C-rich Miras with P $<$ 470 d might have an age of the order of 3.1 Gyr with initial masses of the order of 1.5 $M_{\odot}$ whereas those with P $>$ 470 d might have an age of the order of 1.3 Gyr with initial masses of the order of 2.1 $M_{\odot}$, suggesting that the longer period

C Miras are younger with higher initial masses than the shorter period ones.

In light of the work of Feast et al. (2006) and Figure 3.4, most of the Miras discussed in this work would have an age of the order of 3.1 Gyr with initial masses of the order of 1.5 $M_{\odot}$. This suggests that the assumption of Cioni & Habing (2005), discussed in section 1.3, is reasonable.

3.2 Colour-Magnitude Diagram and carbon stars

3.2.1 Colour-Magnitude Diagram

Figure 3.5 shows the near-infrared (J-K_S, K_S) colour-magnitude diagram (CMD) for the resolved sources detected in the observed $7.5^{'}$ x $21.1^{'}$ area of NGC 6822. The location of the large amplitude AGB variables is shown. Sources which were observed at least 10 times in each of the J, H and K_S bands are considered in the present analysis. Fourier mean magnitudes are used for Miras and SRs while arithmetic mean magnitudes are used for other objects.

Since NGC 6822 is located at a relatively low Galactic latitude (see section 1.1), foreground objects are expected to make a non-negligible contribution in our data. Most of the sources with J-$K_S < 0.9$ are expected to be in the foreground. Due to their relative proximity, many of the foreground sources are expected to be relatively bright and bluer than the objects in NGC 6822. The vertical sequence at J-$K_S \sim 1.0$ will include many supergiants, while most of the redder objects are expected to be low and intermediate mass stars. Most of the stars brighter than the TRGB (K_S=17.2) and redder than J-K_S= 1.0 are expected to be on the AGB. The CMD shows a horizontal sequence made up of objects redder than J-K_S ≈2.0 and extending to J-K_S ≈4.5. This sequence is sometimes referred to as the extended AGB. Objects on the extended AGB have a small range of K_S magnitudes at a given J-K_S and their very red colours suggest high mass-loss rates.

All the sources, except one (this is the object 12080), with J-$K_S > 2.3$

and most of those with $2.0 \lesssim J - Ks < 2.3$ have satisfied the selection criteria of the large amplitude AGB variables discussed in section 3.1. Most of these variables are probably carbon stars as discussed in the next section. I have investigated 12080 and found that it is not a variable, its red colour (J-K_S=2.82) suggests that the object might be a background galaxy.

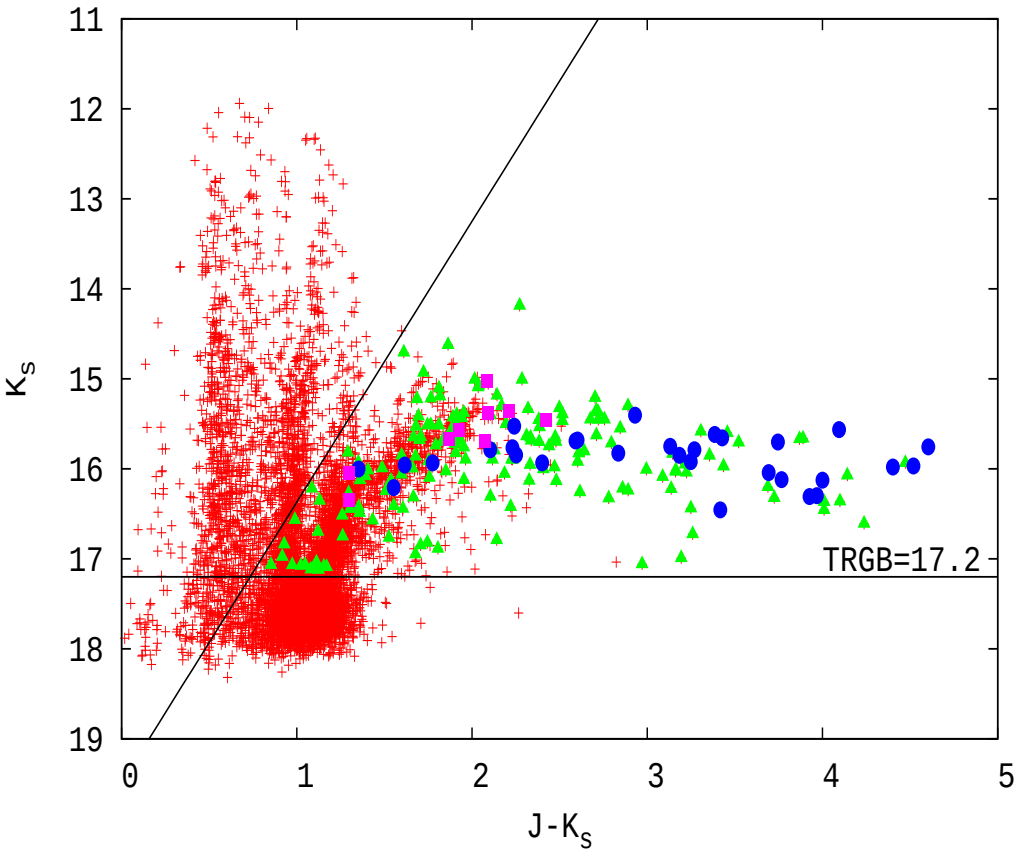

Figure 3.5: Colour-magnitude diagram for the sources detected in NGC 6822, emphasing the location of large amplitude AGB variables. Only sources with at least 10 observations at K_S are illustrated here. Objects brighter than the TRGB (K_S=17.2) and fainter than the slanted line given by $K_S = -3.12(J - K_S) + 19.49$ (see also Figure 3.1) are considered as the most probable AGB stars. Miras and SRs are shown by filled ellipses and rectangles, respectively, whereas other probable large amplitude AGB variables are indicated by filled triangles. Crosses indicate other objects detected in NGC 6822.

3.2.2 Carbon stars

Spectroscopy (Sp) is the clearest way to distinguish between carbon and M stars. However, in the absence of spectra, it is possible to make a reasonable discrimination between carbon and M stars on the basis of colour criteria. In this section, I review some previous work which involved the identification of carbon stars in various galaxies and from the previous results, I deduce the colour criterion which I will use to classify the large amplitude AGB variables in NGC 6822 into probable carbon and M stars.

Hughes & Wood (1990) obtained infrared JHK photometry and spectra for a large sample of long-period variables (LPVs) in the LMC. Based on spectral classification, they found J-K=1.6 as a colour that statistically discriminates C-rich from O-rich stars. They found, further, that all but three of the 121 stars with oxygen-rich spectral types have J-K$\leq$ 1.6. They noticed that three M-type stars that have J-K $>$ 1.6 are very luminous with $M_{bol} \leq$ -5.5 and long periods P $>$ 600 d. Futhermore, they found that there are 15 stars of a total of 87 with C-rich spectra, that have J-K $<$ 1.6.

Cioni et al. (2001) used spectra to separate 126 AGB stars into C- and O-rich groups in the LMC. They found J-K_S $\sim$1.5 as the colour that statistically distinguishes between C- and O-rich stars. Their results show that the J-K_S colours of most of the C stars fall within the range
$1.5 \lesssim$ J-$K_S \lesssim 3$, but there are also two O-rich stars with $2 <$ J-$K_S < 3$ and a few C-rich stars with $1 <$ J-$K_S < 1.5$.

Using 2MASS data, Demers et al. (2002) identified, on the basis of magnitude and colour criteria, 26 C stars in the Fornax dwarf spheroidal galaxy. Most of them are spectrocopically confirmed and their colours fall within the range 1.4 $<$ J-K $<$ 1.9.

Kang et al. (2006), who also investigated AGB stars in NGC 6822, adopted the conditions which discriminate between C stars and M giants, available in the literature, and distinguished C from M stars in NGC 6822

by assuming that stars with J-K > 1.53 and H-K > 0.50 are C-rich.

In light of the above-mentioned previous results, the separation between O and C stars on the basis of colours gives a reasonable estimate, but does not discriminate completely C from O stars.

Although there are no spectra available for the stars involved in this work, based on the above previous results, it is reasonable to assume that large amplitude AGB variables, identified in NGC 6822 as discussed in section 3.1, with J-$K_S \geq 1.5$ are most probably C stars. On this assumption, 132 large amplitude AGB variables are found to be most probably C stars whereas 30 of them are found to be most probably O stars. All but one of the 30 Miras are found to be most probably C stars. Seven of the nine SRs are found to be most probably C stars. In Appendix A, probable carbon large amplitude AGB variables are marked by a symbol C_p, while probable oxygen ones are marked by a symbol O_p.

3.3 Colour-colour diagram

Infrared J-H vs H-K_S diagrams have proved to be an efficient way to discriminate between different stages of stellar evolution (e.g. Bessell & Brett (1988)). This makes it possible for one to identify a region of the two-colour diagram where the stars of interest are located.

Figure 3.6 shows the location on a two-colour diagram of the sources detected in NGC 6822. Large amplitude AGB variables are shown and one can see that they lie in a region spreading to very red colours. However, the distribution of the sources in the various regions of a two-colour diagram might be blurred by photometric errors and depends to some extent on extinction and metallicity, but it is always easy to identify the objects that are probably on the extended AGB.

The slanted dashed line represents infrared colours of black bodies given in Glass (1999). This line is compared with the infrared colours of the

sources detected in NGC 6822 and the reason for this comparison is explained as follows. The photospheres of some stars radiate approximately like black bodies of a given temperature and in addition to this radiation, the circumstellar dust shells surrounding those stars radiate like black bodies of a lower temperature (Glass, 1999). Consequently, one would expect the late stages of stellar evolution, which are characterised by high mass-loss rates and therefore are surrounded by thick layers of dust, to radiate approximately like a combination of black bodies.

The locus of Galactic C Miras in a J-H vs H-K_S diagram is shown by the solid slanted line and compared with the one for Miras in NGC 6822. As can be seen, most of the NGC 6822 Miras fall below but close to the solid line.

Figure 3.7 illustrates the loci of the probable large amplitude carbon and oxygen variables on a two-colour diagram. C stars spread to much redder colours than O stars. These two groups can be distinguished, on the basis of a two-colour diagram, with a reasonable degree of certainty. However, as discussed in detail in section 3.2.2, the separation between O and C stars on the basis of colours, which is the case in this work, does not discriminate completely C from O stars, although it seems likely that the reddest (J-K_S $\gtrsim$ 3) long-period AGB variables are C stars.

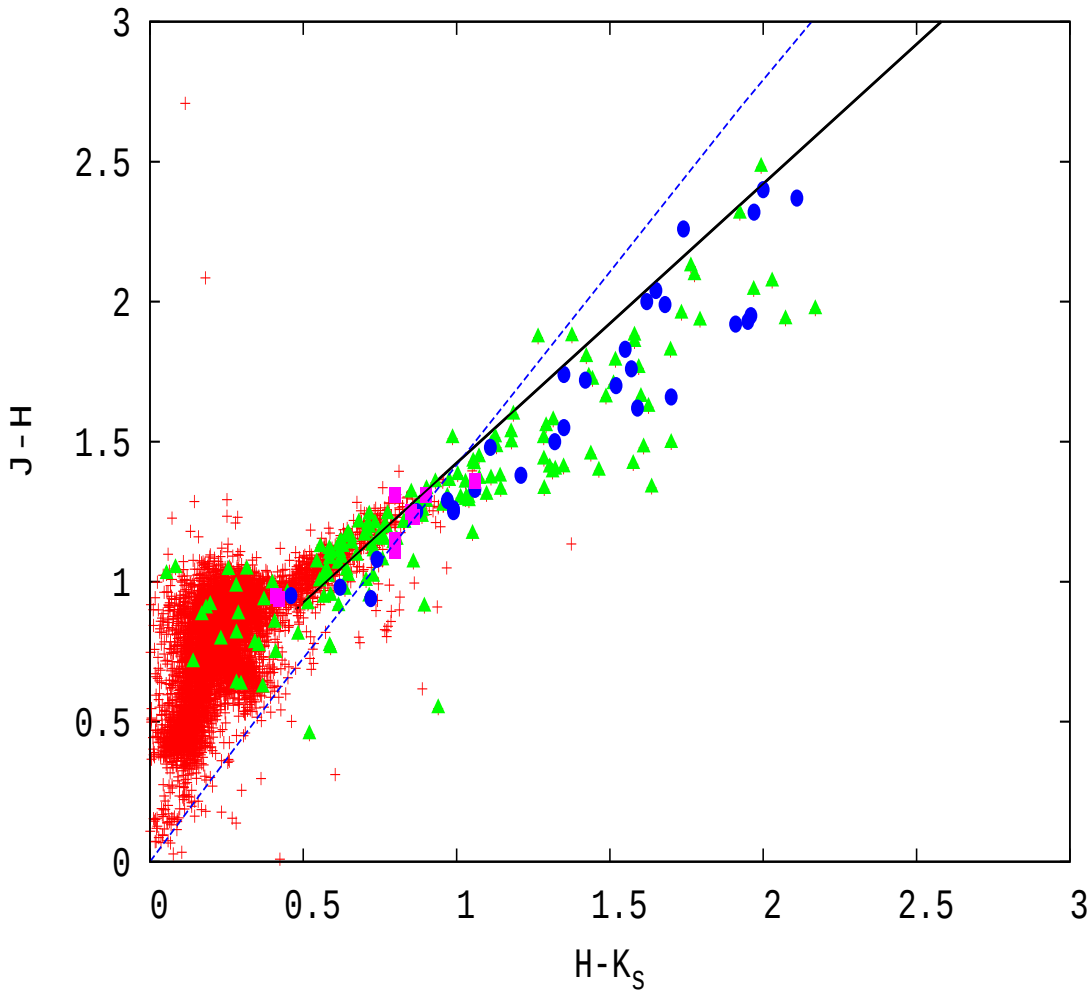

Figure 3.6: Colour-colour diagram of the sources detected in NGC 6822, emphasing the location of large amplitude AGB variables. Symbols are the same as in Figure 3.5. The solid line shows the locus of Galactic carbon Miras and is given by $(\text{H-K})_0 = -0.428 + 1.003(J-H)_0$. This is equation 2 from Whitelock et al. (2006), converted on to the 2MASS system. The dashed line represents infrared colours of black bodies given in Glass (1999).

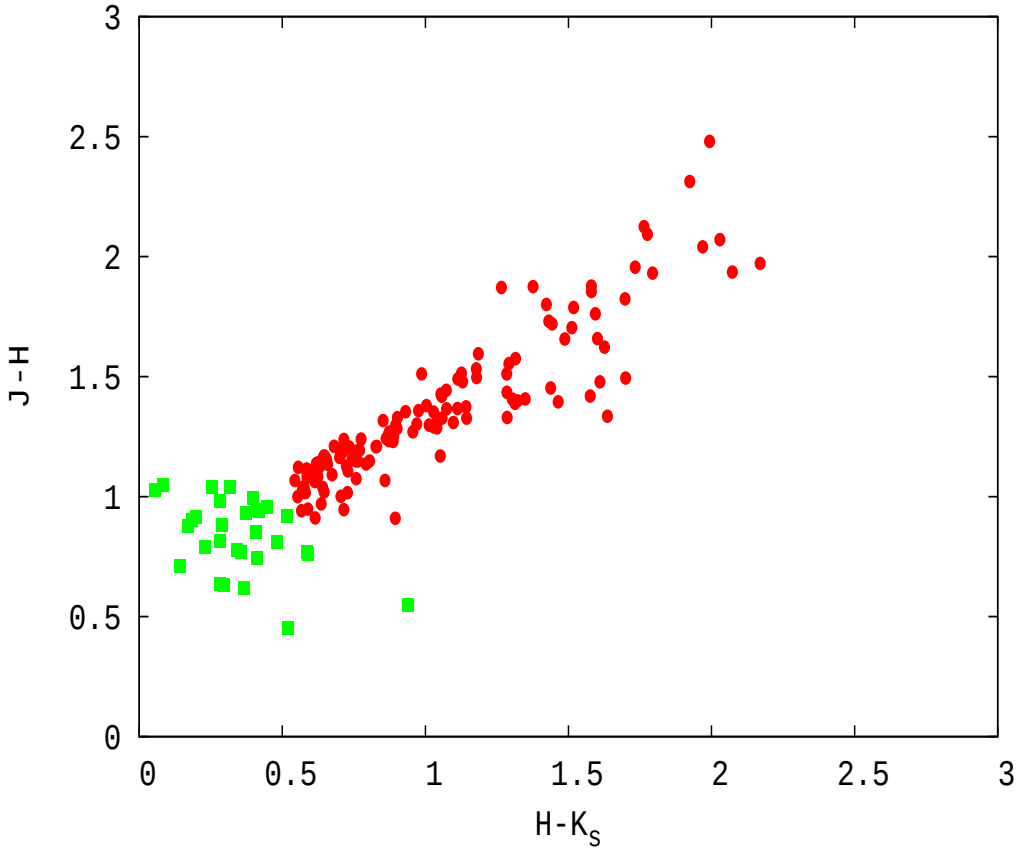

Figure 3.7: The location of large amplitude carbon/oxygen variables on a two-colour diagram. Filled ellipses represent the probable carbon variables, whereas filled rectangles represent the probable oxygen ones.

3.4 K period-luminosity relation for Miras

As in section 1.4, the existence of a PL relation for Miras at different wavelengths has been discussed and confirmed by various authors. The K PL, PL(K), relation for Miras has been proved to be more practical than the ones at J and H when Miras are to be used as distance indicators, since it is narrower for both O and C Miras and in addition to that, K is less sensitive to interstellar reddening than J and H (e.g. Feast et al. (1989)). In this section, the PL(K) relation for Miras in NGC 6822 is presented and a comparison with its most recent LMC counterpart by Whitelock et al. (2008) is made and discussed.

In Figure 3.8, the PL(K) relation for Miras and SRs in NGC 6822 is shown.

The absolute K magnitudes were determined on the assumption that the distance modulus to NGC 6822 is 23.43 (see section 3.5). The line is for the LMC Miras and is given by

$$M_K = -3.51[log(P) - 2.38] - 7.15. \tag{3.1}$$

Equation 3.1 was derived by Whitelock et al. (2008) assuming a distance modulus of 18.39 for the LMC. The relation shows a larger scatter for Miras than for SRs. All but one of the SRs fall above the LMC line whereas many of the Miras, particularly the longer period ones, fall below the line.

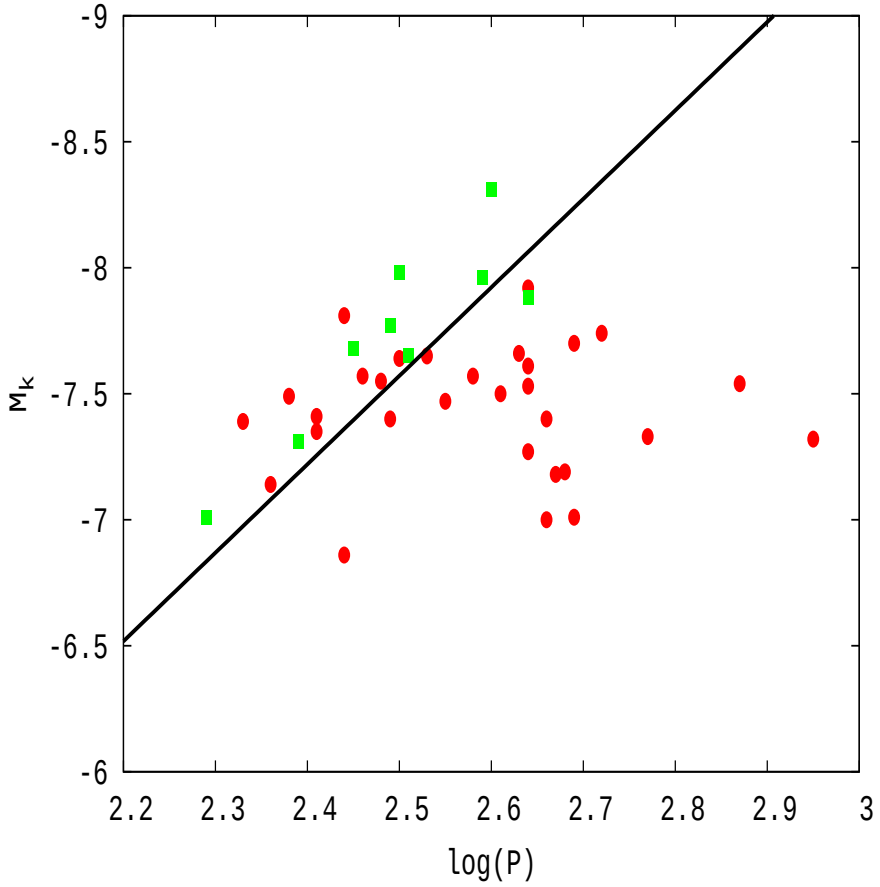

Figure 3.8: PL(K) relation for Miras and SRs in NGC 6822, on the assumption that the distance modulus to NGC 6822 is 23.43 (see section 3.5). Filled ellipses represent Miras while filled rectangles represent SRs. The line is the PL(K) relation for Miras in the LMC and is given by $M_K = -3.51[log(P) - 2.38] - 7.15$ (Whitelock et al., 2008).

In Figure 3.9, the differences (dM_{K_S}) between the observed magnitudes and those predicted by equation 3.1 are plotted against the J-K_S colours. The arrowed line in Figure 3.9 shows the locus for interstellar extinction of strength A_V=10 mag, where A_V is the visual extinction. This value of A_V was found using the colour excess ratios given in Table 5.2 in Glass (1999), from which I deduced A_K=0.91, E(J-K)=1.72 and therefore A_K/E(J-K)=0.53, the slope of the arrowed line.

One can see from Figure 3.9 that for J-$K_S \lesssim 2$, the dM_{K_S} are relatively small, while for J-$K_S \gtrsim 2$ they increase proportionally with J-K_S colour. Clearly, the slope of the arrowed line is comparable to that of the relation illustrated in Figure 3.9 for the sources with J-$K_S \gtrsim 2$ and this suggests that we are observing the effects of extinction. The extinction is maximum at J-$K_S \approx 4.5$ and minimum at J-$K_S \approx 1.5$.

In Figure 3.10, the dM_{K_S} are plotted against the K amplitudes of pulsation ($\triangle K$) for both Miras and SRs. It turns out that the dM_{K_S} increase with increasing $\triangle K$. The maximum of the dM_{K_S} is at $\triangle K \approx$1.5 mag and the minimum is at $\triangle K \approx 0.3$ mag.

From Figures 3.8, 3.9 and 3.10, one can conclude that fainter K mean magnitudes for the LPVs that lie below the LMC Mira PL(K) relation are due to extinction within their circumstellar dust shells. As the amplitude of pulsation increases, the circumstellar dust shell becomes thicker and the deviation of the star in question from the LMC PL(K) becomes larger.

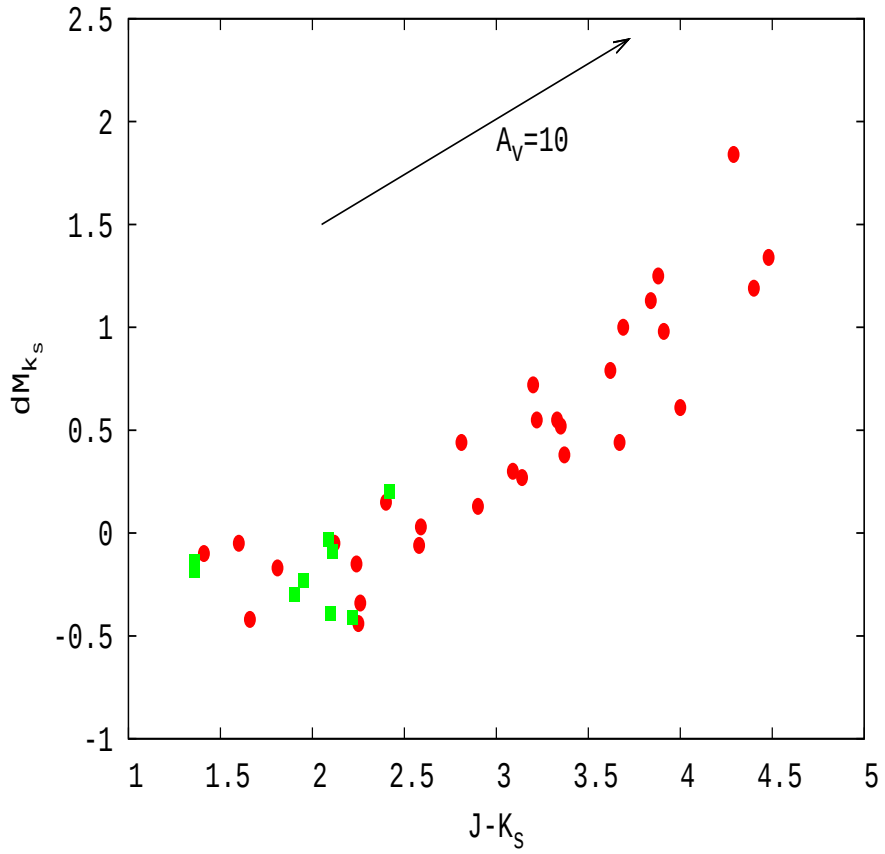

Figure 3.9: The differences (dM_{K_S}) between the observed K magnitudes and those predicted from the LMC PL(K) as a function of J-K_S colours. Symbols are the same as in Figure 3.8. The arrowed line indicates the locus of interstellar reddening of strength A_V=10 mag. This value of A_V was found using the colour excess ratios given in Table 5.2 in Glass (1999).

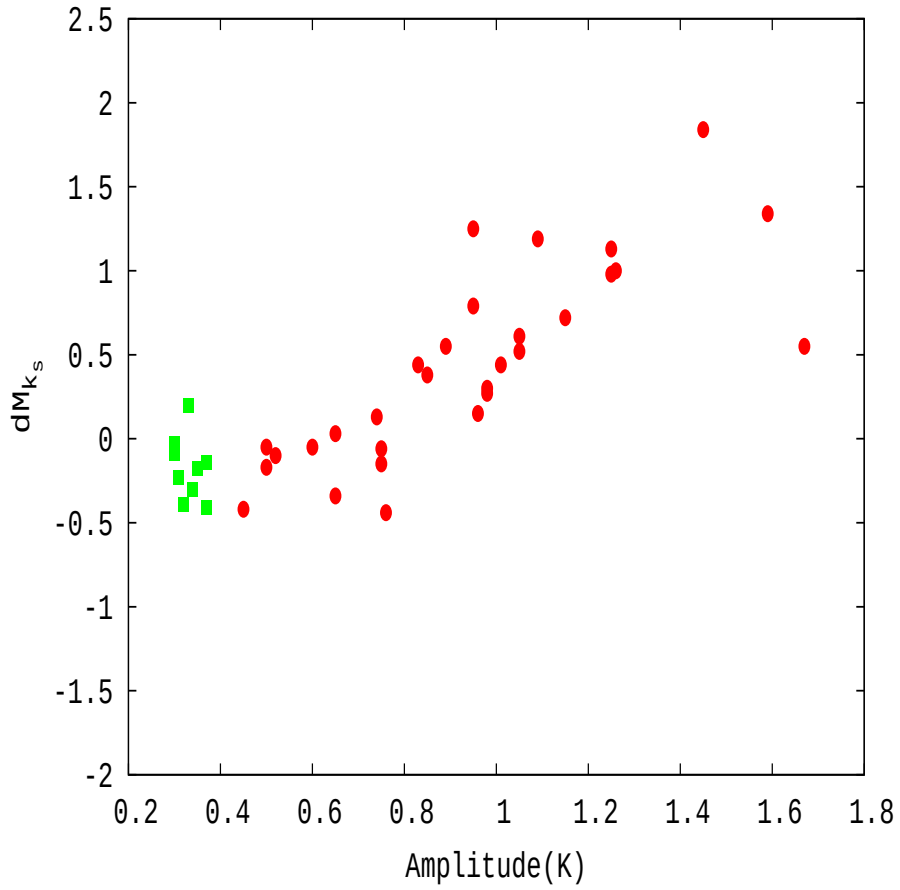

Figure 3.10: The differences (dM_{K_S}) between the observed magnitudes and those predicted from the LMC PL(K) as a function of K amplitudes of pulsation. Symbols are the same as in Figure 3.8.

In light of the results illustrated in Figures 3.8, 3.9 and 3.10, the argument that Miras obey the same PL relation irrespective of the environment is not refuted, but it is noteworthy that the large amplitude AGB variables in NGC 6822 suffer a huge amount of mass loss resulting in a significant circumstellar extinction, which is not corrected for in the present analysis, such that the PL(K) relation of such very red stars will not be useful for distance determination. In the next section, I derive the bolometric PL relation for Miras which will be used for determining the distance to NGC 6822.

3.5 Bolometric period-luminosity relation for Miras

The bolometric magnitude measures the total energy output of a star over all wavelengths, including those unobserved due to various sources of extinction and observational constraints. The apparent bolometric magnitude (m_{bol}) of a star is related to its apparent magnitude m_λ, at λ wavelength, by

$$m_{bol} = BC_\lambda + m_\lambda \tag{3.2}$$

where BC_λ is a correction that must be made at λ. Apparent bolometric magnitudes were calculated using the (J-K_S) and (H-K_S) colour-dependent bolometric corrections in the same way as they were for Miras in the Fornax dwarf spheroidal galaxy by Whitelock et al. (2009) (see also Whitelock et al. (2006) for more informations about the bolometric corrections). The results are shown in column 6 of Table 3.2.

Various observations, e.g. Rejkuba (2004), suggest that the slope of the PL relation of Miras is universal. In the following discussion, I adopt this argument and use the LMC M_{bol} PL relation of C Miras given by

$$M_{bol} = -3.31(\pm 0.24)[log(P) - 2.5] - 4.271(\pm 0.03) \tag{3.3}$$

to find the distance to NGC 6822. Equation 3.3 is A1 in Whitelock et al. (2009) and was derived on the assumption that the distance modulus to the LMC is 18.39.

The distance to NGC 6822 can be established by fitting a line with the LMC slope of -3.31 to the NGC 6822 data given in Table 3.2, as shown in Figure 3.11. This line is given by

$$m_{bol} = -3.31[log(P) - 2.5] + 19.154 \tag{3.4}$$

The absolute difference in the zero-points of equations 3.3 and 3.4 yields the distance modulus to NGC 6822. To find the distance, different groups of Miras are considered depending on the range of their periods, the quality of the data and the quality of the light curves. Various values of the distance moduli obtained in this way are compared.

If all Miras are considered, the distance modulus is found to be m-M=23.43 $\pm$ 0.04 (statistical error). Considering only Miras with periods P$<$ 490 d, I obtain m-M=23.42 $\pm$ 0.04 (statistical error). Excluding Miras with poor quality J data (marked in Table 3.2), I get m-M=23.42 $\pm$ 0.04 (statistical error). If only Miras with very good quality of light curves (Q=1) are considered, I obtain m-M=23.43 $\pm$ 0.05 (statistical error). Considering only shorter periods Miras (P $<$ 490 d) with very good quality of light curves (Q=1) and excluding those with poor quality J data (see Table 3.2), I get m-M=23.39 $\pm$ 0.06 (statistical error). The statistical error excludes the error on the LMC distance. The distance moduli obtained above by considering different groups of Miras agree quite well. In the subsequent discussion, the distance modulus found using all 30 Miras will be considered.

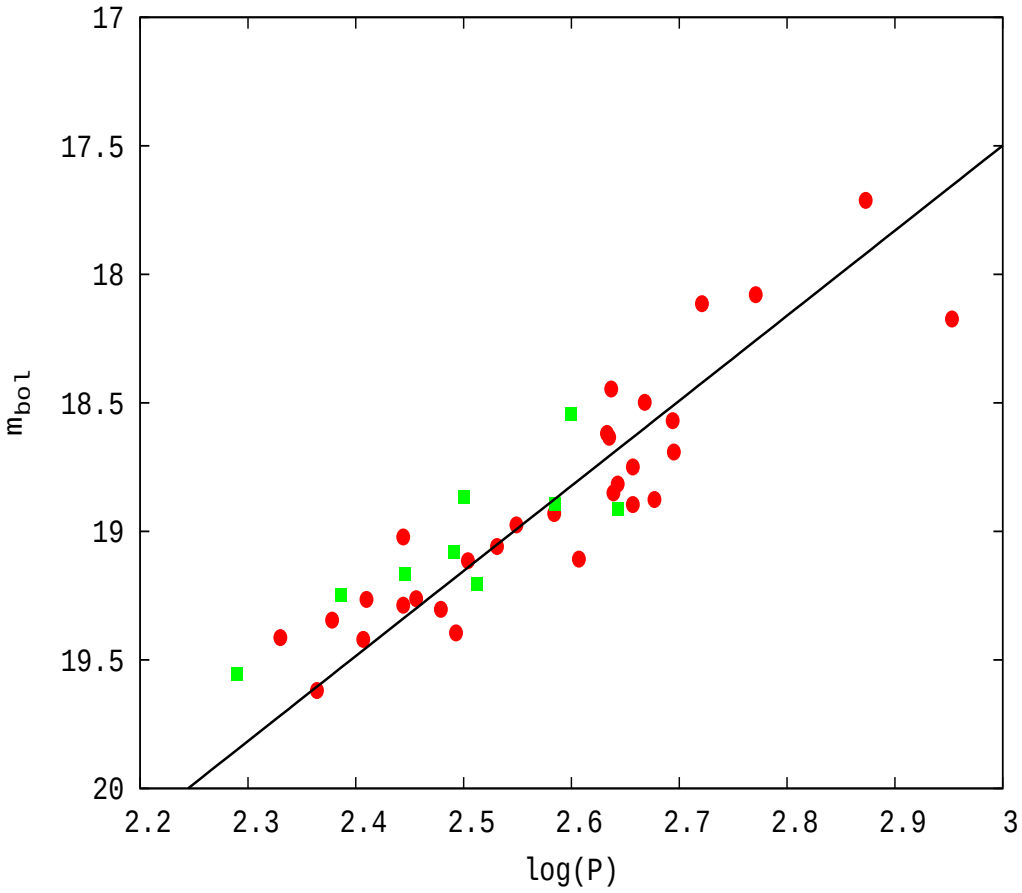

Figure 3.11: m_{bol} PL relation for Miras and SRs in NGC 6822. Symbols are the same as in Figure 3.8. The line is given by $m_{bol} = -3.31[\log(P)\text{-}2.5] + 19.154$ (equation 3.4).

Although the LMC slope was assumed above in order to estimate the distance to NGC 6822, this may not be appropriate for NGC 6822. In the following discussion, I derive the slope suitable for NGC 6822 and this will be compared to its LMC counterpart.

Least squares fits of the form

$$m_{bol} = a[log(P) - 2.5] + b \tag{3.5}$$

to the NGC 6822 Miras yield the values of "a" and "b" as well as the scatter (σ) around the PL relation. Different values of a, b and σ were obtained by considering different groups of Miras defined above and those are listed in Table 3.3.

Table 3.3: Parameters associated to the equation 3.5

Group	Group size	a	b	σ
[1]	30	-2.81 ± 0.24	19.11 ±0.04	0.19
[2]	24	-2.48 ± 0.30	19.12 ± 0.03	0.16
[3]	19	-2.40 ± 0.31	19.13 ± 0.03	0.14
[4]	20	-2.71 ± 0.30	19.10 ± 0.06	0.20
[5]	10	-2.31 ± 0.50	19.11 ± 0.05	0.17

1=All Miras.

2=Miras with P< 490 d.

3=Miras excluding the ones with poor quality J data (see Table 3.2).

4=Miras with very good quality of light curves (Q=1).

5=Miras with P< 490 d and Q=1, excluding those with poor quality J data.

It can be noted from Table 3.3 that the values of the slope found by considering different groups of NGC 6822 Miras are in good agreement. The slope (-2.81 ± 0.24) found by considering all Miras is comparable to its LMC counterpart (-3.31 ± 0.24).

Some values of the slope and scatter of the LMC Mira PL(bol) relations from the literature are presented in Table 3.4.

Table 3.4: Values of the slope and scatter of the LMC Mira PL(bol) relations from the literature

Reference	Group	Group size	a	σ	Periods
1	C-Miras	22	-3.31 ± 0.24	0.12	P< 490 d
2	C-Miras	20	-1.86 ± 0.30	0.13	P< 420 d
2	O-Miras	29	-3.00 ± 0.24	0.16	P< 420 d
2	Both(together)	49	-2.34 ± 0.19	0.17	P< 420 d

1=Whitelock et al. (2009).

2=Feast et al. (1989).

2=Feast et al. (1989).

2=Feast et al. (1989).

There is some difference between the slopes found by Feast et al. (1989) and Whitelock et al. (2009), but it is also important to note that this depends on how the bolometric corrections are calculated.

Using the distance modulus to NGC 6822 found above, the relation

$$M_{bol} = -2.81(\pm 0.24)[log(P) - 2.5] - 4.32 \pm 0.04 \tag{3.6}$$

is obtained and compared to its LMC counterpart (equation 3.3). The results are shown in Figure 3.12. Clearly, although the scatter around the PL relation for Miras in NGC 6822 (σ=0.19) is somewhat larger than the one for its LMC counterpart (σ=0.12), the difference between the NGC 6822 and LMC PL relations is not significant. It is difficult to be certain of the

sources underlying these minor deviations, but one of the possible factors might be the poor quality of J data for some stars of interest. Clearly, the uncertainties in the J magnitudes result in the uncertainties in the bolometric corrections.

The agreement of the two PL relations illustrated in Figure 3.12 confirms other determinations that the PL relation for Miras is universal and therefore Miras can be used as distance indicators in populations of different metallicity, a result which is of particular importance for extragalactic applications. In the next section, I will compare the distance modulus to NGC 6822 found above to the ones from the literature.

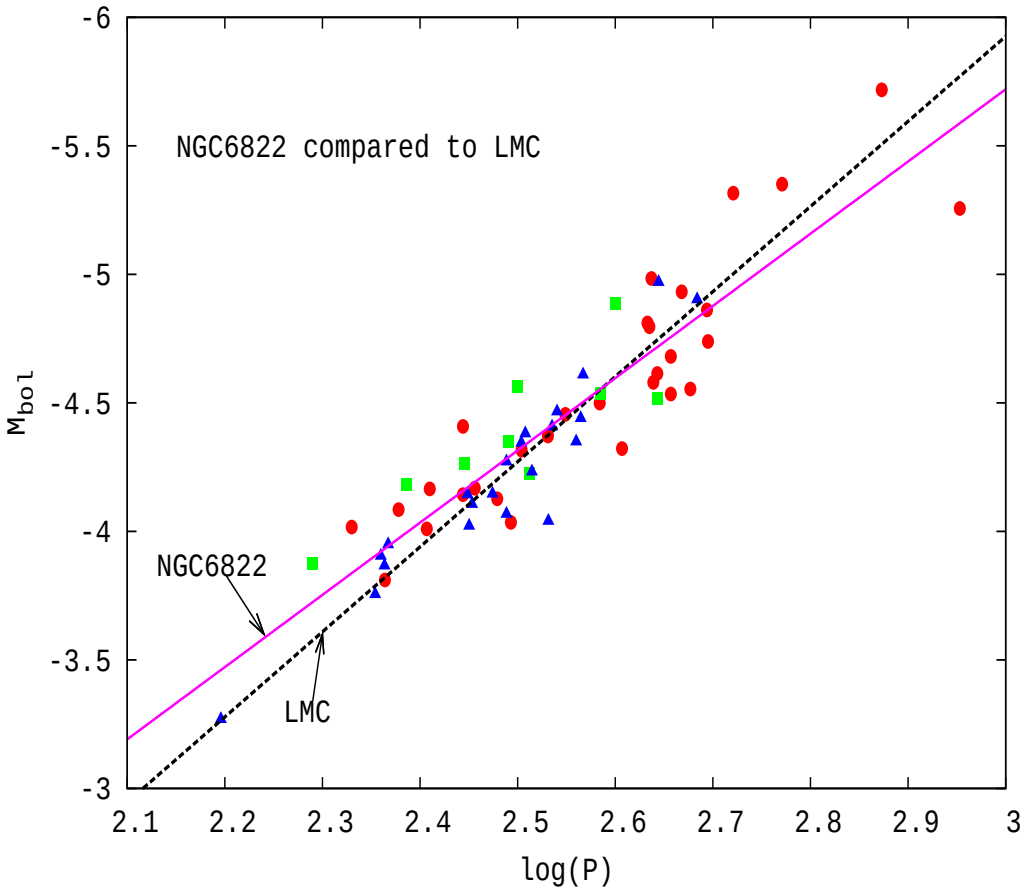

Figure 3.12: M_{bol} PL relation for Miras and SRs in NGC 6822 and LMC. Filled ellipses and rectangles represent, respectively, Miras and SRs in NGC 6822 while filled triangles represent 22 C Miras in the LMC (Whitelock et al., 2009). The solid line is a result of a least squares fit to the NGC 6822 Miras and is given by $M_{bol} = -2.81[log(P) - 2.5] - 4.32$, whereas the dashed line results from a least squares fit to the LMC C Miras and is given by $M_{bol} = -3.31[log(P) - 2.5] - 4.271$ (Whitelock et al., 2009).

3.6 Distance to NGC 6822

Several estimates of the distance to NGC 6822 have been made by various authors, using different approaches. In this section, I compare the distance modulus to NGC 6822 found using Miras to the existing ones from the literature. Table 3.5 contains various estimates of the distance moduli to NGC 6822, from the literature. The distance modulus to NGC 6822 estimated in the present work using Miras is presented at the bottom of Table 3.5.

Table 3.5: Estimates of the distance modulus to NGC 6822 from the literature

Bandpass	Method	m-M	Reference
J	TRGB	23.35 ± 0.26	Sohn et al. (2008)
H	TRGB	23.20 ± 0.42	Sohn et al. (2008)
K	TRGB	23.27 ± 0.50	Sohn et al. (2008)
bol	TRGB	23.41 ± 0.17	Sohn et al. (2008)
V	RRs	23.36 ± 0.17	Clementini et al. (2003)
VIJK	Cepheids	23.31 ± 0.021	Gieren et al. (2006)
BVRI	Cepheids	23.49 ± 0.08	Gallart et al. (1996b)
H	Cepheids	23.47 ± 0.11	McAlary et al. (1983)
3.6 μm	Cepheids	23.57 ± 0.06	Madore et al. (2009)
4.5 μm	Cepheids	23.55 ± 0.07	Madore et al. (2009)
5.8 μm	Cepheids	23.60 ± 0.09	Madore et al. (2009)
8.0 μm	Cepheids	23.51 ± 0.08	Madore et al. (2009)
V, I and W_I	Cepheids	23.34 ± 0.04	Pietrzyński et al. (2004)
bol	Miras	23.43 ± 0.04	This work

Although the distance to NGC 6822 could not be estimated using the PL(K) relation for all of the Miras, for the reasons discussed earlier, it is useful to estimate the distance using the PL(K) relation for those Miras which have relatively little circumstellar extinction and see how this compares with the value obtained using the PL(bol) relation.

Using 10 Miras with $|dM_K| < 0.3$, the PL(K) relation for these stars yields K-M_K=23.37 ± 0.04 where M_K is given by equation 3.1. This is in remarkably good agreement with the value obtained for the bolometric

magnitudes and in reasonable agreement with the values obtained by other authors. However, by selecting for sources with $|dM_K| < 0.3$ we will naturally find a relation with very little scatter and therefore measure a low error on the mean. For this reason, and because of the large number of stars involved, the determination of distance modulus from the bolometric PL relation is to be preferred.

Chapter 4

Discussion of the results and recommendations

Analysis of the data used in this work reveals the presence of a large number of large amplitude AGB variables in NGC 6822. Analysis of their light curves suggests that many of these undergo erratic changes. Many of the variables with regular or semiregular light curves have been fully characterised leading to a classificaction of stars into Miras and SRs. It is likely that the list of Miras and SRs in NGC 6822 presented in this work is not exhaustive, as the approach used here did not take into account those which undergo erratic variations. The last mentioned variables are most likely to be found among those listed in Appendix A and I would recommend their further investigation, if more adequate means are available. This would probably result in a larger number of Miras in NGC 6822 and therefore a better estimate of the distance to this galaxy.

I have carefully analysed the star 30920. Based on the conditions on variability, amplitude and period defined in section 1.4 this star is a Mira, but its light curve suggests an odd variation. The reasons for this are not clear to me and I recommend further investigation of this star.

Sources with some probability of being large amplitude AGB variables, given their red colours, but which have been observed less than 10 times and therefore have not been selected in section 2.2.2 as candidate large

amplitude variables are listed in Appendix B. I would recommend sufficient observations of these objects in order to draw relevant conclusions about them.

Appendix C contains objects with J-K_S $\geq$ 2, observed more than 10 times, but which have not satisfied the selection criterion for the large amplitude variables in NGC 6822. It would be interesting to investigate the cause of the very red colours of these objects.

The colour criterion (J-K_S $\geq$1.5) adopted on the basis of previous work suggests that most of the large amplitude AGB variables identified in this work are most probably C stars. However, many investigators of AGB stars, e.g. Cioni et al. (2001), using spectroscopy, have found M stars with J-K_S >1.5 although these are few. I would recommend another classification of the large amplitude AGB variables in NGC 6822 into C and O stars, when spectra become available.

One of the most interesting results of this work is the agreement between the bolometric PL relation for Miras in NGC 6822 and its LMC counterpart. However, as can be seen from Figure 3.12, there are some minor deviations. It is difficult to be certain of the sources underlying these minor deviations, but one of the possible factors might be the poor quality of J data for some stars of interest. As mentioned earlier, AGB stars are fainter at shorter wavelengths. Observation of these stars at J is sometimes difficult. Obviously, the poor quality of J data results in uncertainty in the mean J magnitudes and therefore in the bolometric corrections and magnitudes. The extreme cases of such stars are marked in Table 3.2 and I would recommend their further investigation.

Chapter 5

Conclusion

In this work J, H and K_S data obtained by the SIRIUS camera centred on NGC 6822 have been analysed. The purpose of the analysis was to identify and characterise the large amplitude AGB variables. 162 probable large amplitude AGB variables have been identified and some of these have been fully characterised. Their location in the CMD suggests that NGC 6822 has a large population of evolved low and intermediate mass stars, a result which confirms previous work by various authors (see section 1.3). The colours of known carbon stars suggest that most of the large amplitude AGB variables found in NGC 6822 are most probably carbon stars.

On the basis of the light curves and periodogram analysis, 30 Miras and 9 SRs have been found and fully characterised. Their characteristic parameters such as pulsation periods, amplitudes and Fourier mean J, H and K_S magnitudes have been determined. It has been found that Miras and SRs have periods which fall in the range 190 <P< 900 d and K amplitudes in the range $0.2 < \triangle K < 1.8$ mag.

The PL(K) relation for Miras in NGC 6822 has been discussed and compared to its LMC counterpart. It has been found that many of the longer period Miras are fainter than the LMC PL(K). Further investigation of these stars indicates that many of the large amplitude AGB variables in NGC 6822 suffer a huge mass loss, resulting in thicker circumstellar dust shells, an im-

portant source of extinction for these objects. As a result of this, as long as the magnitudes of Miras are not dereddened, the PL(K) can not be used to determine the distance to NGC 6822.

Following the work of Whitelock et al. (2009) for the Fornax dwarf spheroidal galaxy, apparent bolometric magnitudes of Miras and SRs have been found and used to determine the distance modulus to NGC 6822, adopting the universality of the Mira PL relation. I have found the distance modulus to NGC 6822 to be m-M=23.43 $\pm$ 0.04 (statistical error only). Using this value of the distance modulus, a comparison of the M_{bol} PL relation for Miras in NGC 6822 to its LMC counterpart has been made. It has been found that these two period-luminosity relations are very similar, confirming other determinations that the PL relation for Miras is universal.

Bibliography

Baud, B. & Habing, H. J. 1983, A&A, 127, 73

Bessell, M. S. & Brett, J. M. 1988, PASP, 100, 1134

Blöcker, T. & Schönberner, D. 1991, A&A, 244, L43

Bonnarel, F., Fernique, P., Bienaymé, O., Egret, D., Genova, F., Louys, M., Ochsenbein, F., Wenger, M., & Bartlett, J. G. 2000, A&AS, 143, 33

Brandenburg, H. J. & Skillman, E. D. 1998, in Bulletin of the American Astronomical Society, Vol. 30, Bulletin of the American Astronomical Society, 1354–+

Cioni, M., Blommaert, J. A. D. L., Groenewegen, M. A. T., Habing, H. J., Hron, J., Kerschbaum, F., Loup, C., Omont, A., van Loon, J. T., Whitelock, P. A., & Zijlstra, A. A. 2003, A&A, 406, 51

Cioni, M. & Habing, H. J. 2005, A&A, 429, 837

Cioni, M., Marquette, J., Loup, C., Azzopardi, M., Habing, H. J., Lasserre, T., & Lesquoy, E. 2001, A&A, 377, 945

Clementini, G., Held, E. V., Baldacci, L., & Rizzi, L. 2003, ApJ, 588, L85

Cohen, J. G. & Blakeslee, J. P. 1998, AJ, 115, 2356

Cutri, R. M., Skrutskie, M. F., van Dyk, S., Beichman, C. A., Carpenter, J. M., Chester, T., Cambresy, L., Evans, T., Fowler, J., Gizis, J., Howard,

E., Huchra, J., Jarrett, T., Kopan, E. L., Kirkpatrick, J. D., Light, R. M., Marsh, K. A., McCallon, H., Schneider, S., Stiening, R., Sykes, M., Weinberg, M., Wheaton, W. A., Wheelock, S., & Zacarias, N. 2003, 2MASS All Sky Catalog of point sources., ed. Cutri, R. M., Skrutskie, M. F., van Dyk, S., Beichman, C. A., Carpenter, J. M., Chester, T., Cambresy, L., Evans, T., Fowler, J., Gizis, J., Howard, E., Huchra, J., Jarrett, T., Kopan, E. L., Kirkpatrick, J. D., Light, R. M., Marsh, K. A., McCallon, H., Schneider, S., Stiening, R., Sykes, M., Weinberg, M., Wheaton, W. A., Wheelock, S., & Zacarias, N.

Davidge, T. J. 2003, PASP, 115, 635

Demers, S., Dallaire, M., & Battinelli, P. 2002, AJ, 123, 3428

Feast, M. W. 1984, MNRAS, 211, 51P

Feast, M. W., Glass, I. S., Whitelock, P. A., & Catchpole, R. M. 1989, MNRAS, 241, 375

Feast, M. W., Whitelock, P. A., & Menzies, J. W. 2006, MNRAS, 369, 791

Gallart, C., Aparicio, A., Bertelli, G., & Chiosi, C. 1996a, AJ, 112, 2596

Gallart, C., Aparicio, A., & Vilchez, J. M. 1996b, AJ, 112, 1928

Gieren, W., Pietrzyński, G., Nalewajko, K., Soszyński, I., Bresolin, F., Kudritzki, R., Minniti, D., & Romanowsky, A. 2006, ApJ, 647, 1056

Glass, I. S. 1999, Handbook of Infrared Astronomy, ed. Glass, I. S.

Glass, I. S. & Feast, M. W. 1982, MNRAS, 199, 245

Glass, I. S. & Lloyd Evans, T. L. 1981, Nature, 291, 303

Hodge, P., Lee, M. G., & Kennicutt, Jr., R. C. 1988, PASP, 100, 917

Hodge, P. W. 1977, ApJS, 33, 69

Hubble, E. 1925, Contributions from the Mount Wilson Observatory / Carnegie Institution of Washington, 304, 1

Hughes, S. M. G. & Wood, P. R. 1990, AJ, 99, 784

Iben, Jr., I. 1964, ApJ, 140, 1631

—. 1975, ApJ, 196, 525

Iben, Jr., I. & Renzini, A. 1983, ARA&A, 21, 271

Kang, A., Sohn, Y., Kim, H., Rhee, J., Kim, J., Hwang, N., Lee, M. G., Kim, Y., & Chun, M. 2006, A&A, 454, 717

Kippenhahn, R., Thomas, H. C., & Weigert, A. 1965, Zeitschrift fur Astrophysik, 61, 241

Kukarkin, B. V. 1985, General catalogue of variable stars. Vol.1: Constellations Andromeda - Crux; Vol.2: Constellations Cygnus - Orion; Vol.3: Constellations Pavo-Vulpecula, ed. Kukarkin, B. V.

Letarte, B., Demers, S., Battinelli, P., & Kunkel, W. E. 2002, AJ, 123, 832

Madore, B. F., Rigby, J., Freedman, W. L., Persson, S. E., Sturch, L., & Mager, V. 2009, ApJ, 693, 936

Massey, P., Armandroff, T. E., Pyke, R., Patel, K., & Wilson, C. D. 1995, AJ, 110, 2715

McAlary, C. W., Madore, B. F., McGonegal, R., McLaren, R. A., & Welch, D. L. 1983, ApJ, 273, 539

Menzies, J. W. & Whitelock, P. A. 1985, MNRAS, 212, 783

Nagashima, C., Nagayama, T., Nakajima, Y., Tamura, M., Sugitani, K., Nagata, T., Hirao, T., Nakaya, H., Yanagisawa, K., & Sato, S. 1999, in Star Formation 1999, ed. T. Nakamoto, 397–398

Nagayama, T., Nagashima, C., Nakajima, Y., Nagata, T., Sato, S., Nakaya, H., Yamamuro, T., Sugitani, K., & Tamura, M. 2003, in Society of Photo-Optical Instrumentation Engineers (SPIE) Conference Series, Vol. 4841, Society of Photo-Optical Instrumentation Engineers (SPIE) Conference Series, ed. M. Iye & A. F. M. Moorwood, 459–464

Paczyński, B. 1971, Acta Astronomica, 21, 271

Pietrzyński, G., Gieren, W., Udalski, A., Bresolin, F., Kudritzki, R., Soszyński, I., Szymański, M., & Kubiak, M. 2004, AJ, 128, 2815

Reimers, D. 1975, Memoires of the Societe Royale des Sciences de Liege, 8, 369

Rejkuba, M. 2004, A&A, 413, 903

Sackmann, I. & Boothroyd, A. I. 1992, ApJ, 392, L71

Scalo, J. M., Despain, K. H., & Ulrich, R. K. 1975, ApJ, 196, 805

Schechter, P. L., Mateo, M., & Saha, A. 1993, PASP, 105, 1342

Schulz, N. S. 2005, From Dust To Stars Studies of the Formation and Early Evolution of Stars, ed. Schulz, N. S.

Sohn, Y., Kang, A., Han, W., Park, J., Kim, H., Kim, J., Shin, I., & Chun, S. 2008, Journal of Astronomy and Space Sciences, 25, 249

Tolstoy, E., Irwin, M. J., Cole, A. A., Pasquini, L., Gilmozzi, R., & Gallagher, J. S. 2001, MNRAS, 327, 918

van den Bergh, S. 2000, The Galaxies of the Local Group, ed. van den Bergh, S. (Cambridge)

Vassiliadis, E. & Wood, P. R. 1993, ApJ, 413, 641

Venn, K. A., Lennon, D. J., Kaufer, A., McCarthy, J. K., Przybilla, N., Kudritzki, R. P., Lemke, M., Skillman, E. D., & Smartt, S. J. 2001, ApJ, 547, 765

Whitelock, P. A., Feast, M. W., Marang, F., & Groenewegen, M. A. T. 2006, MNRAS, 369, 751

Whitelock, P. A., Feast, M. W., & van Leeuwen, F. 2008, MNRAS, 386, 313

Whitelock, P. A., Menzies, J. W., Feast, M. W., Matsunaga, N., Tanabé, T., & Ita, Y. 2009, MNRAS, 394, 795

Wood, P. R., Alcock, C., Allsman, R. A., Alves, D., Axelrod, T. S., Becker, A. C., Bennett, D. P., Cook, K. H., Drake, A. J., Freeman, K. C., Griest, K., King, L. J., Lehner, M. J., Marshall, S. L., Minniti, D., Peterson, B. A., Pratt, M. R., Quinn, P. J., Stubbs, C. W., Sutherland, W., Tomaney, A., Vandehei, T., & Welch, D. L. 1999, in IAU Symposium, Vol. 191, Asymptotic Giant Branch Stars, ed. T. Le Bertre, A. Lebre, & C. Waelkens, 151–+

Wood, P. R., Bessell, M. S., & Paltoglou, G. 1985, ApJ, 290, 477

Wood, P. R. & Zarro, D. M. 1981, ApJ, 247, 247

Wyder, T. K. 2000, in Bulletin of the American Astronomical Society, Vol. 32, Bulletin of the American Astronomical Society, 1444–+

Wyder, T. K., Hodge, P. W., & Zucker, D. B. 2000, PASP, 112, 1162

Appendix A

Probable large amplitude AGB variables in NGC 6822

Name	α(2000)	δ(2000)	J	H	K_S	J-K$_S$	Sp
40520	19:44:41.4	-14:44:25	18.09	16.66	15.37	2.72	C$_p$
40623	19:44:41.5	-14:44:49	20.38	18.34	16.37	4.01	C$_p$
40275	19:44:41.8	-14:45:02	17.13	15.92	15.09	2.04	C$_p$
40363	19:44:41.8	-14:51:25	19.08	17.68	16.22	2.86	C$_p$
40102	19:44:41.9	-14:45:04	19.55	17.43	15.66	3.89	C$_p$
40446	19:44:41.9	-14:51:38	18.57	17.55	16.82	1.75	C$_p$
40501	19:44:42.0	-14:50:52	17.26	16.13	15.52	1.75	C$_p$
40114	19:44:42.4	-14:51:42	20.19	18.69	16.99	3.19	C$_p$
40493	19:44:42.6	-14:44:16	18.21	16.80	15.45	2.76	C$_p$
10425	19:44:42.7	-14:47:58	17.32	16.11	15.40	1.91	C$_p$
11299	19:44:42.9	-14:46:35	19.21	17.45	15.85	3.36	C$_p$
12751	19:44:43.0	-14:45:35	17.98	16.96	16.32	1.67	C$_p$
13106	19:44:43.1	-14:50:58	19.18	17.46	16.02	3.16	C$_p$
12445	19:44:43.1	-14:47:26	20.85	18.53	16.61	4.24	C$_p$
11389	19:44:43.2	-14:45:48	17.59	16.46	15.66	1.93	C$_p$
10839	19:44:43.2	-14:49:37	18.13	16.63	15.45	2.68	C$_p$
10433	19:44:43.3	-14:47:45	17.45	16.30	15.54	1.91	C$_p$
10755	19:44:43.6	-14:50:18	17.42	16.23	15.52	1.91	C$_p$
12147	19:44:43.8	-14:48:39	19.89	17.94	16.20	3.69	C$_p$
10748	19:44:43.9	-14:50:20	18.62	17.19	16.14	2.48	C$_p$
12373	19:44:44.0	-14:47:45	18.63	17.56	16.95	1.68	C$_p$
11174	19:44:44.1	-14:47:22	18.98	17.32	15.83	3.14	C$_p$
12784	19:44:44.1	-14:45:22	18.53	17.04	15.92	2.60	C$_p$
11273	19:44:44.2	-14:46:47	17.63	16.47	15.72	1.90	C$_p$
10968	19:44:44.5	-14:48:46	19.14	17.27	15.89	3.25	C$_p$

Continued on Next Page...

Table A.1 – Continued

Name	α(2000)	δ(2000)	J	H	K_S	J-K$_S$	Sp
10876	19:44:46.0	-14:49:21	17.70	16.40	15.50	2.19	C$_p$
12660	19:44:46.2	-14:46:10	18.40	16.84	15.55	2.85	C$_p$
11059	19:44:46.6	-14:48:05	18.44	16.96	15.83	2.61	C$_p$
10917	19:44:46.7	-14:49:04	17.47	16.16	15.30	2.17	C$_p$
10152	19:44:46.7	-14:49:05	16.32	15.25	14.71	1.61	C$_p$
10261	19:44:47.1	-14:50:53	17.28	16.14	15.52	1.77	C$_p$
10400	19:44:47.2	-14:48:23	17.03	15.79	15.01	2.02	C$_p$
11296	19:44:47.2	-14:46:35	18.18	16.81	15.70	2.48	C$_p$
12208	19:44:47.4	-14:48:24	18.02	16.73	15.69	2.34	C$_p$
10408	19:44:47.5	-14:48:13	16.92	15.76	15.11	1.81	C$_p$
10635	19:44:47.6	-14:51:35	17.92	16.67	15.80	2.13	C$_p$
10817	19:44:47.7	-14:49:50	17.66	16.71	16.00	1.66	C$_p$
11665	19:44:47.7	-14:51:25	19.13	17.68	16.24	2.89	C$_p$
10249	19:44:48.2	-14:51:14	17.51	16.40	15.67	1.84	C$_p$
11021	19:44:48.3	-14:48:21	17.53	16.40	15.74	1.79	C$_p$
13364	19:44:48.3	-14:49:22	18.29	16.99	15.96	2.33	C$_p$
10343	19:44:48.5	-14:49:07	17.32	16.11	15.43	1.89	C$_p$
10310	19:44:48.8	-14:49:47	18.34	16.81	15.63	2.71	C$_p$
11335	19:44:48.9	-14:46:21	17.51	16.28	15.41	2.11	C$_p$
11391	19:44:49.6	-14:45:47	18.45	16.93	15.81	2.64	C$_p$
10809	19:44:49.7	-14:49:54	18.08	16.89	16.12	1.95	C$_p$
11403	19:44:50.4	-14:45:40	18.42	17.17	16.31	2.11	C$_p$
10838	19:44:50.5	-14:49:36	17.54	16.42	15.86	1.68	C$_p$
11401	19:44:50.6	-14:45:41	18.08	16.71	15.70	2.38	C$_p$
11305	19:44:51.0	-14:46:31	17.91	16.54	15.39	2.52	C$_p$
10501	19:44:51.9	-14:46:24	17.99	16.54	15.47	2.52	C$_p$
10753	19:44:51.9	-14:50:18	18.45	17.13	15.98	2.47	C$_p$
20542	19:44:52.1	-14:42:37	17.88	16.75	16.03	1.85	C$_p$
11991	19:44:52.2	-14:49:22	18.46	17.17	16.13	2.33	C$_p$
11271	19:44:53.1	-14:46:49	17.44	16.26	15.56	1.88	C$_p$
20657	19:44:53.3	-14:39:09	17.84	16.49	15.46	2.38	C$_p$
20547	19:44:53.5	-14:42:32	17.38	16.27	15.68	1.70	C$_p$
10356	19:44:53.6	-14:48:56	17.01	15.84	15.20	1.82	C$_p$
20375	19:44:54.2	-14:44:53	18.13	16.71	15.65	2.48	C$_p$
10371	19:44:54.3	-14:48:43	17.29	15.94	15.01	2.29	C$_p$
11140	19:44:54.3	-14:47:36	18.51	17.00	15.72	2.80	C$_p$
20417	19:44:54.4	-14:44:25	18.06	16.66	15.35	2.71	C$_p$
10859	19:44:54.4	-14:49:29	17.67	16.55	15.92	1.75	C$_p$
11132	19:44:54.6	-14:47:40	17.66	16.65	16.06	1.60	C$_p$
21234	19:44:54.9	-14:40:26	20.05	18.12	16.33	3.73	C$_p$
21671	19:44:55.0	-14:43:13	19.41	17.55	15.97	3.44	C$_p$

Continued on Next Page...

Table A.1 – Continued

Name	α(2000)	δ(2000)	J	H	K_S	J-K$_S$	Sp
20399	19:44:55.2	-14:44:36	17.72	16.57	15.76	1.95	C$_p$
14105	19:44:56.0	-14:45:28	19.19	17.46	16.03	3.16	C$_p$
12496	19:44:56.0	-14:47:06	18.19	16.82	15.75	2.44	C$_p$
20539	19:44:56.1	-14:42:41	17.92	16.60	15.54	2.39	C$_p$
20428	19:44:56.1	-14:44:14	17.49	16.34	15.59	1.90	C$_p$
20774	19:44:56.2	-14:44:53	18.69	17.78	16.89	1.81	C$_p$
11032	19:44:56.7	-14:48:16	18.12	16.85	15.90	2.23	C$_p$
10633	19:44:56.7	-14:51:38	18.56	17.56	16.85	1.71	C$_p$
20540	19:44:56.7	-14:42:38	17.97	16.97	16.41	1.55	C$_p$
20438	19:44:57.3	-14:44:05	19.17	17.47	15.95	3.22	C$_p$
10807	19:44:57.7	-14:49:55	20.22	18.25	16.08	4.14	C$_p$
21316	19:44:57.7	-14:38:33	18.65	17.48	16.42	2.22	C$_p$
20439	19:44:57.7	-14:44:05	18.89	17.11	15.59	3.31	C$_p$
12711	19:44:58.1	-14:45:51	18.93	17.68	16.79	2.14	C$_p$
12400	19:44:58.1	-14:47:38	18.13	16.80	15.90	2.23	C$_p$
11139	19:44:58.3	-14:47:37	17.99	16.63	15.65	2.33	C$_p$
20195	19:44:58.9	-14:44:43	17.11	16.01	15.42	1.70	C$_p$
10330	19:44:58.9	-14:49:27	17.33	16.16	15.52	1.81	C$_p$
13293	19:44:59.0	-14:49:50	20.47	18.53	16.46	4.01	C$_p$
10439	19:44:59.1	-14:47:38	17.33	16.09	15.38	1.95	C$_p$
20614	19:44:59.1	-14:40:50	18.88	17.55	16.26	2.62	C$_p$
10412	19:44:59.3	-14:48:10	17.33	16.06	15.19	2.14	C$_p$
13390	19:44:59.3	-14:49:16	19.99	18.33	16.73	3.26	C$_p$
21217	19:44:59.7	-14:40:41	17.75	16.81	16.25	1.51	C$_p$
10411	19:45:00.2	-14:48:09	16.91	15.81	15.23	1.69	C$_p$
21029	19:45:00.5	-14:43:06	19.23	17.41	15.71	3.52	C$_p$
12466	19:45:00.5	-14:47:19	18.41	17.10	16.00	2.41	C$_p$
10460	19:45:00.6	-14:47:17	17.32	16.24	15.65	1.67	C$_p$
10743	19:45:00.6	-14:50:23	17.60	16.45	15.69	1.91	C$_p$
11372	19:45:00.8	-14:46:03	17.53	16.46	15.70	1.83	C$_p$
20311	19:45:01.1	-14:39:59	17.21	16.17	15.53	1.68	C$_p$
20608	19:45:01.6	-14:40:57	19.01	17.59	16.01	3.00	C$_p$
10200	19:45:01.7	-14:46:00	16.49	15.32	14.62	1.86	C$_p$
20569	19:45:01.8	-14:41:52	19.18	17.70	16.09	3.09	C$_p$
10850	19:45:02.1	-14:49:33	17.86	16.67	15.90	1.96	C$_p$
12177	19:45:02.3	-14:48:32	20.41	17.93	15.94	4.47	C$_p$
20496	19:45:02.4	-14:43:26	17.36	16.27	15.65	1.71	C$_p$
20239	19:45:02.4	-14:43:32	17.95	16.65	15.64	2.31	C$_p$
21419	19:45:02.6	-14:44:57	19.69	18.07	16.44	3.25	C$_p$
20558	19:45:02.6	-14:42:10	18.19	16.62	15.30	2.89	C$_p$
20213	19:45:03.0	-14:44:16	18.18	16.78	15.45	2.72	C$_p$

Continued on Next Page...

Table A.1 – Continued

Name	α(2000)	δ(2000)	J	H	K_S	J-K$_S$	Sp
20784	19:45:03.0	-14:44:49	20.46	18.39	16.36	4.10	C$_p$
11633	19:45:03.2	-14:51:42	20.03	18.70	17.06	2.97	C$_p$
11210	19:45:03.6	-14:47:13	17.49	16.42	15.56	1.93	C$_p$
20363	19:45:03.7	-14:45:01	17.59	16.54	15.97	1.62	C$_p$
10293	19:45:04.0	-14:50:11	17.83	16.31	15.33	2.50	C$_p$
20578	19:45:04.0	-14:41:47	17.86	16.72	16.10	1.76	C$_p$
11238	19:45:04.2	-14:47:01	17.73	16.58	15.83	1.91	C$_p$
30928	19:45:04.6	-14:54:36	19.11	17.51	16.33	2.78	C$_p$
30285	19:45:04.9	-14:52:41	16.98	15.89	15.22	1.77	C$_p$
30611	19:45:04.9	-14:52:04	18.24	16.96	16.06	2.19	C$_p$
30244	19:45:05.3	-14:54:14	17.38	16.17	15.44	1.94	C$_p$
30271	19:45:05.3	-14:53:11	16.66	15.55	14.93	1.72	C$_p$
20182	19:45:05.5	-14:45:02	17.11	15.90	15.07	2.04	C$_p$
20356	19:45:05.5	-14:45:04	19.54	17.45	15.67	3.87	C$_p$
31168	19:45:06.1	-14:52:13	19.06	17.18	15.60	3.46	C$_p$
30924	19:45:06.1	-14:54:39	19.36	17.49	16.22	3.14	C$_p$
30767	19:45:06.5	-14:57:42	18.05	17.08	16.44	1.61	C$_p$
30268	19:45:06.6	-14:53:17	16.46	15.16	14.19	2.27	C$_p$
30920	19:45:06.7	-14:54:42	19.27	17.47	16.04	3.22	C$_p$
20588	19:45:06.9	-14:41:29	17.66	16.37	15.34	2.32	C$_p$
10609	19:45:06.9	-14:51:54	17.45	16.42	15.85	1.60	C$_p$
31328	19:45:07.0	-14:50:51	18.29	17.38	16.77	1.53	C$_p$
21141	19:45:07.0	-14:41:51	17.91	16.53	15.21	2.70	C$_p$
10599	19:45:07.4	-14:52:00	18.02	16.79	15.90	2.12	C$_p$
10597	19:45:07.5	-14:52:01	17.67	16.72	16.13	1.54	C$_p$
40538	19:45:07.8	-14:45:05	17.28	16.52	15.93	1.35	O$_p$
12790	19:45:08.1	-14:45:19	18.01	17.09	16.57	1.43	O$_p$
11226	19:45:08.2	-14:47:05	17.43	16.47	16.02	1.41	O$_p$
11794	19:45:08.5	-14:50:34	17.78	16.84	16.43	1.35	O$_p$
11884	19:45:08.6	-14:50:03	18.12	17.24	17.07	1.05	O$_p$
12070	19:45:08.9	-14:48:58	17.48	16.93	15.99	1.49	O$_p$
21302	19:45:09.0	-14:38:54	17.77	17.14	16.84	0.93	O$_p$
12557	19:45:09.0	-14:46:49	18.24	17.50	17.09	1.15	O$_p$
10935	19:45:09.1	-14:49:00	17.49	16.55	16.13	1.36	O$_p$
12477	19:45:09.3	-14:47:15	17.92	17.21	17.07	0.85	O$_p$
11637	19:45:09.7	-14:51:43	18.15	17.24	17.04	1.11	O$_p$
12191	19:45:09.8	-14:48:28	17.82	17.04	16.70	1.12	O$_p$
11820	19:45:10.4	-14:50:24	18.26	17.38	17.09	1.17	O$_p$
20367	19:45:10.8	-14:45:00	17.78	16.93	16.52	1.26	O$_p$
11626	19:45:11.0	-14:51:44	18.01	17.03	16.75	1.26	O$_p$
20463	19:45:11.0	-14:43:45	17.85	16.81	16.49	1.36	O$_p$

Continued on Next Page...

Table A.1 – Continued

Name	α(2000)	δ(2000)	J	H	K_S	J-K$_S$	Sp
10615	19:45:11.2	-14:51:50	17.75	16.82	16.45	1.30	O$_p$
21238	19:45:11.5	-14:40:21	17.90	17.26	16.98	0.92	O$_p$
20357	19:45:11.5	-14:45:05	17.31	16.54	15.96	1.36	O$_p$
20359	19:45:11.7	-14:45:03	17.11	16.30	15.82	1.29	O$_p$
11131	19:45:11.7	-14:47:41	17.57	16.53	16.27	1.30	O$_p$
30478	19:45:11.7	-14:54:32	17.56	16.94	16.57	0.99	O$_p$
20726	19:45:11.7	-14:45:13	18.25	17.48	17.12	1.12	O$_p$
11034	19:45:11.8	-14:48:16	17.31	16.40	16.22	1.09	O$_p$
11349	19:45:11.8	-14:46:16	17.47	16.48	16.08	1.39	O$_p$
20707	19:45:11.8	-14:37:31	17.48	16.44	16.35	1.13	O$_p$
31373	19:45:11.8	-14:58:19	18.10	17.31	17.08	1.02	O$_p$
31332	19:45:11.9	-14:50:49	18.20	17.38	17.10	1.10	O$_p$
21157	19:45:12.1	-14:41:33	18.04	17.59	17.07	0.97	O$_p$
31370	19:45:12.1	-14:58:21	18.20	17.17	17.12	1.08	O$_p$

Appendix B

Potential large amplitude variables observed less than 10 times in NGC 6822

Name	α(2000)	δ(2000)	J	H	K_S	J-K_S	NK
30734	19:44:55.2	-14:50:51	18.62	17.74	15.26	3.37	1
30583	19:45:12.0	-14:52:43	18.48	17.01	15.87	2.61	9
30720	19:45:12.3	-14:52:07	18.70	17.89	14.87	3.83	2
30961	19:45:12.4	-14:54:13	19.46	17.62	15.98	3.49	7
12287	19:45:12.7	-14:48:05	18.34	17.10	16.16	2.18	8
20840	19:45:12.8	-14:44:30	18.66	17.00	15.89	2.77	8
21517	19:45:13.1	-14:44:23	18.38	17.37	16.25	2.13	6

Appendix C

Other red objects detected in NGC 6822

Name	α(2000)	δ(2000)	J	H	K_S	J-K$_S$
40356	19:44:41.2	-14:44:43	17.52	16.27	15.45	2.07
40007	19:44:41.4	-14:51:35	17.91	16.67	15.77	2.14
40500	19:44:42.0	-14:50:55	17.42	16.22	15.42	2.00
40476	19:44:48.5	-14:44:12	17.71	16.44	15.50	2.20
40419	19:44:48.8	-14:51:59	18.05	16.78	15.84	2.21
10370	19:44:49.5	-14:48:48	17.33	16.05	15.27	2.06
10496	19:44:51.4	-14:46:32	17.37	16.13	15.33	2.04
11200	19:44:51.6	-14:47:15	18.24	16.94	16.14	2.10
10957	19:44:51.7	-14:48:50	17.56	16.25	15.44	2.12
10943	19:44:52.0	-14:48:56	17.50	16.22	15.40	2.09
10455	19:44:52.9	-14:47:23	17.50	16.19	15.35	2.14
10406	19:44:54.3	-14:48:15	17.37	16.14	15.37	2.01
10936	19:44:54.8	-14:49:00	17.89	16.56	15.80	2.10
10374	19:44:54.8	-14:48:41	17.37	16.12	15.34	2.03
11392	19:44:55.2	-14:45:48	18.40	17.01	15.96	2.45
10448	19:44:55.4	-14:47:31	17.31	16.01	15.17	2.14
11187	19:44:55.8	-14:47:17	17.89	16.50	15.68	2.21
10756	19:44:56.1	-14:50:16	17.64	16.40	15.63	2.01
11364	19:44:56.6	-14:46:09	17.62	16.28	15.38	2.23
11173	19:44:56.6	-14:47:22	18.28	17.07	16.14	2.14
10391	19:44:57.3	-14:48:32	17.25	16.03	15.23	2.02
20236	19:44:57.4	-14:43:35	17.38	16.15	15.36	2.02
21021	19:44:57.8	-14:43:10	18.74	17.39	16.43	2.31
20892	19:44:57.9	-14:44:11	18.27	17.07	16.12	2.14
20215	19:44:58.2	-14:44:13	17.71	16.42	15.50	2.21

Continued on Next Page...

Table C.1 – Continued

Name	α(2000)	δ(2000)	J	H	K_S	J-K$_S$
11002	19:44:58.2	-14:48:31	17.83	16.60	15.78	2.06
10521	19:44:58.5	-14:45:54	17.28	16.06	15.26	2.01
12004	19:44:58.5	-14:49:16	18.81	17.55	16.73	2.08
12075	19:44:59.1	-14:48:57	19.87	17.78	17.60	2.27
21184	19:44:59.7	-14:41:11	18.48	17.22	16.30	2.18
20194	19:44:59.9	-14:44:43	17.53	16.26	15.44	2.09
10422	19:45:00.4	-14:48:00	17.01	15.75	14.98	2.03
10384	19:45:02.0	-14:48:34	17.43	16.15	15.37	2.06
11764	19:45:02.0	-14:50:46	18.75	17.48	16.52	2.23
20319	19:45:02.9	-14:39:04	17.63	16.37	15.45	2.18
20245	19:45:03.2	-14:43:26	17.15	15.88	15.06	2.09
21826	19:45:04.4	-14:41:09	19.13	18.08	17.11	2.02
30204	19:45:05.6	-14:55:36	17.28	16.03	15.27	2.01
30934	19:45:06.2	-14:54:31	18.04	16.90	15.53	2.51
31138	19:45:06.5	-14:52:29	18.60	17.24	16.28	2.32
30511	19:45:07.7	-14:53:48	17.59	16.30	15.44	2.15
12080	19:45:10.3	-14:48:57	19.86	17.15	17.04	2.82

Appendix D

Phased K light curves for Miras in NGC 6822

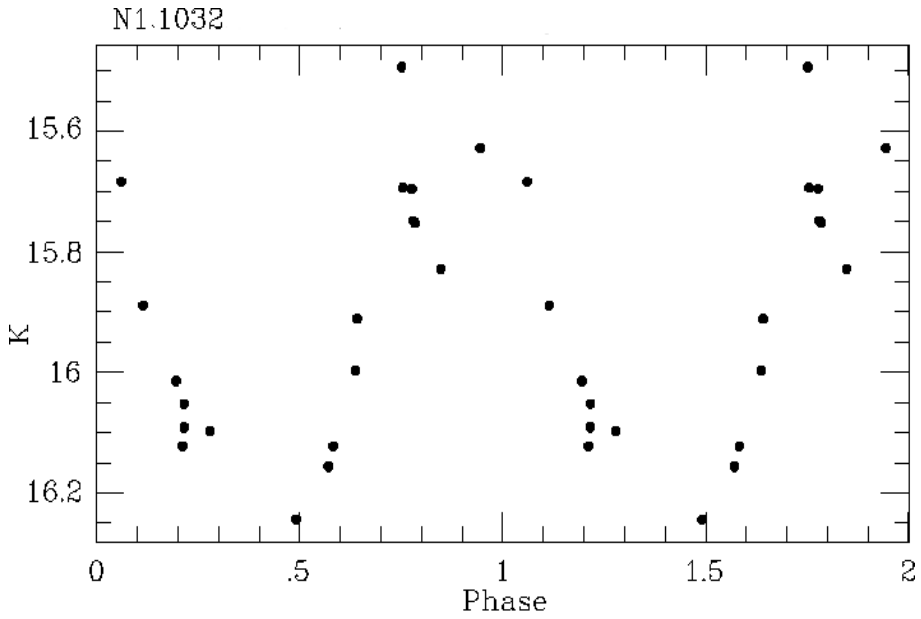

Figure D.1: Phased K light curve for 11032.

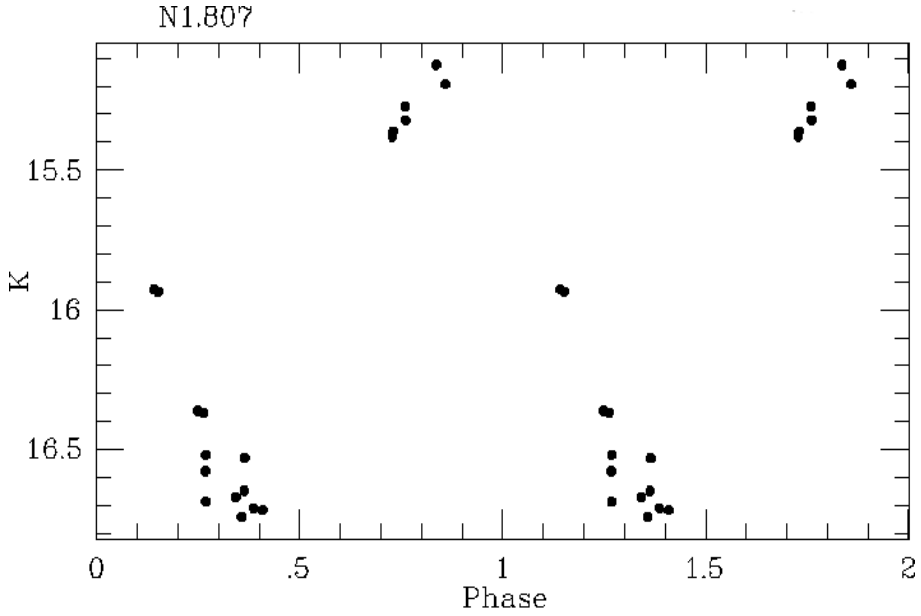

Figure D.2: Phased K light curve for 10807.

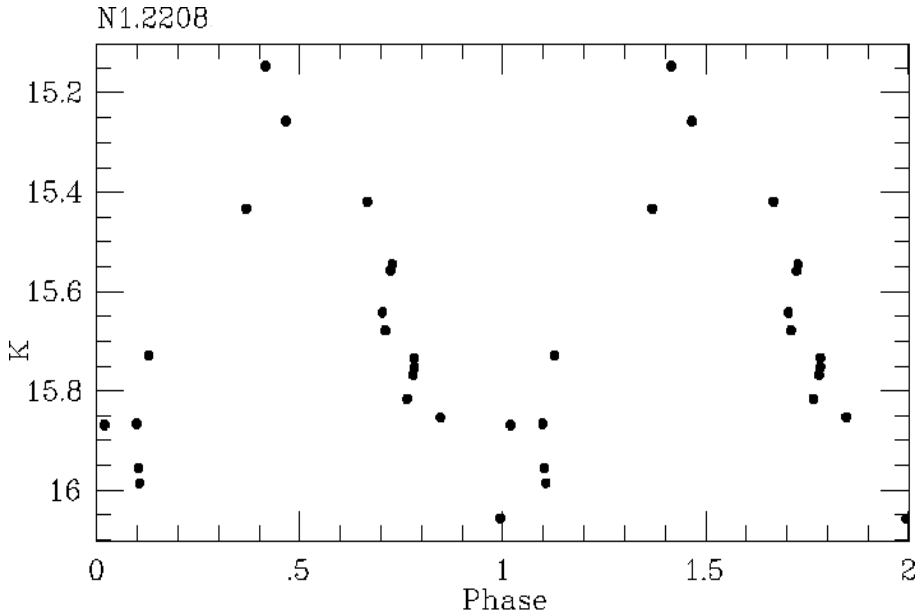

Figure D.3: Phased K light curve for 12208.

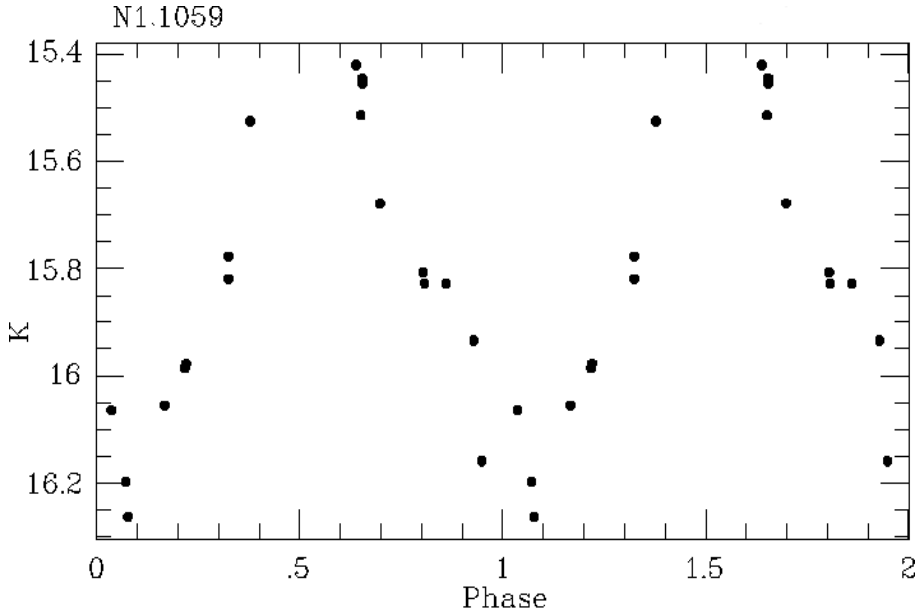

Figure D.4: Phased K light curve for 1059.

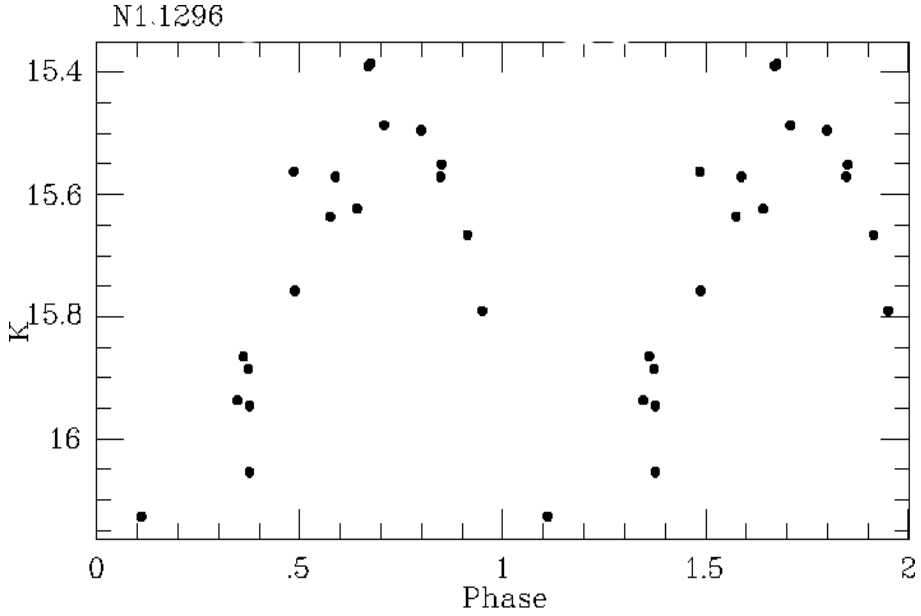

Figure D.5: Phased K light curve for 11296.

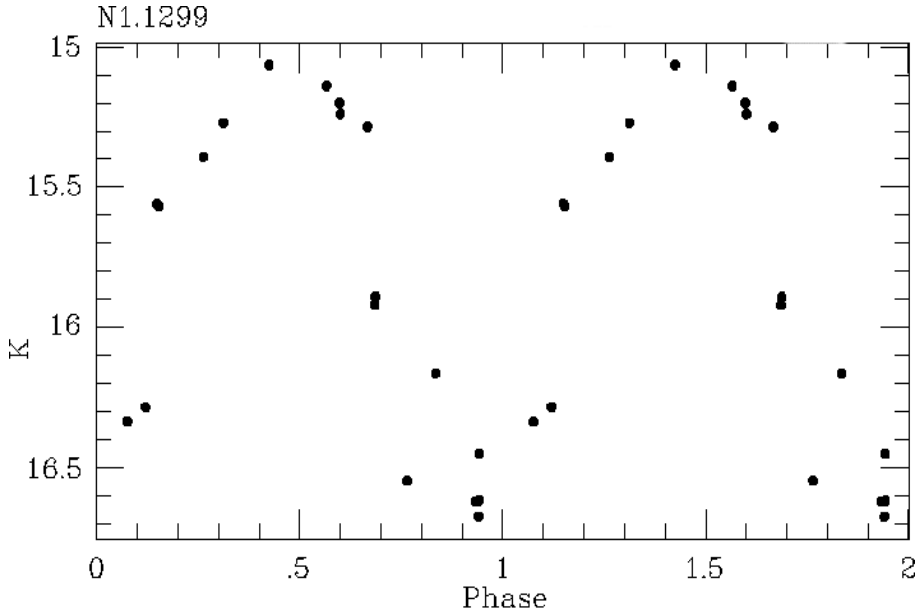

Figure D.6: Phased K light curve for 11299.

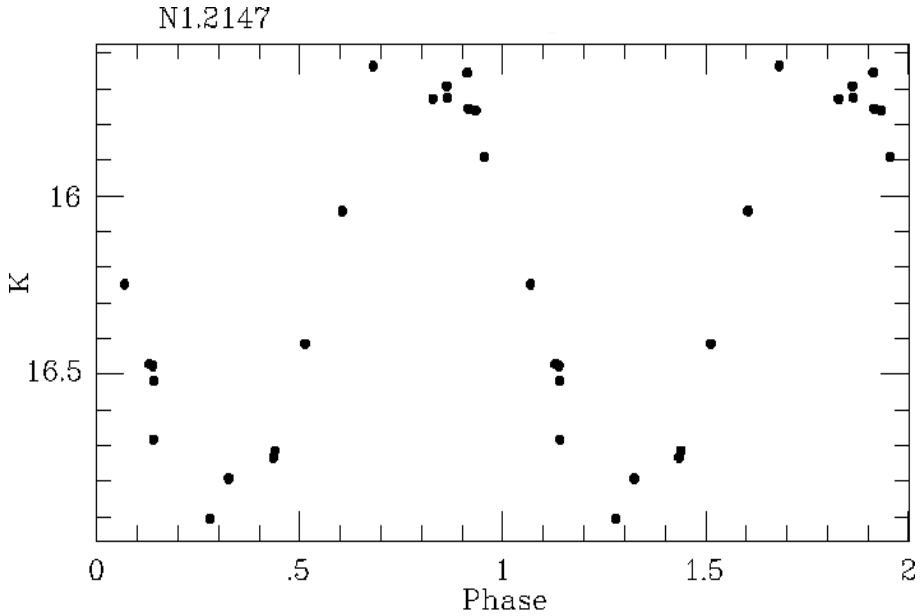

Figure D.7: Phased K light curve for 12147.

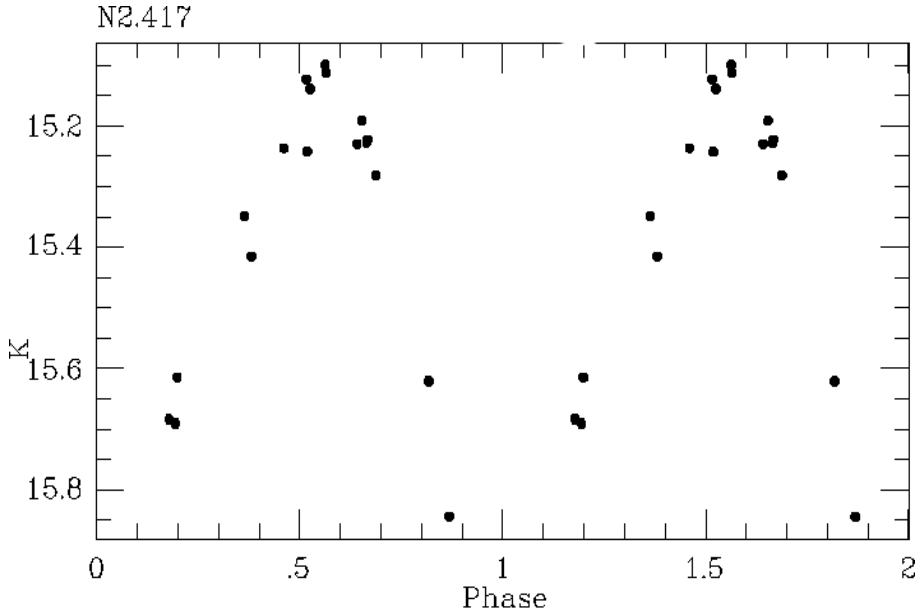

Figure D.8: Phased K light curve for 20417.

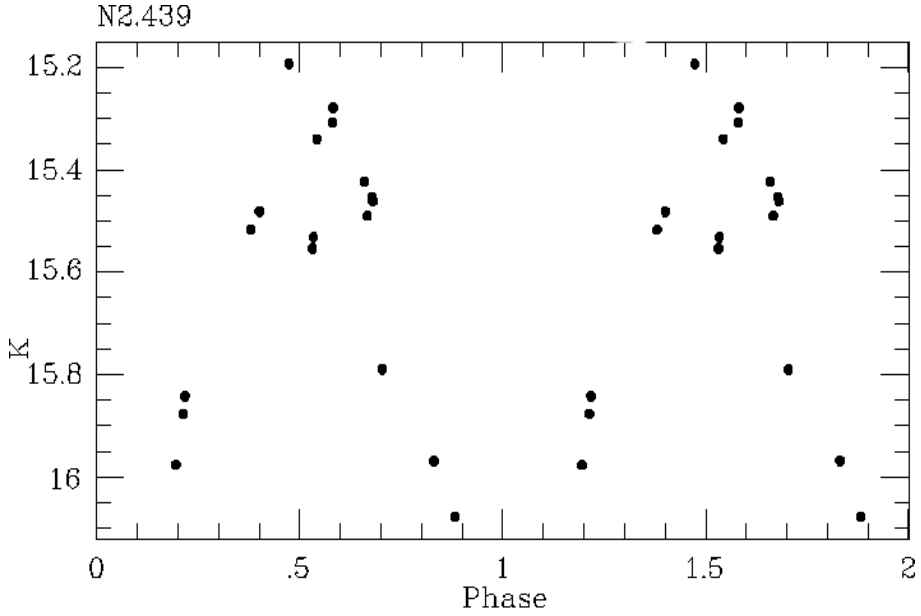

Figure D.9: Phased K light curve for 20439.

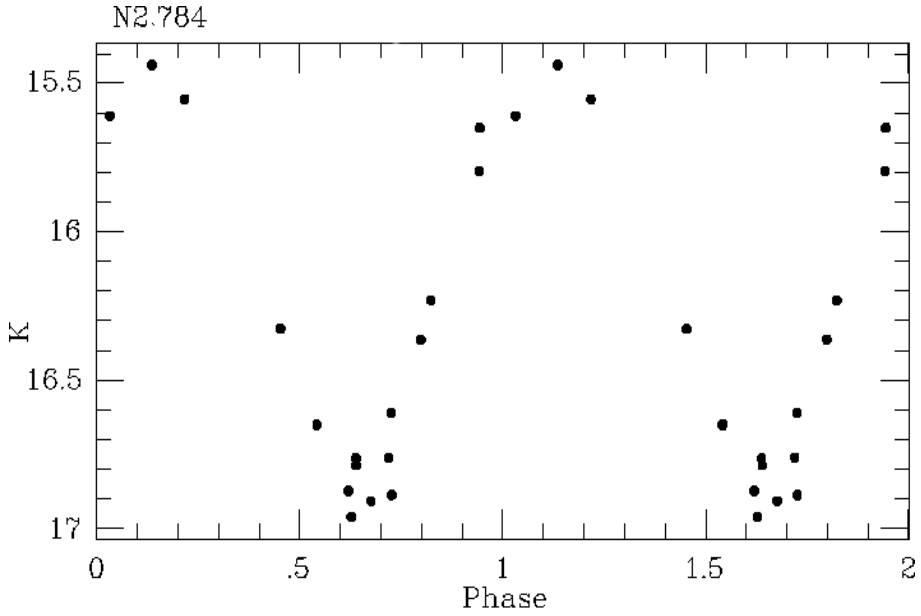

Figure D.10: Phased K light curve for 20784.

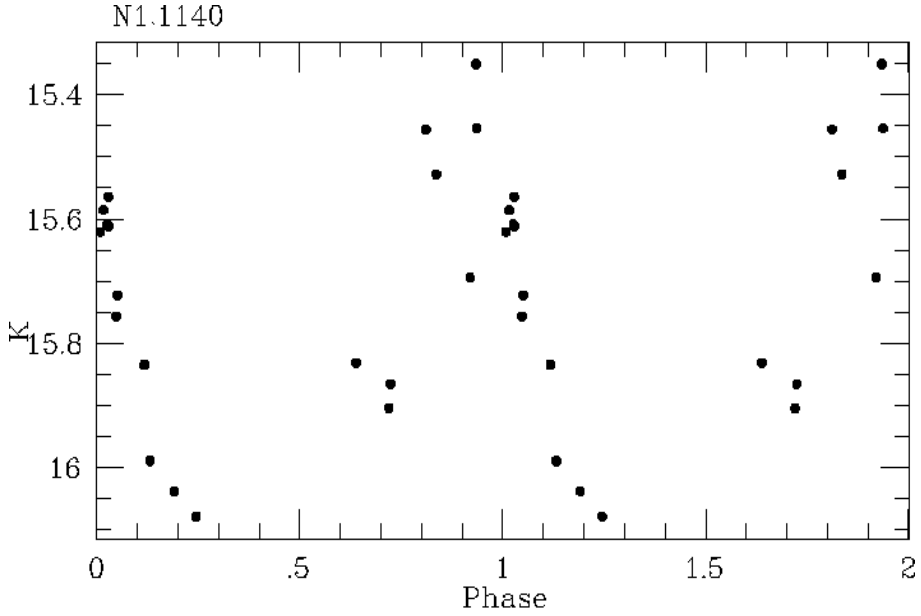

Figure D.11: Phased K light curve for 11140.

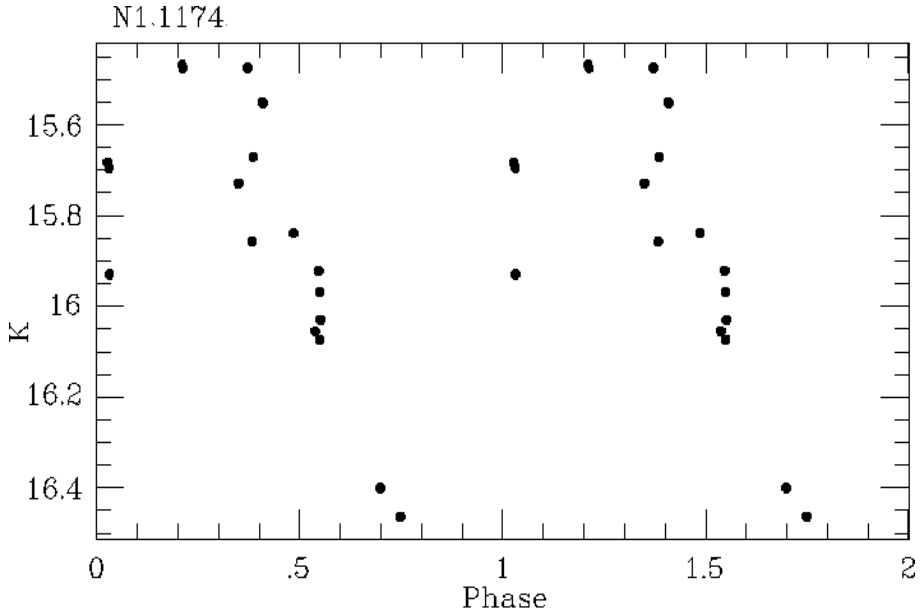

Figure D.12: Phased K light curve for 11174.

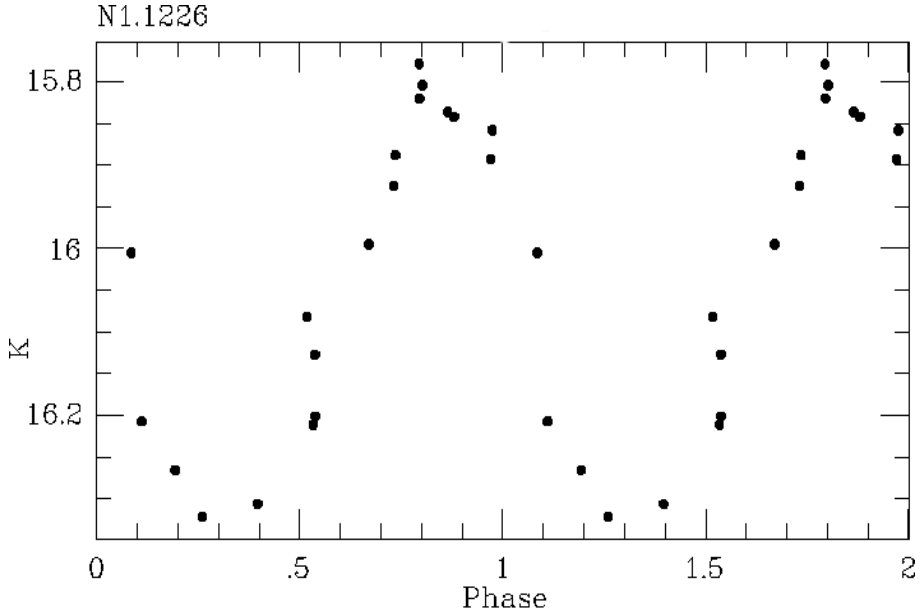

Figure D.13: Phased K light curve for 11226.

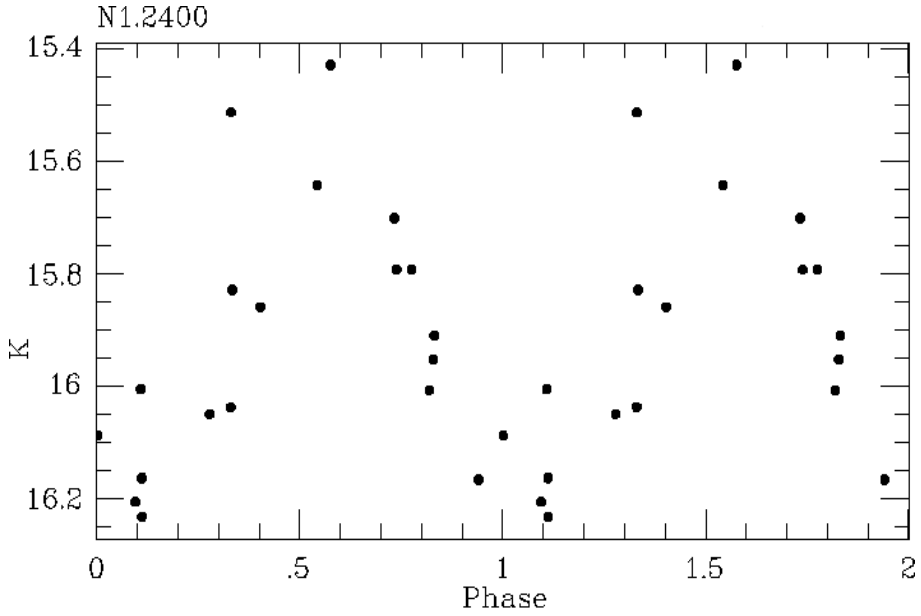

Figure D.14: Phased K light curve for 12400.

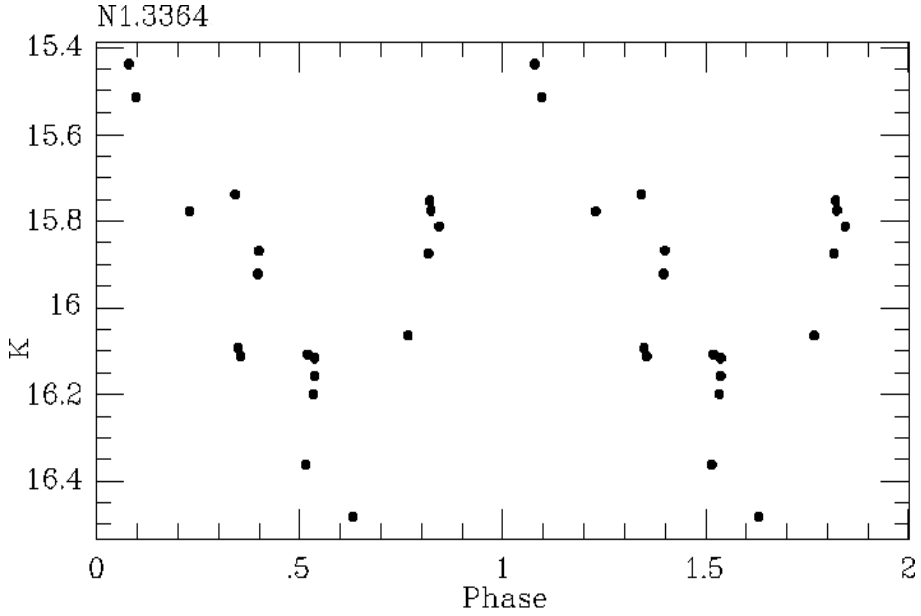

Figure D.15: Phased K light curve for 13364.

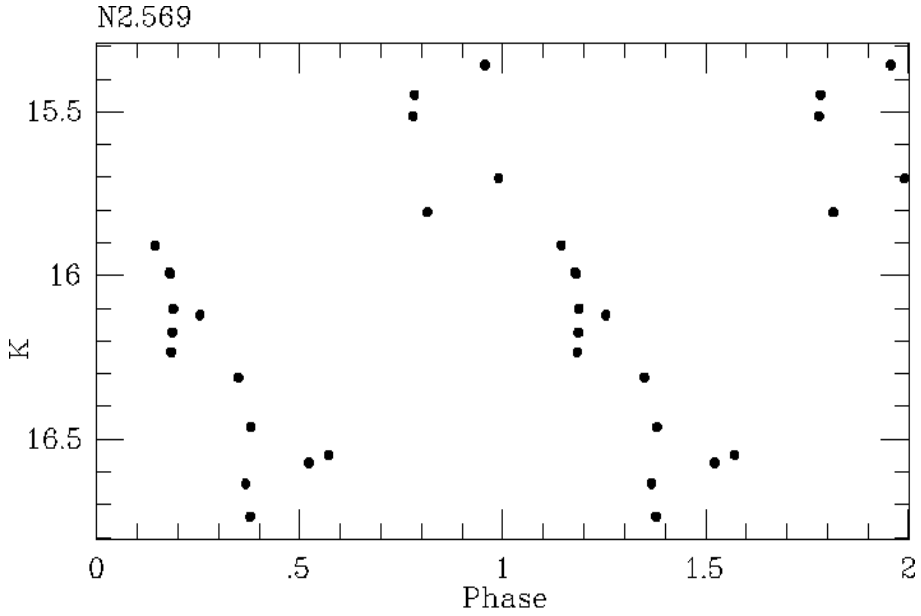

Figure D.16: Phased K light curve for 20569.

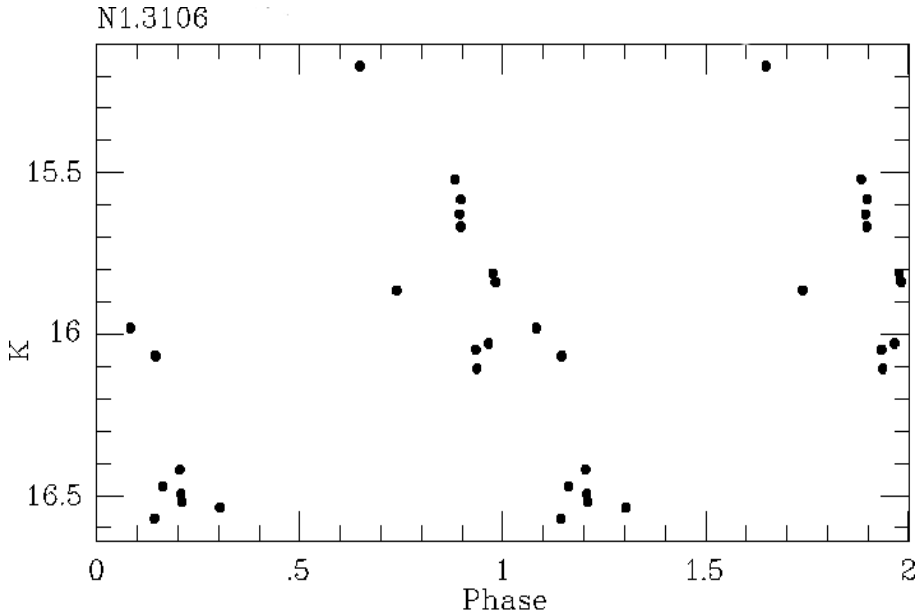

Figure D.17: Phased K light curve for 13106.

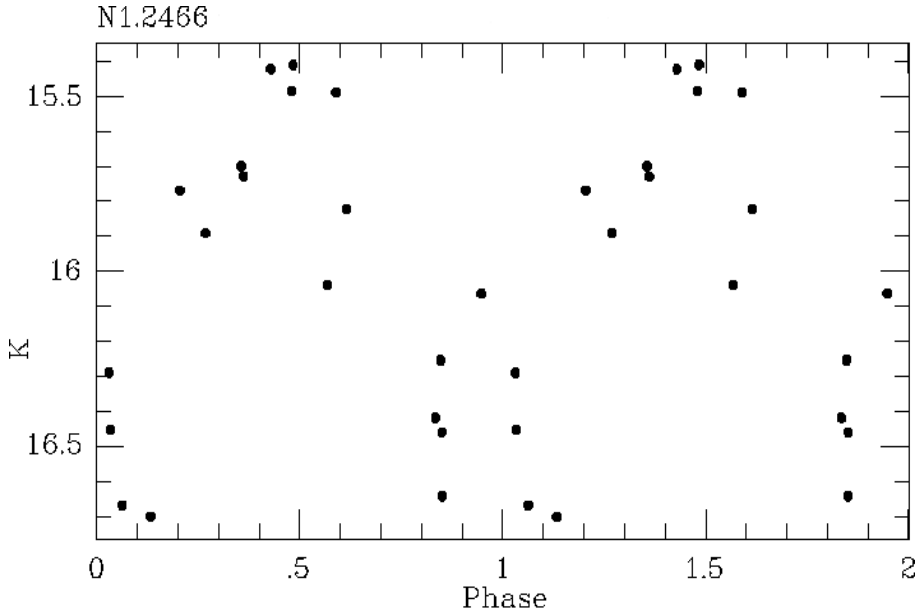

Figure D.18: Phased K light curve for 12466.

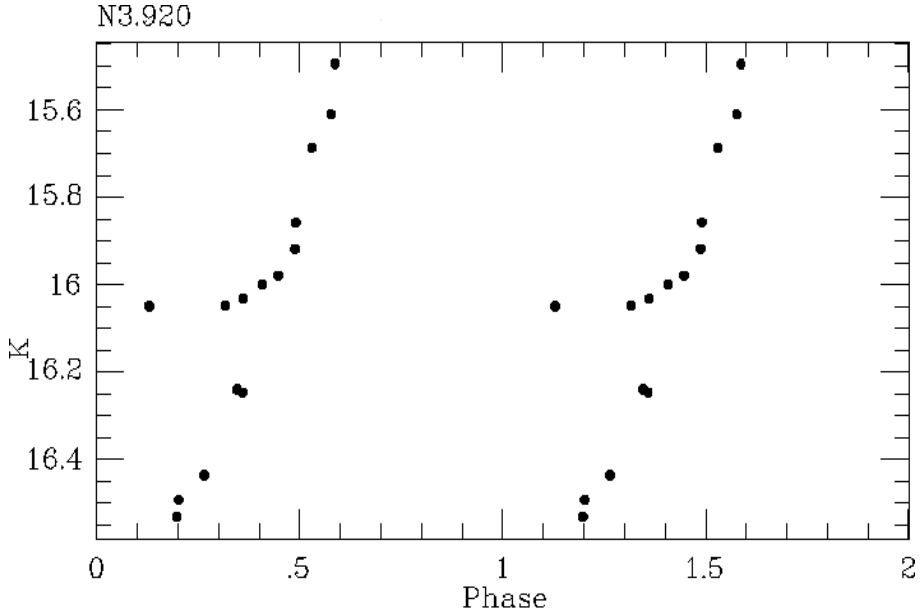

Figure D.19: Phased K light curve for 30920.

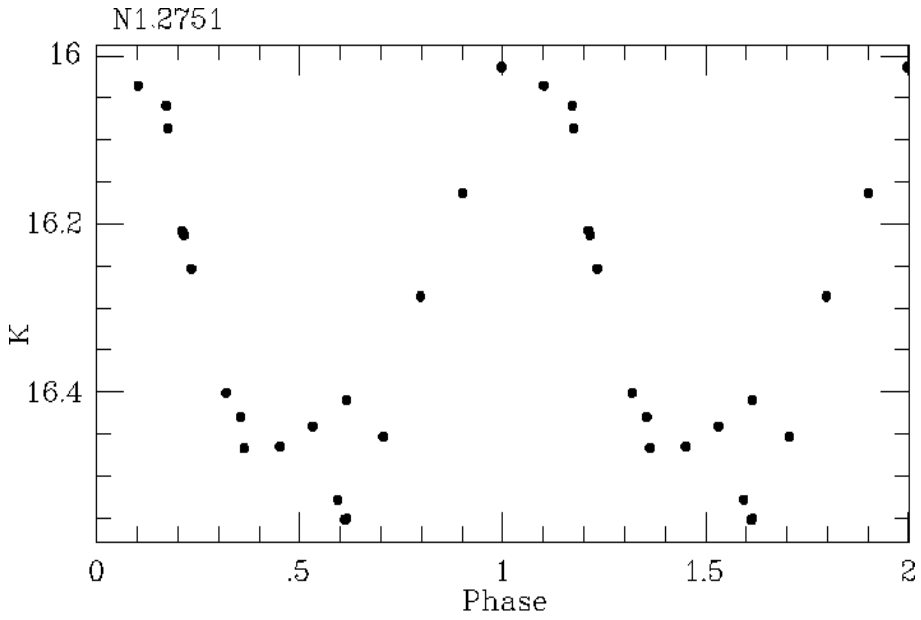

Figure D.20: Phased K light curve for 12751.

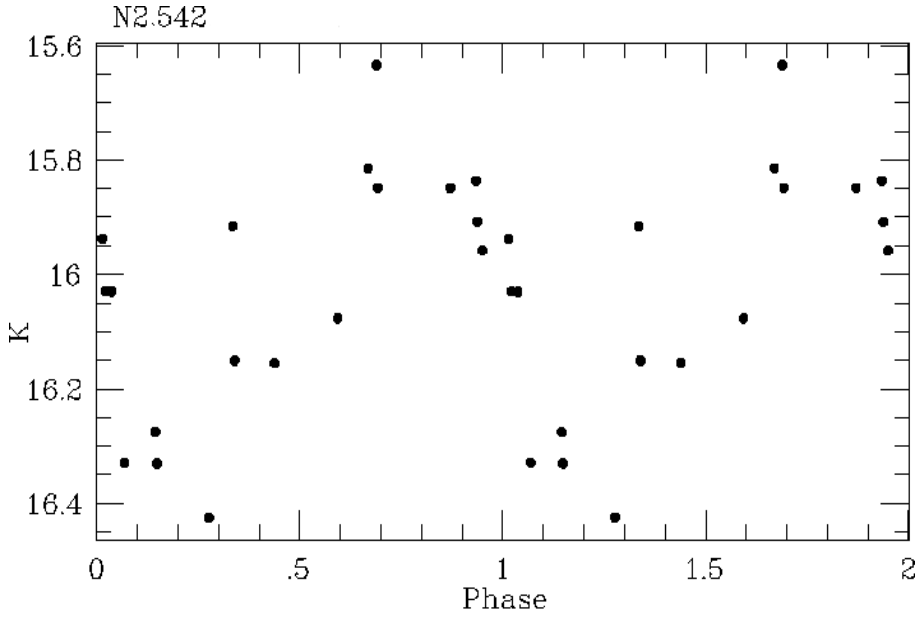

Figure D.21: Phased K light curve for 20542.

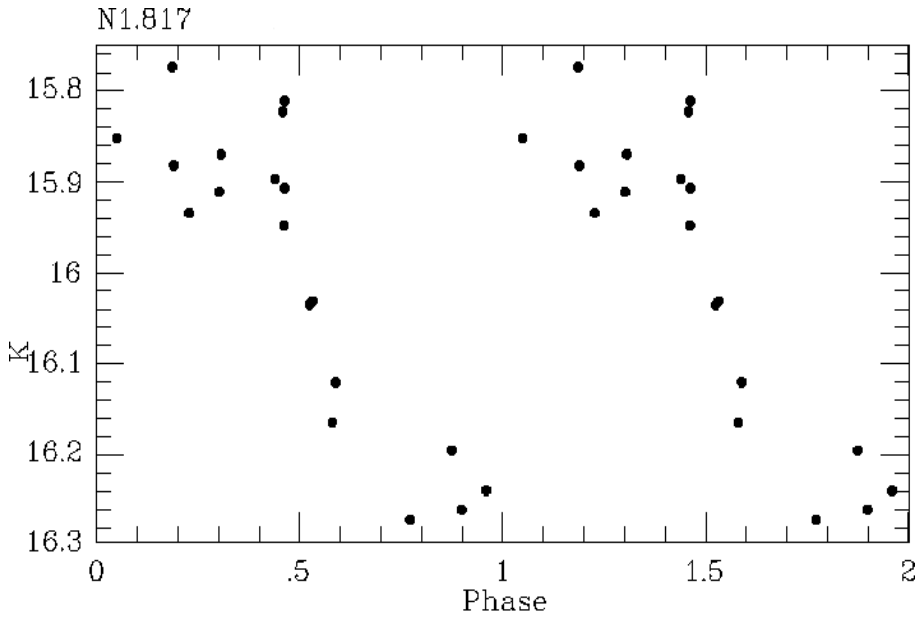

Figure D.22: Phased K light curve for 10817.

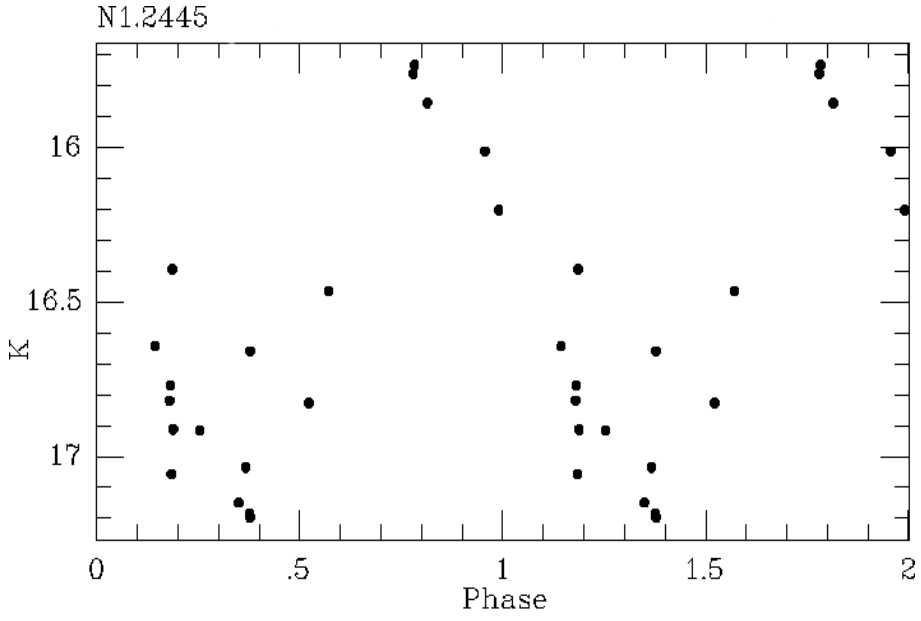

Figure D.23: Phased K light curve for 12445.

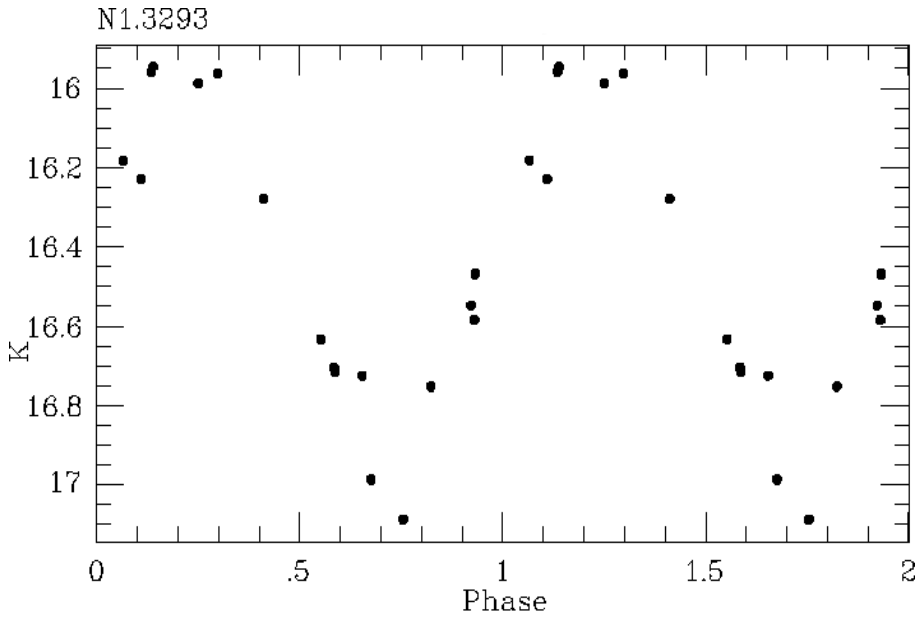

Figure D.24: Phased K light curve for 13293.

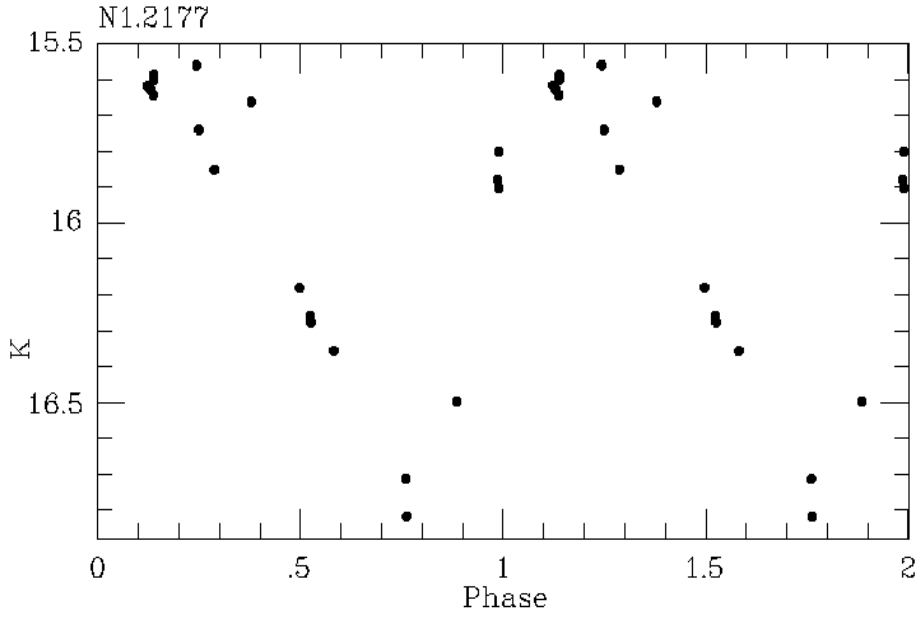

Figure D.25: Phased K light curve for 12177.

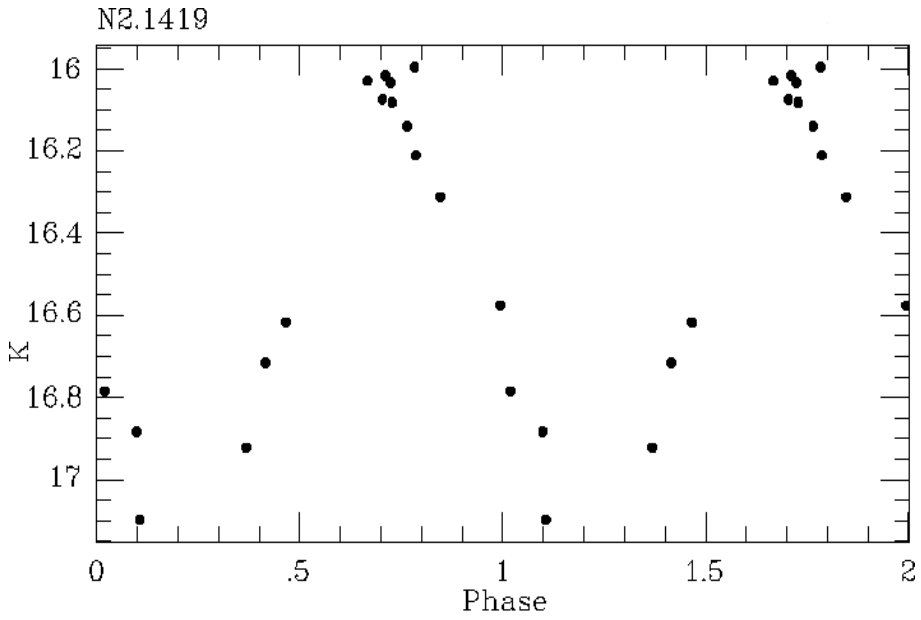

Figure D.26: Phased K light curve for 21419.

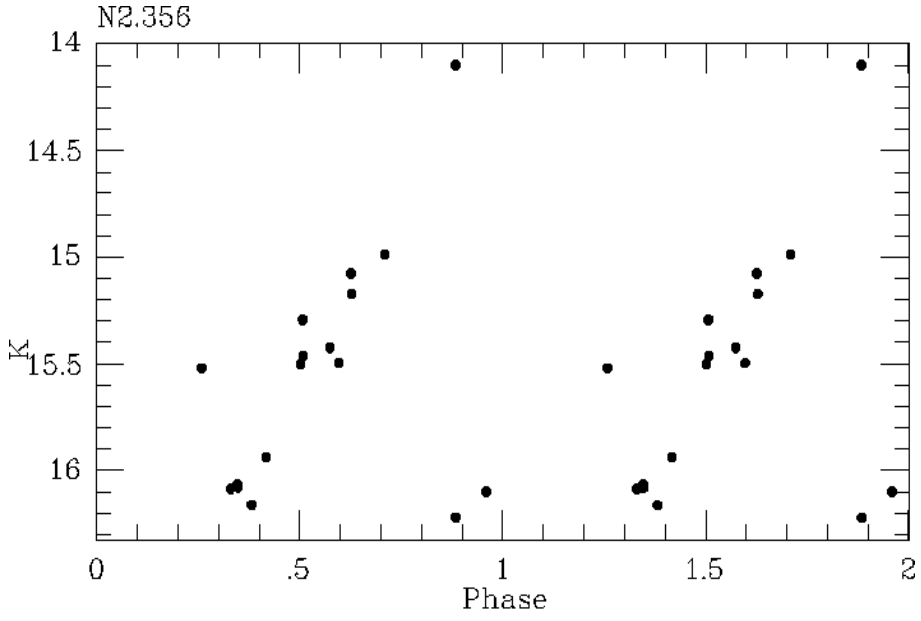

Figure D.27: Phased K light curve for 20356.

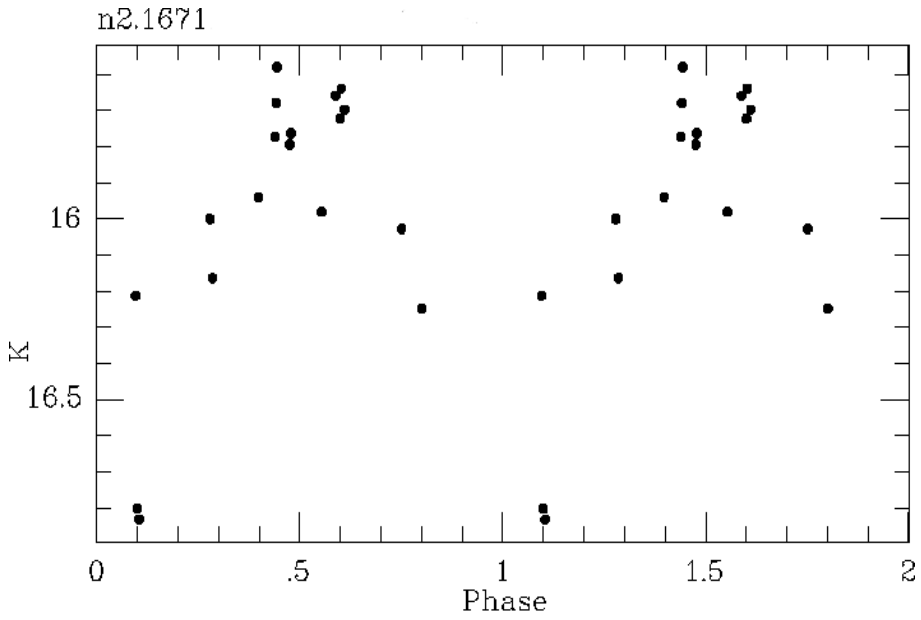

Figure D.28: Phased K light curve for 21671.

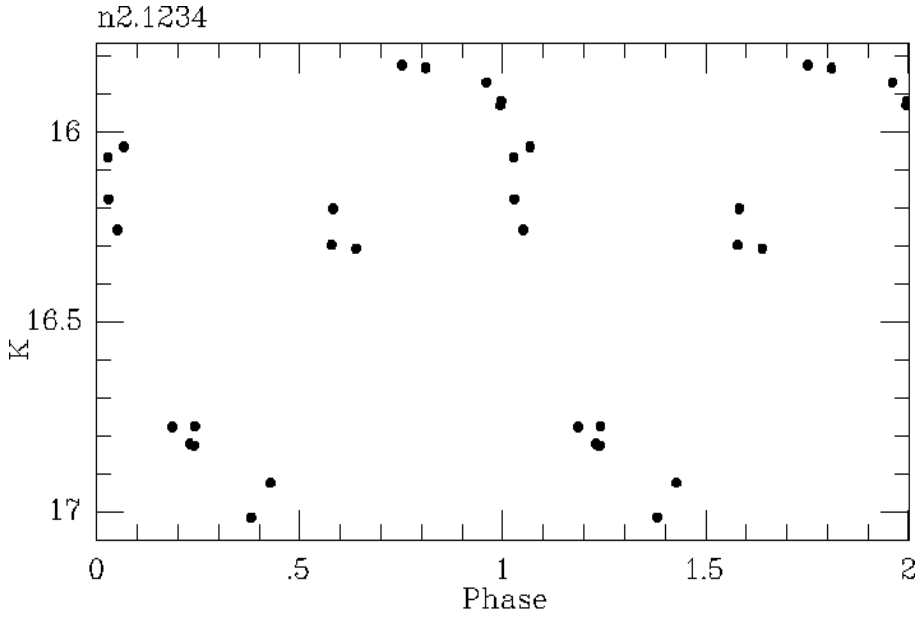

Figure D.29: Phased K light curve for 21234.

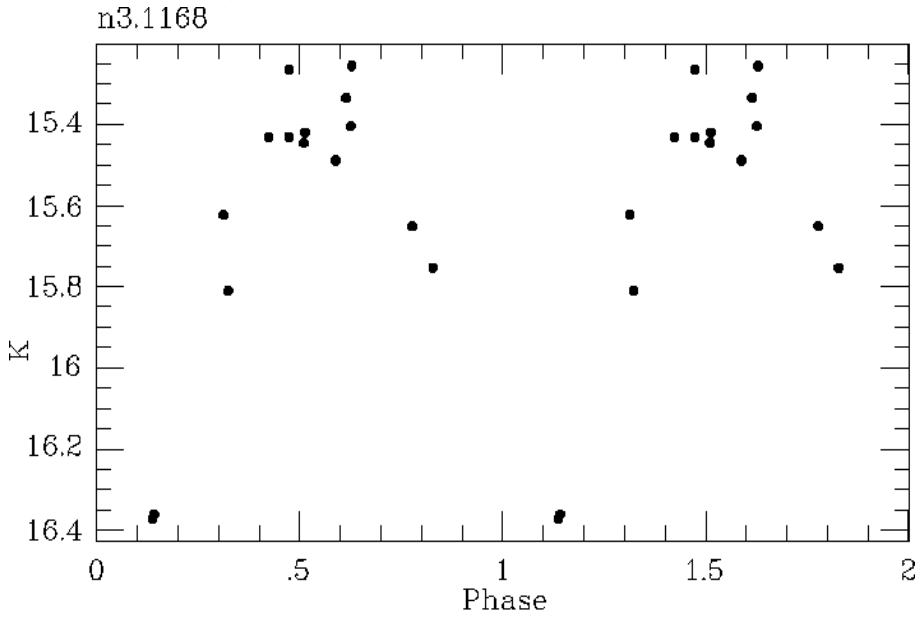

Figure D.30: Phased K light curve for 31168.

Appendix E

Phased K light curves for SRs in NGC 6822

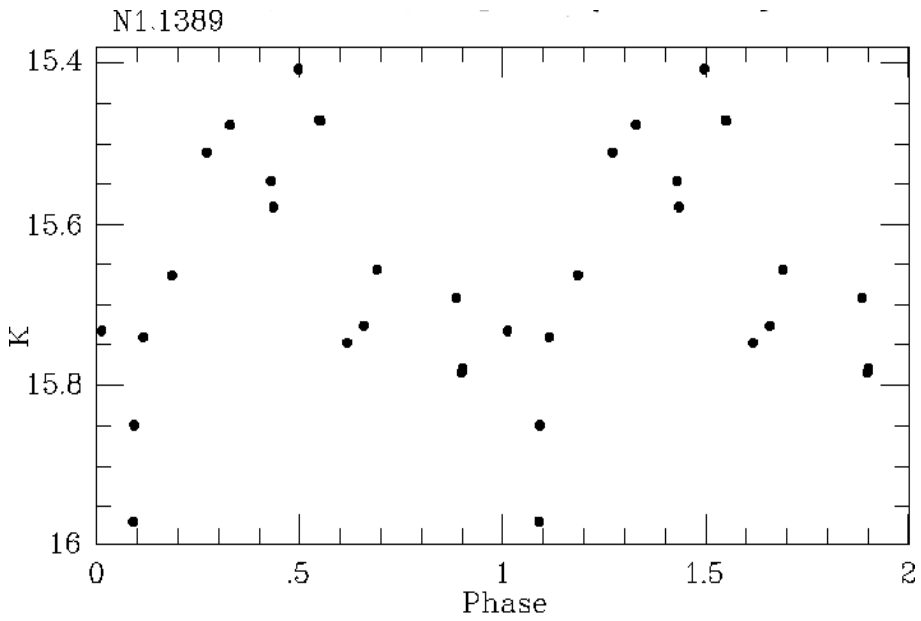

Figure E.1: Phased K light curve for 11389.

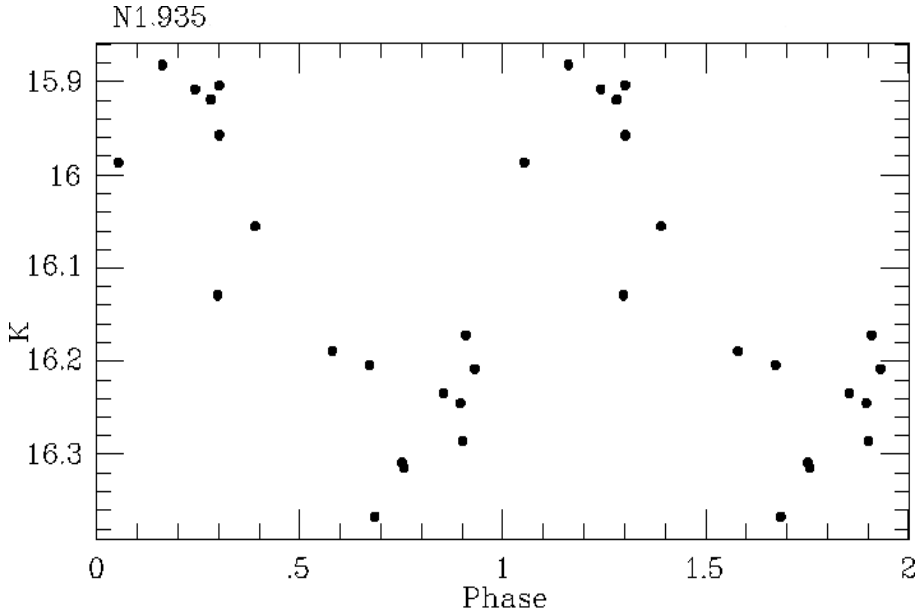

Figure E.2: Phased K light curve for 10935.

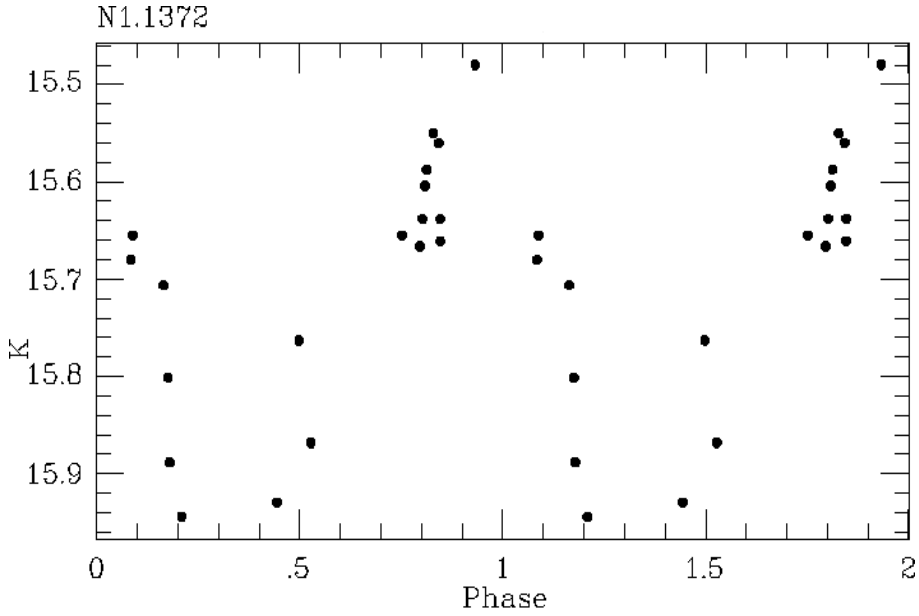

Figure E.3: Phased K light curve for 11372.

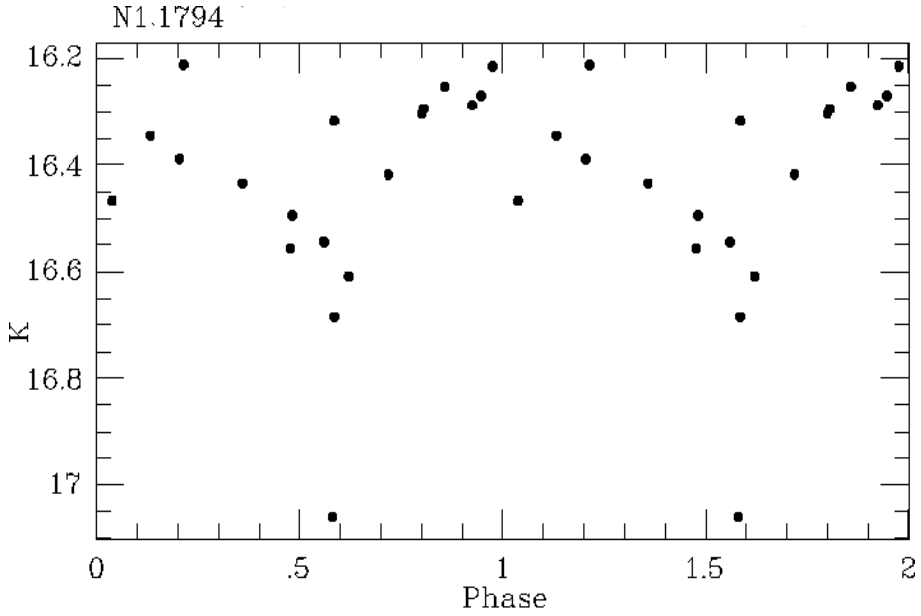

Figure E.4: Phased K light curve for 11794.

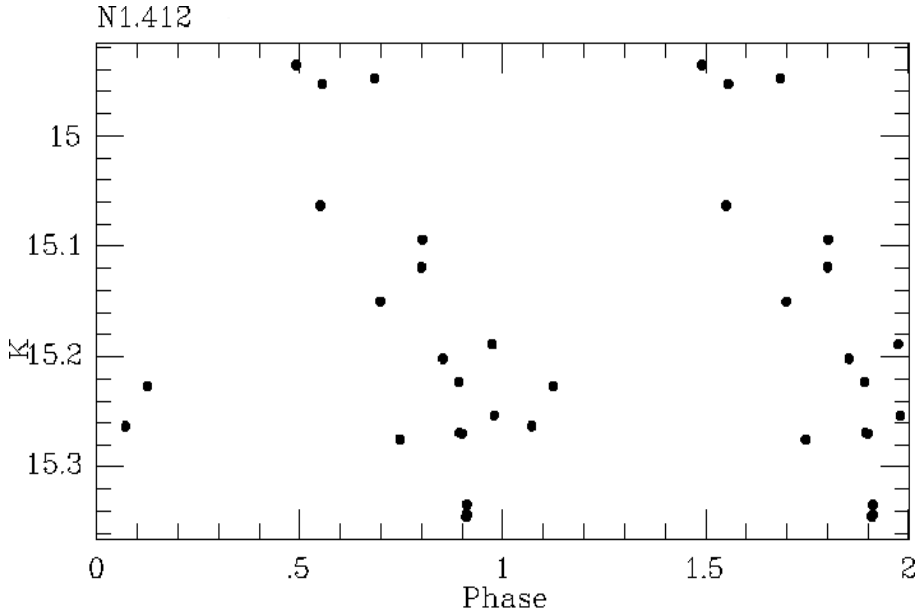

Figure E.5: Phased K light curve for 10412.

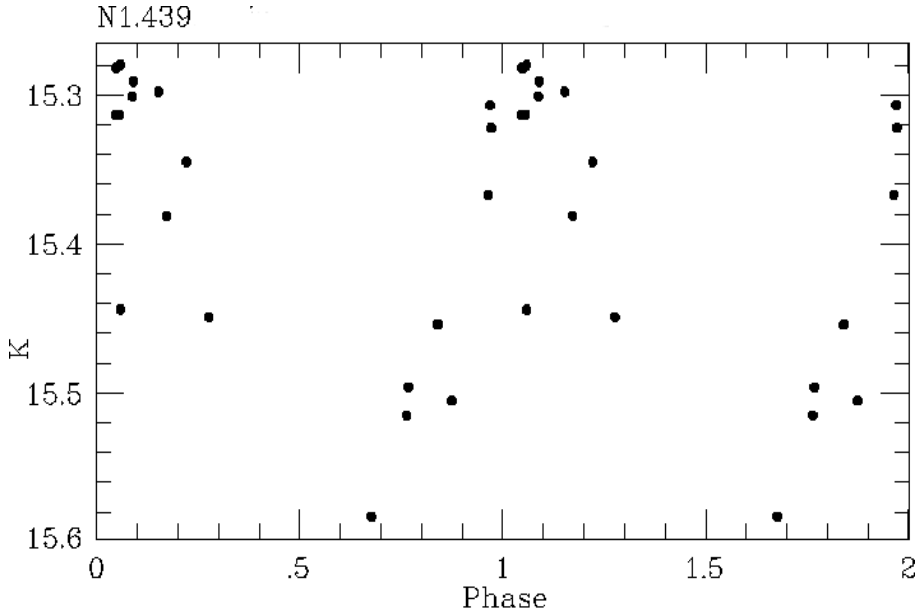

Figure E.6: Phased K light curve for 10439.

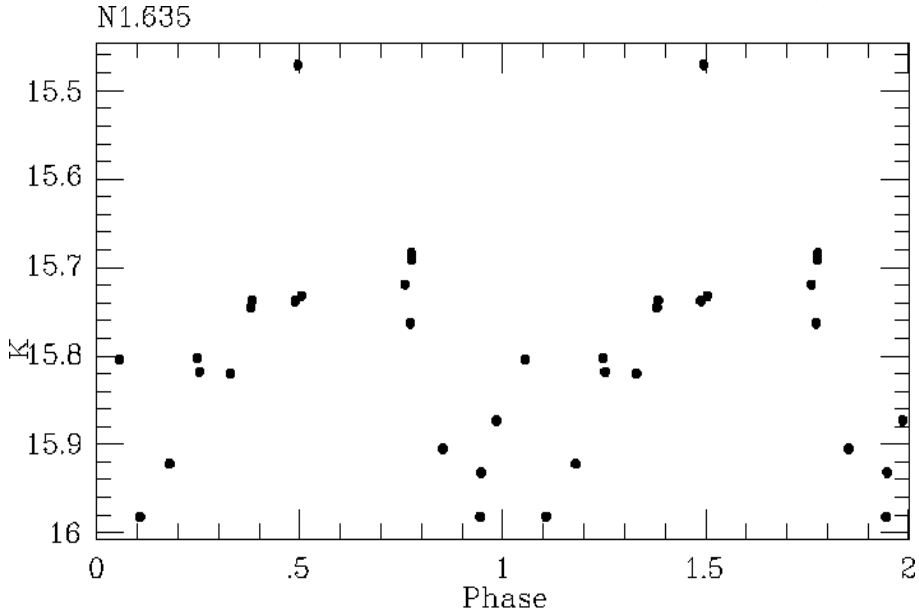

Figure E.7: Phased K light curve for 10635.

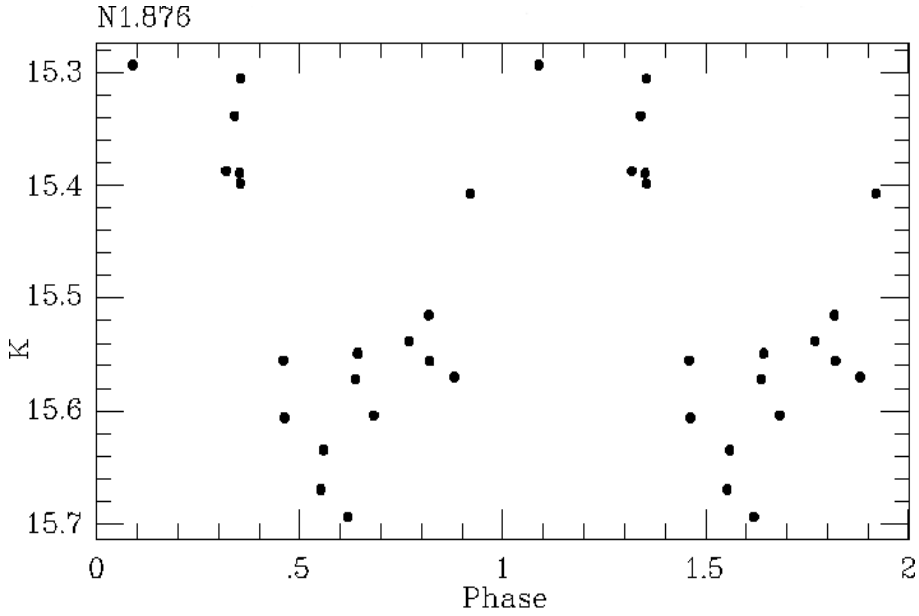

Figure E.8: Phased K light curve for 10876.

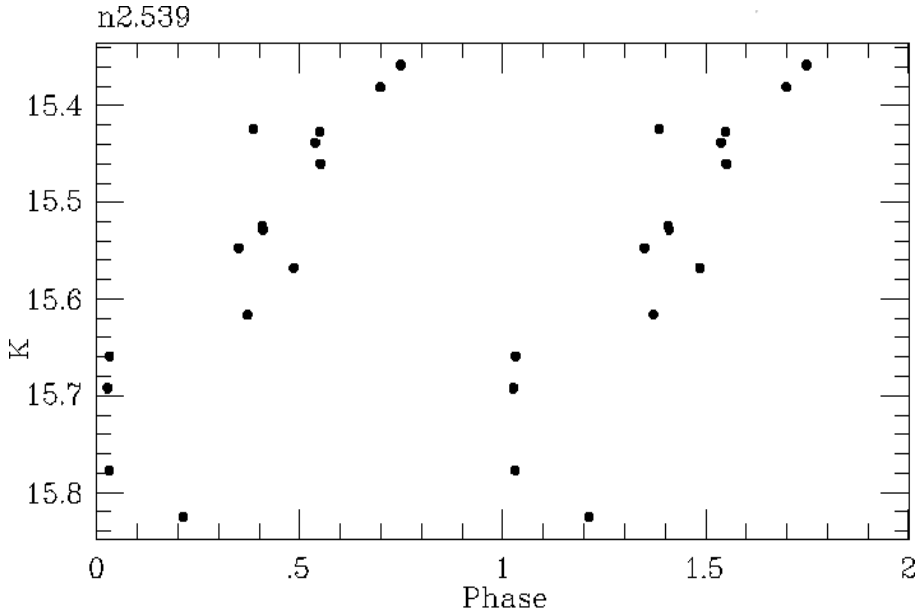

Figure E.9: Phased K light curve for 20539.